Albert-Ludwig-University Freiburg
Faculty of Environment and Natural Resources

MODELING THE DROUGHT IMPACT ON THE PRODUCTIVITY OF A SCOTS PINE FOREST

Master-thesis submitted in partial fulfillment of the requirements for the degree of
Master of Science Forest Science
by

Kenta Koyanagi
Student number: 4776318

First supervisor: Dr. Jens Lange, University of Freiburg
Second supervisor: Dr. Andreas Christen, University of Freiburg

Freiburg i.Br. / Germany
Date of submission:
August 22th, 2019

Abstract

European forestry is expected to broadly be influenced by intensified droughts under changing climate. Drought-induced forest productivity reduction has been recently studied based on remotely sensed data, however, it is still difficult to predict the stand-level growth reduction as stand-level meteorological, hydrological, and biological processes of damaged forests are generally poorly understood. Therefore, this study aimed (1) to collect and compile long-term monitoring data of a drought-affected forest stand, (2) to simulate localized soil moisture and plant water uptake (PWU) dynamics of the last 40 years, and (3) to examine the effects of intensified drought on stand-level forest productivity. Considering the availability of long-term monitoring data and the occurrence of drought-induced forest damages, 60-year-old Scots pine (*Pinus sylvestris*) plantation forest located in southwestern Germany (Hartheim forest) was selected for this study. I employed a newly developed 1-D hydrological model (SPWisoM), which was calibrated and validated in reference to measured soil moisture data (θ_{meas}), actual evapotranspiration data (ET_{act}), and the Kling-Gupta Efficiency (KGE). Time-series productivity of the study site was represented by tree-ring width data (RWI) from 80 Scots pine trees.

KGE values indicated sufficiency of SPWisoM in modeling soil moisture dynamics (KGE at 5, 15, and 35 cm = 0.211, 0.253 and 0.014). PWU dynamics, on the other hand, was only simulated adequately in terms of relative distribution. From 1 January 1978 to 31 December 2018, 82% of total plant-available water existed at shallow depth (0-20cm) and 65% of total PWU also occurred from this depth. This study also revealed that both mean daily soil moisture ($R^2 = 0.5263$, $p < 0.001$) and mean daily PWU ($R^2 = 0.5257$, $p < 0.001$) have been significantly decreasing since 1978, assumably attributed both to increasing annual mean temperature ($R^2 = 0.1717$, $p = 0.007$) and to increasing total annual potential evapotranspiration ($R^2 = 0.3117$, $p < 0.001$) at the study site. Radial growth of Scots pine trees was positively correlated to the soil moisture during the summer period (June – August) and to the PWU during the winter period (December – February), implying an importance of pre-summer PWU and earlywood formation for the productivity of Scots pine trees. Time-series growth rate suggested that fast-growing trees were relatively more vulnerable to recent severe droughts, likely due to lower water-use efficiency combined with drought-prone growing conditions. My findings demonstrated that intra-species drought tolerance and intra-stand microenvironment were the main factors which determined the stand-level forest growth reduction related to drought events. Thus, further efforts should be accordingly made to examine and document detailed growing conditions of individual Scots pine trees. Due to the changing microclimatic condition and decreasing plant-available water, this forest stand would presumably be more unsuitable for existing Scots pine trees, requiring immediate forestry-based climate change adaptations.

Table of Contents

List of Figures

List of Tables

List of Abbreviations and Acronyms

A0	Litter layer
Ah	Denseley rooted silty sand layer
Ah/C	Transition layer between Ah and C layers
alpha	Scale parameter inversely proportional to mean pore diameter
C	Sparsely rooted alluvial gravel sand layer
DOY	Day of the year
DWD	Deutscher Wetterdienst (German Meteorological Service)
ETact	Actual evapotranspiration
FAO	Food and Agriculture Organization of the United Nations
Grad_H	Global radiation at Hartheim forest
hc	Health classes of Scots pine trees
KGE	Kling-Gupta efficiency
KGE_15cm	Kling-Gupta efficiency value at 15 cm
KGE_35cm	Kling-Gupta efficiency value at 35 cm
KGE_5cm	Kling-Gupta efficiency value at 5 cm
Ksat	Saturated hydraulic conductivity
LAI	Leaf area index
NPP	Net primary production
PET	Potential Evapotranspiration
Prec_F	Daily precipitation at Freiburg DWD station
Prec_H	Daily precipitation at Hartheim forest
Press_F	Daily mean atmospheric pressure at Freiburg DWD station
Press_FS	Daily mean atmospheric pressure at Feldberg/Schwarzwald DWD station
Press_H	Daily mean atmospheric pressure at Hartheim forest
PWU	Plant Water Uptake
r	Pearson´s correlation coefficient
RH	Relative humidity
RH_F	Daily mean relative humidity at Freiburg DWD station
RH_FS	Daily mean relative humidity at Feldberg/Schwarzwald DWD station
RH_H	Daily mean relative humidity at Hartheim forest
RWI	Ring width index
SOM	Soil Organic Matter
SPAC	Soil-Plant-Atmosphere Continuum
SPWisoM	Soil, Plant, Water, and isotope Model
Sun_F	Relative sunshine hours at Freiburg DWD station
SWRC	Soil water retention curve
Temp_F	Mean daily temperature at Freiburg DWD station
Temp_H	Mean daily temperature at Hartheim forest
W10_F	Daily mean wind speed at Freiburg DWD station, measured at 10 m a.g.l.
W10_FS	Daily mean wind speed at Feldberg/Schwarzwald DWD station, measured at 10 m a.g.l.
W2_H	Daily mean wind speed at Hartheim forest, measured at 2 m a.g.l.
WAI	Woody area index
θ	Soil moisture
θmeas	Measured soil moisture

θmod	Modeled soil moisture
θr	Residual water content
θs	Saturated water content
ψ	Water potential

List of Appendices

1 Introduction

Drought hazards may trigger catastrophic damages on human society, economy, and environment. Globally, the intensity of drought is expected to increase in southern and central Europe, central North America, Central America and Mexico, northeast Brazil and southern Brazil, implying increasing drought-related hazard risks such as food and water shortage (Stanke et al., 2013). In case of the USA, a single drought hazard in 2011 caused 1.4 billion USD of economic losses, including direct economic impacts on the agricultural sector and other secondary effects (Ding et al., 2011). Drought also disturbs terrestrial and aquatic environments; drought may decrease productivity and biodiversity of forest and grassland ecosystems (Hanson & Weltzin, 2000; Tilman & Haddi, 1992); declined water level potentially alter species composition and biogeochemical cycles of the aquatic ecosystems (Humphries & Baldwin, 2003). Therefore, international society is increasingly demanded to adapt to the intensified frequency, duration, and severity of the drought hazards.

Forestry is particularly susceptible to drought hazards as the productivity of the forest ecosystem is directly and/or indirectly influenced by the availability of water. Decreased soil moisture and stomatal conductance due to drought directly lead to reduced net primary production (NPP) and water use of forest ecosystem (Dale et al., 2001). Once water transport systems of trees are disconnected by gas emboli, leaves cannot receive enough water for the photosynthesis, often resulting in dehydration and increased mortality (Choat et al., 2012). Based on CO_2 flux measurements, Kljun et al. (2007) estimated that 3-year drought in Canadian boreal forests reduced NPP by 34% lower than pre-drought condition at the 3rd year of the continuous drought. In addition to the direct effects, drought may indirectly decrease forest productivity through degrading vitality of trees and increasing secondary hazards; forest drought potentially increases risks of pest outbreaks and wildfires (Hanson and Weltzin, 2000).

Although there have been regional (e.g., Ciais et al., 2005; Figure 1) to global scale (e.g., Vicente-Serrano et al., 2013; Figure 2) researches for understanding drought effects on forest productivity, those large scale simulations do not always reproduce stand-level response to droughts, due to the influences of stand-specific factors. For instance, Martínez-Vilalta et al. (2012) studied the effects of drought on Scots pine (Pinus sylvestris) productivity, showing tree ring growth under drought was mainly determined by tree- and stand-level variabilities (e.g., the growth rates of individual trees). Dense forests are generally more susceptible to droughts due to higher competition for water resources (D'Amato et al., 2013). Additionally, soil characteristics and subsequent soil water content play an important role in determining drought response of forest ecosystems (Granier et al., 2007). Unfortunately, rapidly developing remotely sensed data usually provides soil moisture data at limited depth below the forest surface (~5cm; Chen et al., 2014), making stand-level hydrological properties underrepresented. For those reasons, it is still hard to predict stand-level forest response to intensified droughts based on recent regional- and global-scale studies.

Therefore, this study aimed to understand the drought impacts on stand-level forest productivity, by combining stand-level meteorological, hydrological, and biological

parameters. This study was conducted at 60-year-old Scots pine (Pinus sylvestris) plantation forest (Hartheim Forest Research Site) in southwestern Germany, where long-term meteorological, hydrological, and forest growth monitoring data were accessible. The Hartheim forest was also suitable for this research because (1) it has been severely damaged by recent drought events (section 3.1) and (2) Scots pine is one of the most widespread and economically important tree species in Europe. I firstly simulated the spatiotemporal distribution of soil water content and plant water uptake (PWU) based on a novel hydrological model (Figure 3). Secondly, this study compared the long-term forest productivity data (i.e., time-series tree ring width data) to the simulated soil moisture and PWU data, for understanding the stand-scale forest response to intensified droughts.

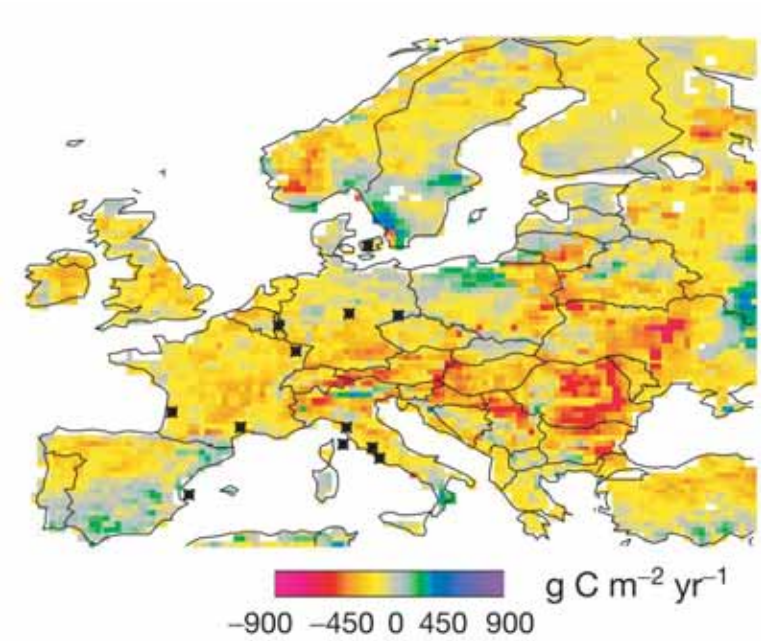

Figure 1. Regional-scale changes of annual mean vegetation growth (net primary productivity: NPP) induced by the 2003 European drought simulated by Ciais et al. (2005). Overall, NPP in 2003 (541 $gCm^{-2}year^{-1}$) was significantly reclined than average value of 1998 – 2002 (644 $gC^{-2}year^{-1}$). NPP reduction was particularly severe in Central and Eastern Europe, while it even increased partly in Northern Europe.

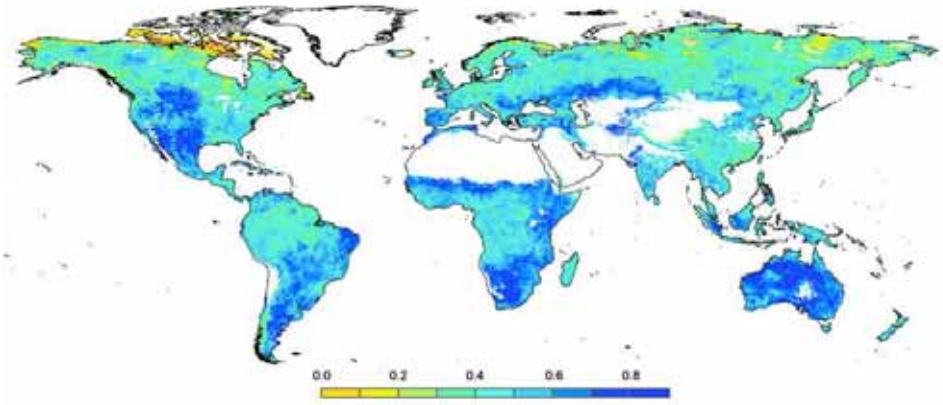

Figure 2. A global-scale study by Vicente-Serrano et al. (2013), showing Pearson coefficient (r) between Standardized Precipitation Evapotranspiration Index (SPEI) and Global Inventory Modeling and Mapping Studies-Normalized Difference Vegetation Index (GIMMS-NDVI). Globally, 72% of vegetated land surface indicate a significant correlation between SPEI and GIMMS-NDVI, suggesting vegetation activity is strongly influenced by droughts across the world.

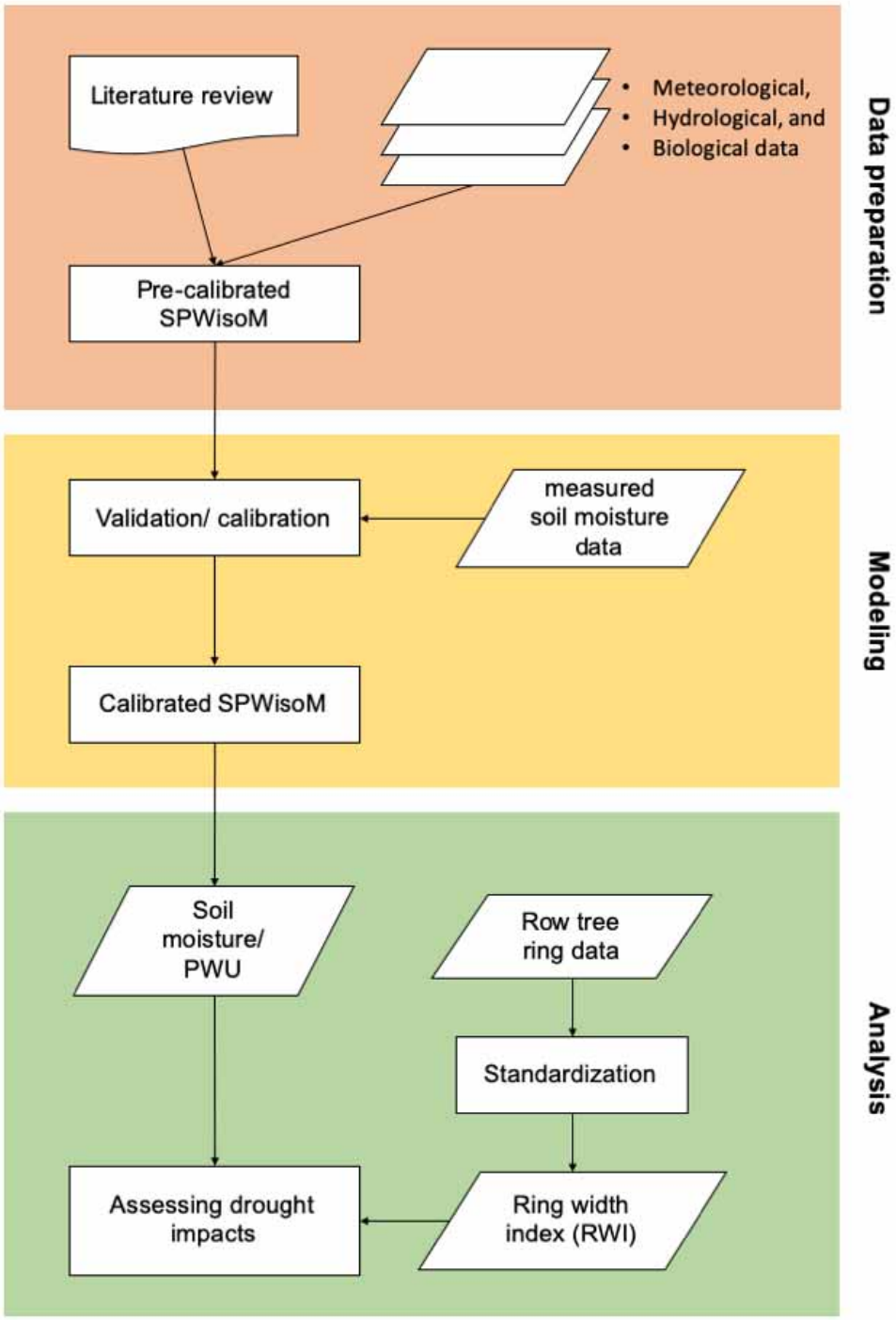

Figure 3. Flowchart of the research: Input parameters were collected from the literature review, long-term monitoring data, and field observation; SPWisoM was validated and calibrated based on measured soil moisture data from 2003-2004; calibrated SPWisoM was finally applied for the period of 1978-2018 and drought impacts on tree growth reduction was analyzed.

2 Literature Review

2.1 Drought impact on European forestry

Drought has been observed across Europe more intensively since the beginning of the 21st century (e.g., 2003, 2010, 2013, and 2015; Hanel et al., 2018), causing forestry damages both for short and long periods. For instance, a drought event induced by the 2003 European heatwave decreased the gross primary productivity of European forests by 30% in total, according to Ciais et al. (2005). Leuzinger et al. (2005) studied the physiological responses of five deciduous tree species in Swiss temperate forest during the 2003 drought, indicating that annual basal area increment has been reduced by 25% compared to previous years. The Mediterranean forest is the most drought-prone in Europe due to warmer and drier weather pattern (see Lindner et al., 2010). In western Europe, Rouault et al. (2006) studied secondary hazards (pest outbreak) associated with the 2003 drought in Western Europe, indicating that water stress-induced risk of pest outbreak varies depending on the feeding resources of insect species.

Moreover, the frequency and intensity of drought are expected to increase in large parts of European forests (see Appendix 1 and Appendix 2). Schlyter et al. (2006) simulated future climatic patterns (2070-2100) and subsequent drought-related forest damages in the boreal forest of Northern Europe, suggesting that extreme weather events such as summer drought would be magnified. As well as the direct impacts, decreased vitality of boreal trees will be threatened by post-drought pest outbreaks and/or windthrow risks according to Schlyter et al. (2006). It is also projected that the forest area of Central Europe, especially in southern Slovakia and Hungary, will be more and more susceptible to droughts (Hlásny et al., 2014). In Mediterranean forests, warmer and drier weather patterns are likely to trigger less nutrient supply from soil (Sardans & Peñuelas, 2004, 2005, 2007) and/or reduced forest productivity (Lindner et al., 2010).

Therefore, several adaptation strategies aimed to regulate climate change impacts have been developed and implemented in European forestry (Lindner et al., 2008). Based on Lindner et al. (2008), adaptation measures against climate change in European forestry can be classified into three different levels, i.e., stand-level, forest management-level, and policy-level; stand-level measures consist of regeneration, tending and thinning, and harvesting; forest management-level measures include forest planning and forest protection; policy-level measures incorporate infrastructure and transporting, nurseries and tree breeding, development and evaluation of adaptation strategies, and scientific researches. In Central Europe, for instance, Hlásny et al. (2014) assessed drought-induced forestry risks and suggested increasing drought tolerance by diversifying genetic variation and changing species composition, as well as improvement of risk monitoring systems. Based on a process-based forest growth model, Sabaté et al. (2002) examined the effect of thinning cycle length under projected climate change in Mediterranean forest, showing shorter thinning period is likely to produce more final timber due to reduced mortality between thinnings. In the European Alps, Elkin et al. (2015) also used a process-based model to study effective thinning regimes to mitigate drought impacts. This study concluded that thinning possibly reduce drought-induced

mortality, but also the effective duration differs depending on stand elevation and timing and intensity of thinning.

2.2 Soil-Plant-Atmosphere Continuum (SPAC)

Drought causes temporal or permanent functional failures in plant water uptake (PWU), lowering the vitality of trees and leading to die-off in extreme cases. Due to the absence of metabolically active pumps like animal heart, water transport inside plant body is passively induced by the gradients of pressure and/or chemical potentials; water is transported from higher to lower water potential (Figure 4). In particular, upward transport of water can be explained to occur based on negative pressure within the plant body caused by transpiration (Cohesion-Tension theory; Tyree, 2007). This, upward water transport which is driven by transpiration happens only when water is connected throughout the soil-root-stem-branch-leaf-stomata of a tree (Kumagai, 2011). The pathway through which water moves from soil to the atmosphere is known as the soil-plant-atmosphere continuum (SPAC). Along the SPAC, processes of PWU can be divided into four sections being consistent with actual sequential order: (1) water movement within soil, (2) water transport from the soil to roots, (3) water transport through the xylems, and (4) water transport from leaf to the atmosphere.

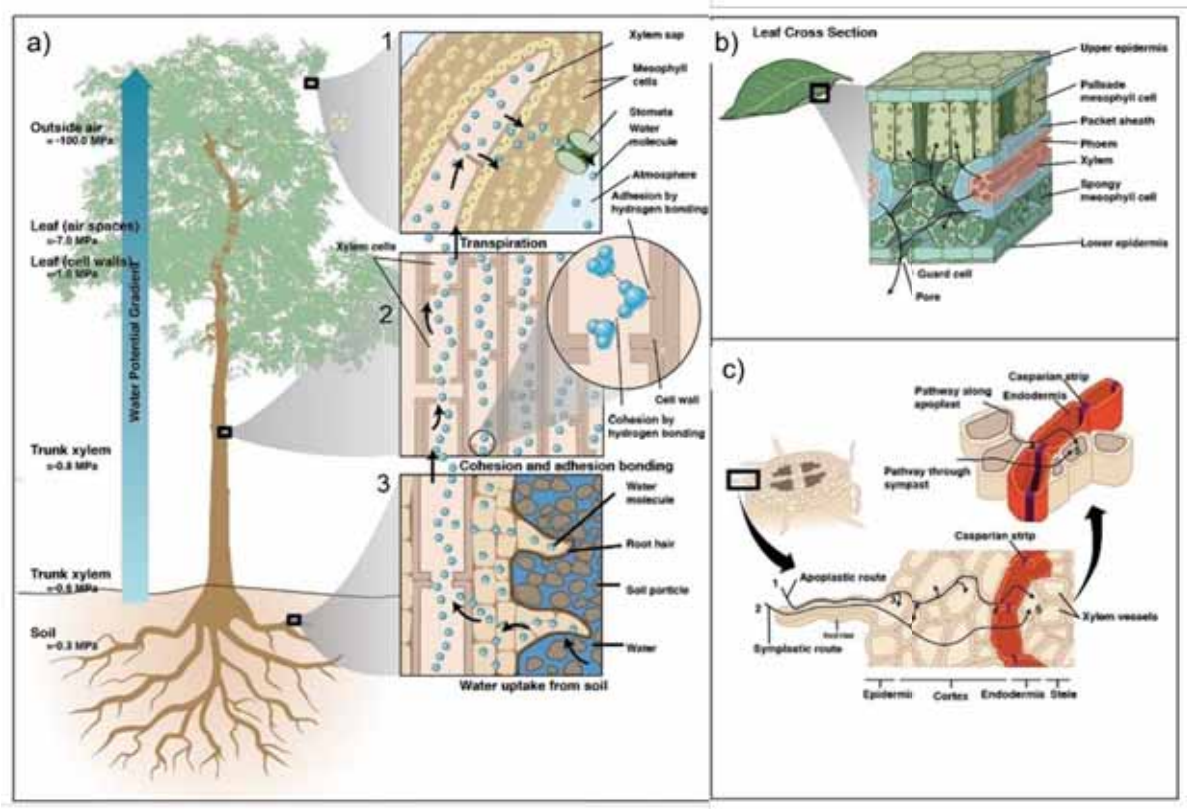

Figure 4. Schematic diagram of the plant water uptake along the soil-plant-atmosphere continuum (SPAC) after McElrone et al. (2013). (a) Water transport occurs from areas with higher water potential (i.e., soil) to the area with lower water potential (i.e., atmosphere outside of the leaves). (1) During leaf transpiration, evaporation of water molecules generates tensions; (2) upward tension is transmitted via cohesive water channel within the xylem; (3) consequently, this upward tension triggers plant water uptake (PWU) through roots from the soil. (b) Water movement from leaf veins through the stomata and (c) water movement from the soil through the fine roots.

The physical properties of soils are of importance when understanding soil moisture and PWU dynamics, since they greatly influence the availability of water for plant roots; plant-available water capacity is determined by the difference between field capacity and permanent wilting point (Silva et al., 2014). Field capacity refers to the amount of soil water stored following complete drainage of excess water, while permanent wilting point is the lower limit of available soil water below which plant cannot extract water from the soil. Field capacity is mainly determined by soil texture, soil structure, and soil depths (Veihmeyer & Hendrickson, 1949). For instance, fine-textured soils such as clay soils are able to hold more water than coarse-textured soils such as sandy soils, representing higher field capacity due to the larger surface area. Soil organic matter (SOM) may also increase field capacity of a given soil by expanding the surface area of the soil (Vengadaramana & Jashothan, 2012). Permanent wilting point is also largely influenced by soil types associated with vegetation types, typically increasing from sandy to clay soils (Slatyer, 1937). The plant-available water, the difference between field capacity and permanent wilting point, is therefore strongly affected by those physical properties of soils. The relationship between water potential (ψ) and water content is called a water retention curve (see section 3.2.1.2.4).

Those physical soil properties also have considerable effects on water movement through soil. Between the groundwater table and soil surface, the soil is normally unsaturated and is known as the "unsaturated zone" or "vadose zone". During infiltration processes, for instance by a precipitation event, water moves downwards by shaping wetting front ununiformly, and the rate at which the wetting front moves is mainly determined by soil texture and soil structure (Radcliffe & Rasmussen, 2002). For example, water generally moves downwards more rapidly (highly conductive) though coarse-textured soils than through fine-textured soils. When soil is mostly drained (below field capacity), on the other hand, water movement becomes relatively slow and the rate at which water flow occurs is mainly determined by capillary forces. Moreover, the existence and connectivity of soil macropores, usually generated from biological processes like root decomposition, may also dynamically alter the direction and speed of water transport through unsaturated soils (Beven & Germann, 2013).

Plant water uptake (PWU) is driven by the hydraulic gradient at the root-water interface; water movement from soil to plant roots is controlled by the transpiration-induced negative hydrostatic pressure and/or nutrient ion-induced positive osmotic pressure (Steudle, 2000; Figure 4c). The amount of plant-available soil water largely depends on the soils properties, vegetation types, and meteorological conditions. Soil characteristics and consequent hydraulic properties stated above play an important role in controlling PWU, i.e., optimal PWU occurs when soil is neither too dry nor too wet (see section 3.2.1.3.1). Plants species with higher capacity of root system development are likely to access relatively more water resources (Franco & Nobel, 1990). Furthermore, mycorrhizal fungi possibly enhance water uptake of some plant species, for instance by enlarging the root surface area contacting with soil water and/or by improving root hydraulic conductivity (Ruiz-Lozano & Azcón, 1995; George & Marschner, 1996). Increased evaporation rate, mostly owing to the higher evaporative demand, from soil surface results in reduced soil moisture and potentially declined plant-available soil water (Jensen et al., 1961), while precipitation patterns and intensity also modify the spatiotemporal distribution of plant-available soil water (Zeppel et al., 2014).

Once water moves into plant xylem, upward water flow is pulled by the transpiration-caused tension as a form of bulk flow (Figure 4a). Besides water, xylem also transports inorganic and organic substances dissolved into water, which is also known as xylem sap flow. The volume and speed of xylem water (or sap) flow are mainly controlled by transpiration rate and anatomical characteristics of xylem. Because xylem water flow is triggered by transpiration, xylem flow rate strongly respond to and is correlated to canopy transpiration rate in general (e.g., Schulze et al., 1985). Therefore, xylem sap flow measurement has been widely applied for the estimation of the transpiration rate, from individual tree-level, stand-level (Granier et al., 1996), regional-level (Köstner, 2001), and to global-level (Poyatos et al., 2016). Additionally, upward xylem water flow is also affected by intra- and inter-species differences in xylem characteristics, such as size and density of xylem pits (Lobet et al., 2014; Figure 5b) which alter the hydraulic conductivity of xylem (López-Bernal et al., 2010). Under drought condition, cavitation and embolism within the xylem may reduce xylem conductivity, possibly causing hydraulic failure and subsequently increased tree mortality.

At the leaf-atmosphere interface, water finally evaporates from plant leave to the atmosphere in the way of transpiration (Figure 4b). Transpiration is mainly driven by the difference of water potential between plant leave and atmosphere, and the rate at which transpiration occurs is regulated by a wide range of factors, including both internal and external factors. The major internal factors include characteristics of leaf and canopy structure, determining the abundance of stomata contributing to transpiration (Wang & Jarvis, 1990; Vertessy et al., 1995). For instance, Oren et al. (1999) measured the effect of reduced leaf area index (LAI) on the transpiration rate, showing 40 % reduced LAI resulted in 18 % declined xylem sap flux density. Moreover, the major external factors are the atmospheric humidity, temperature, photosynthetically active radiation (PAR), and wind speed, simultaneously controlling the resistance and conductivity of stomata as well as evaporative demands (Drake et al., 1970; Collatz et al., 1991). As an example, Meinzer et al. (1993) investigated the effect of lowered humidity on the transpiration rate of tropical tree species, reporting a significant reduction of transpiration rate due to increased evaporative demands.

In addition, summer droughts potentially destroy the connectivity of SPAC which may result in reduced productivity of the forest ecosystem. Increased evaporative demand owing to dry and warm weather enhances both leaf transpiration and soil evaporation, intensifying the tension of the xylem water column. This, strengthened tension often cause the breakage of the water column (i.e., cavitation). Cavitation and associated air-emboli inside the xylem generally reduce the efficiency of the water transport considerably (Figure 5b), eventually triggering the hydraulic failure of a tree (e.g., Brodribb & Cochard, 2009). Combined with reduced photosynthesis (McDowell, 2011) and degraded tree vitality associated with the water stress (Dobbertin, 2005), trees are likely to grow slower and become more vulnerable to biotic and/or abiotic disturbances under drought conditions. Those mechanisms are the most widely supported theory explaining the drought-induced growth reduction and consequently increased mortality of the forest ecosystem (Allen et al., 2010).

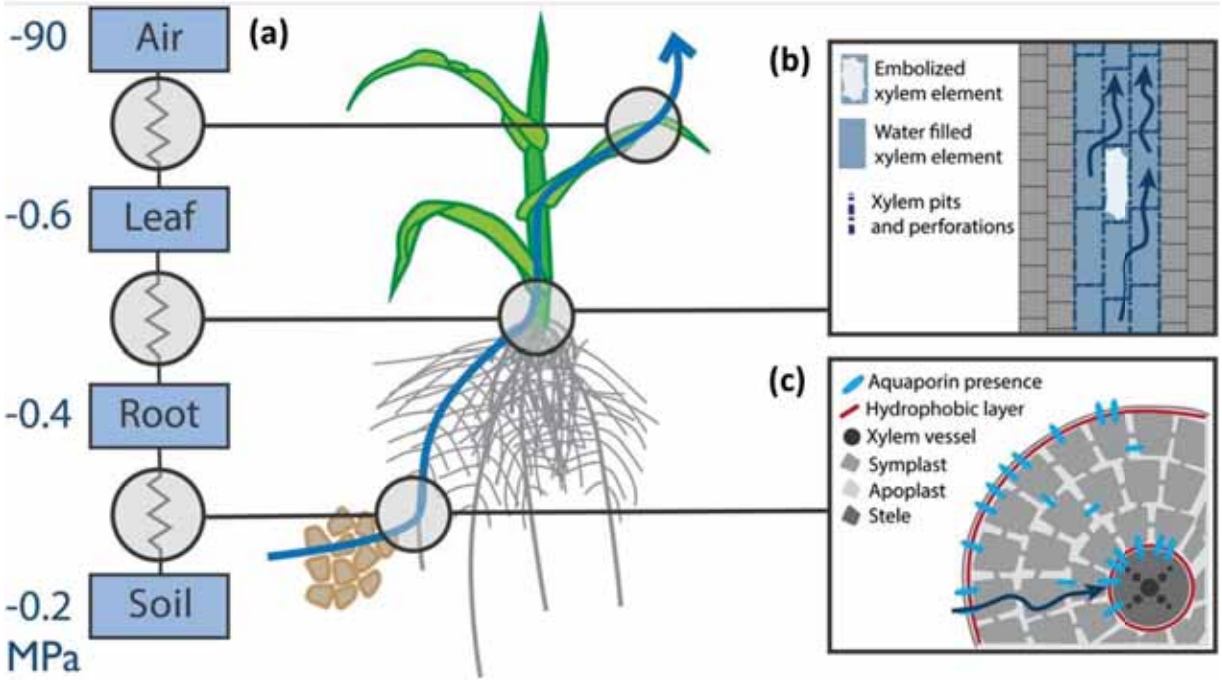

Figure 5. Schematic diagram of plant water uptake (PWU) under dry environment after Lobet et al. (2014). (a) PWU is driven passively by differences of water potential through SPAC. (b) Axial water transport is regulated by the characteristics of the xylem (e.g., size, number, and presence of pits) as well as the presence of cavitation. (c) Radial water transport is affected by the radial properties of the root (e.g., number of cell layers and the presence of hydrophobic layers) for the long-term, while it is governed by the expression and localization of aquaporin for the short-term.

3 Materials and Methods

3.1 Study Site

This study was conducted at the Hartheim Forest Research Site (47.93391°N 7.59814°E; 201m above the sea level), 60-year-old Scots pine (*Pinus sylvestris*) plantation forest at the time of 2019. The Hartheim forest is located in the Upper Rhine valley, 20 km south-west of Freiburg, southwestern Germany (Figure 6). This study area is situated approximately 1m east of the Rhine River, the border between France and Germany. Since 1969, this study site has been managed by the Chair of Environmental Meteorology (formerly known as Meteorological Institute), University of Freiburg, for the purpose of long-term cross-disciplinary studies including meteorological, hydrological, and biological perspectives. While the fenced area for continuous monitoring purposes covers only ca. 0.7 ha, a homogeneous plantation forest extends to the outside of the fenced area (Figure 7). The plantation forest area ranges 10 km from North to South and 1.5 km from West to East, respectively (Jaeger & Kessler, 1997). This study site is situated on an extremely flat ground surface which shapes a part of the Rhine floodplains (Koeninger & Leibundgut, 2001); based on 25m-resolution EU-DEM, the mean slope gradient of the study site (500m-buffered area around the fenced area) is 1.37° (SD: 1.06°) (Figure 8).

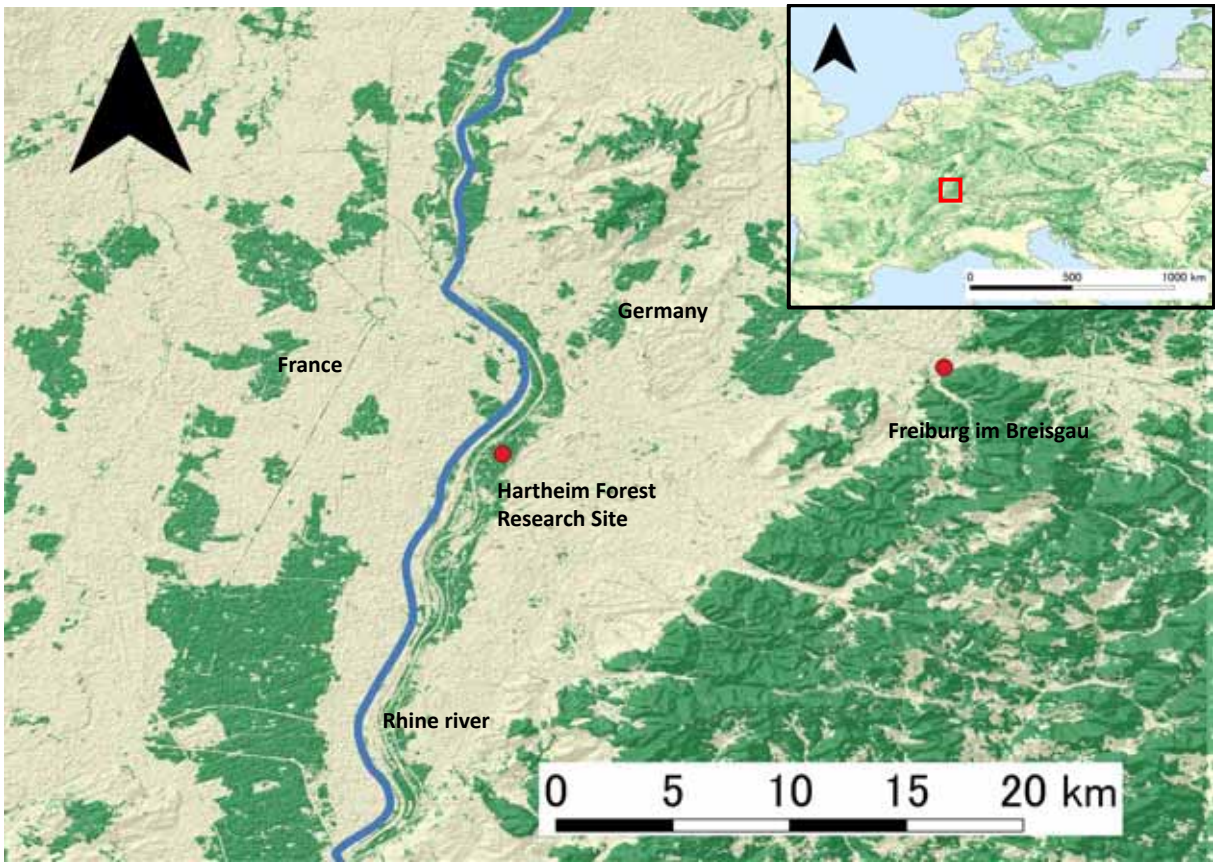

Figure 6. The geographical setting of the Hartheim Forest Research Site, which is located approximately 20km from Freiburg, southwestern Germany. Greenish parts represent forest cover, detected by the Pan-European Forest/Non-Forest Map 2006 (spatial resolution = 25m×25m). Background hillshade was created from the ASTER Global Digital Elevation Model (spatial resolution = 30m×30m). Shapefile of Rhine River was accessed from the European Environmental Agency's WISE Large rivers and large lakes.

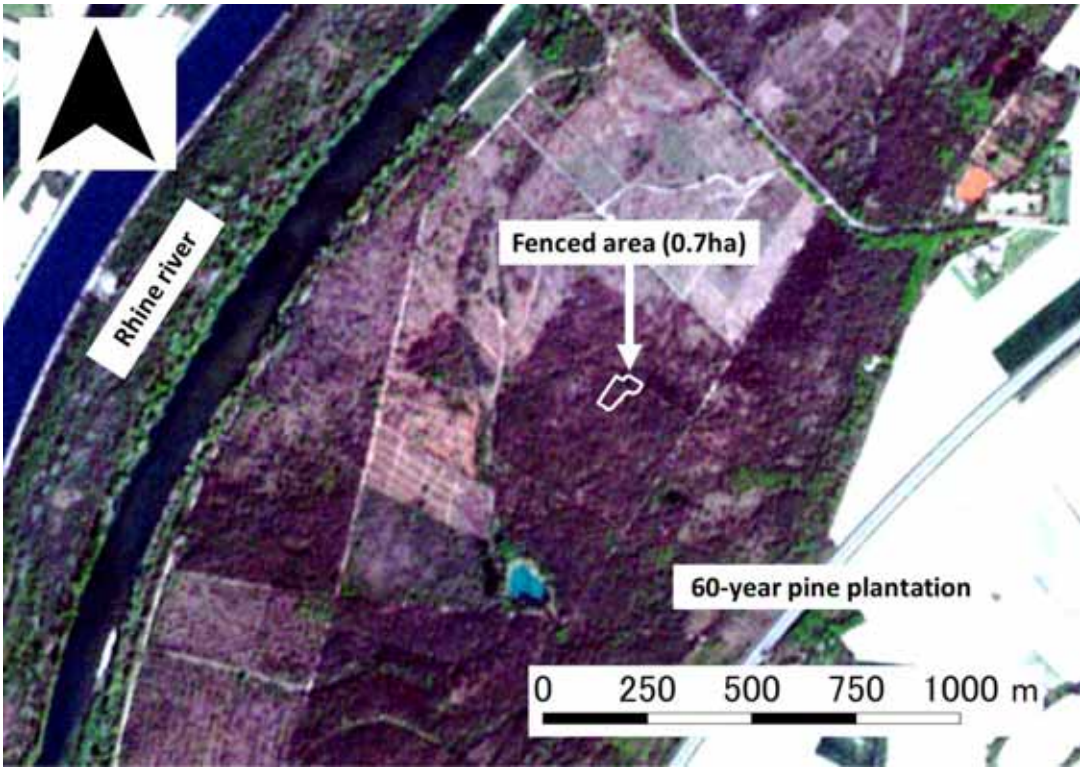

Figure 7. Satellite image (5m-RapidEye image captured on April 20th, 2019) covering the Hartheim forest, including the fenced area (0.7ha) managed by the University of Freiburg. The 60-year-old Scots pine plantation is located adjacent to the Rhine River.

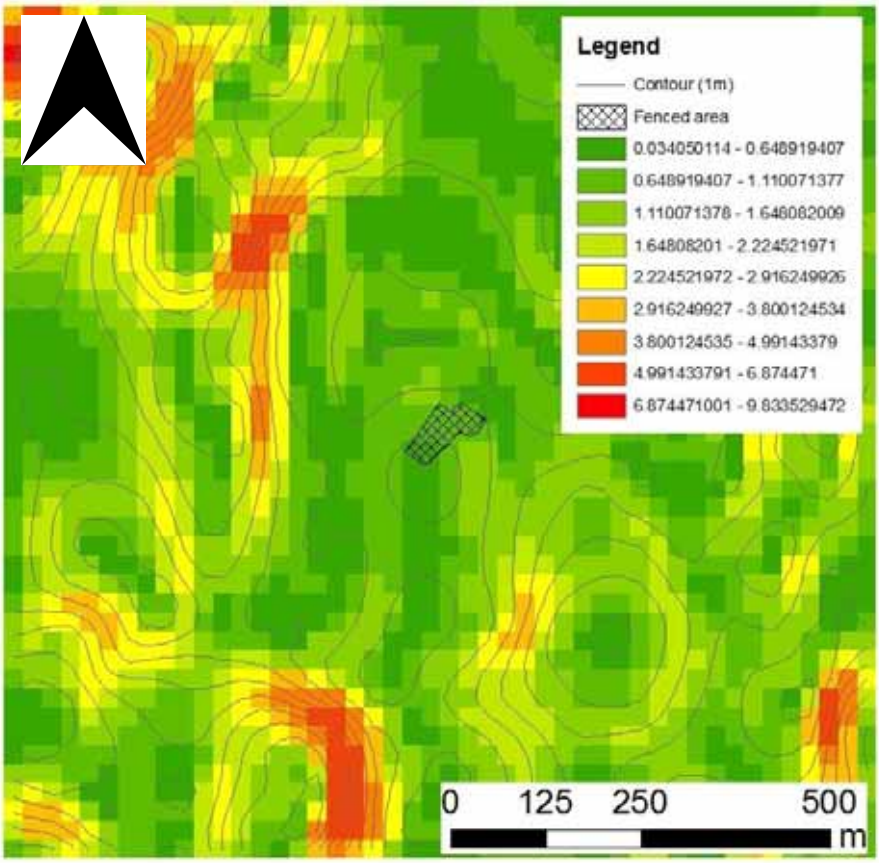

Figure 8. The topography of the Hartheim forest (the 500m-buffered area around the fenced area). Slope gradient was calculated based on 25m-resolution European Digital Elevation Model (EU-DEM), version 1.1. This figure shows the flat surface of the study site with an average slope gradient of 1.37° (SD: 1.06°).

The Hartheim forest mainly consists of homogenous Scots pine (*Pinus sylvestris*), partially mixed with Black pine (*Pinus nigra*). Originally, this area was covered with riparian forest, however, increased mortality of riparian trees due to bypath construction of the Rhine river completely altered species composition of the area; Scots pine plantation was initiated in 1961 with 2-year-old seedlings at the 1.5m of spacing between each tree as a result of subsidies (Jaeger & Kessler, 1997; Ryel et al., 2001; Mayer et al., 2012; Figure 9). Following the plantation, several thinning operations have been carried out: 1970/71; 1981/82; 1993/94; March 2003 (Jaeger & Kessler, 1996; Jung, 2005; Wellpott et al., 2005). While every third row of the Hartheim plantation forest was removed in the first thinning, the rest of following thinnings were conducted only to remove trees around the final crop trees (Jaeger & Kessler, 1997). As a result of these forest management, stand height and stand density of the Hartheim forest have changed from 2.4 m and 22,000 ha^{-1} in 1969 to 17.3 m and 600 ha^{-1} 2019 (Figure 10). Over the last 50 years, the mean annual growth rate was ~0.3 m/year, which is classified as slow-growing conditions according to Holst et al. (2008). In terms of forest floor, approximately 40% are sorely covered with bare soil, litters and/or mosses, while other surfaces are dominated by vascular plant species such as *Carex alba* and *Carex flacca* (Wedler et al., 1996).

Figure 9. Aerial photograph of the pine plantation in 1978 after Jaeger (1978). The homogenous crown surface of the plantation forest can be found from the aerial photograph.

Figure 10. Stand development of Hartheim Forest Research Site from 1969 to 2019. Average stand height has developed from 2.41 m to 17.33 m over the monitoring period. Tree density has been decreased from 22,000 ha^{-1} to 600 ha^{-1} due to repeated artificial thinning.

Due to the topographic effects of the Upper Rhine valley, this study site is governed by a warm and dry climate, referred to as "almost semi-arid hydrological condition" by Kessler & Jaeger (1999). The mean annual total precipitation (mm/year) and mean annual temperature (°C) between 1978 and 2018 are 641 mm/year and 11.0 °C, respectively. Monthly total precipitation (mm/month), monthly mean temperature (°C), and monthly maximum temperature (°C) over the period of 1978-2018 are indicated in Figure 11. Over the

corresponding period, the highest mean temperature on a monthly basis generally occurred in July (ca. 20.0 °C), while the lowest mean temperature normally took place in January (ca. 2.4 °C). In addition, maximum monthly precipitation generally happened in May (ca. 79 mm/month) and minimum monthly precipitation occurred in February (ca. 32 mm/month).

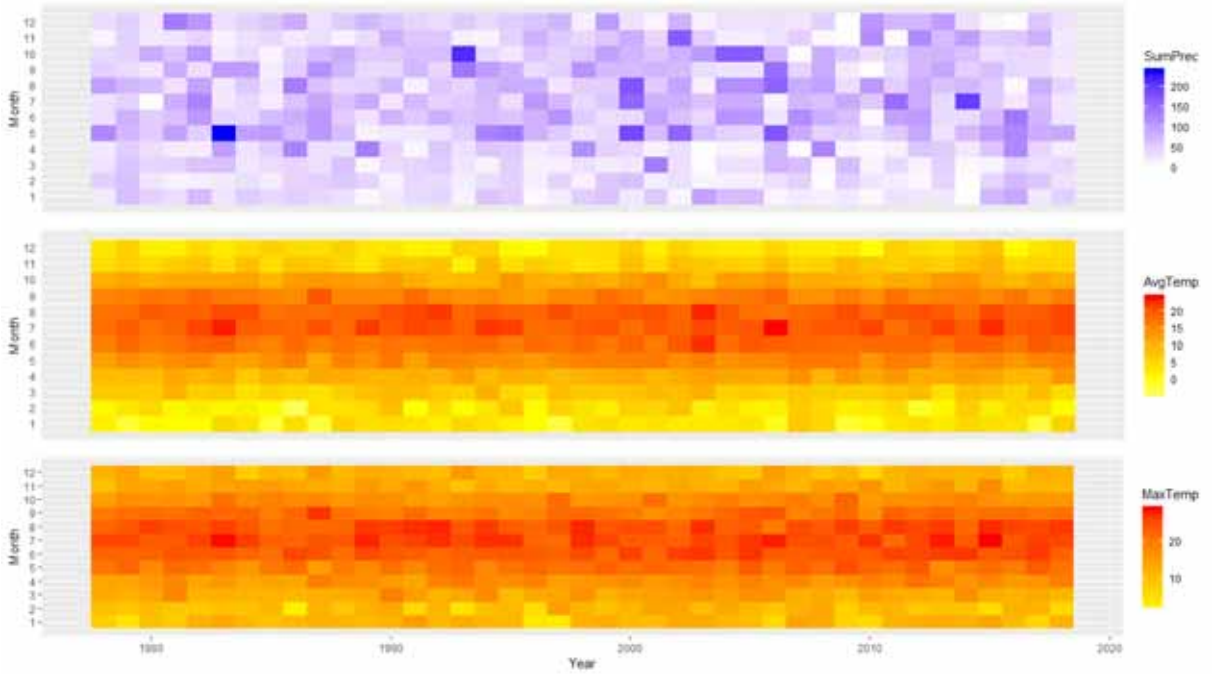

Figure 11. Heat maps showing monthly total precipitation (mm/month), monthly mean temperature (°C), and monthly maximum temperature (°C) from 1978 to 2018.

The soil of the study site is formed with two main layers shaped by flooding of the Rhine River (Sturm et al., 1996) in addition to the humus layer (ca. 1 cm) on the top (Figure 12). The upper layer (Ah-horizon) that ranges from 15cm to 80cm (average depth: 40 cm) is silty sand, followed by the lower layer (C-horizon) consisting of alluvial gravel sand (Sturm et al., 1996). The upper layer exhibits relatively higher field capacity (35.4 Vol%; Königer, 2003) and higher organic content (Goffin et al., 2014), resulting in that most of the tree roots develop within the upper layer (Figure 12). In contrast to the upper layer, the lower layer is less capable of retaining water (field capacity = 3.5 Vol%; Königer, 2003) and less in nutrient, showing limited penetration of the roots. Therefore, only the upper layer (~ 40 cm) contributes to the water uptake of pine roots at the study site (Königer, 2003). Due to the shallowness of the upper silty sand layer, the absolute water storage capacity of the study site is limited to 80 mm (Sturm et al., 1996). In addition, although the study site is located adjacent to the Rhine river, the groundwater table has been lowered to approximately 7m below the ground surface due to artificially modified river morphology of the Rhine (Figure 13); trees of the study site are unable to access to the groundwater, thus, there is no water uptake from the groundwater (Vogt & Jaeger, 1990; Jaeger & Kessler, 1996). Because of the flat and homogenous ground surface, subsurface water flow is dominated by vertical flow and lateral subsurface flow is negligible (Sprenger et al., 2015).

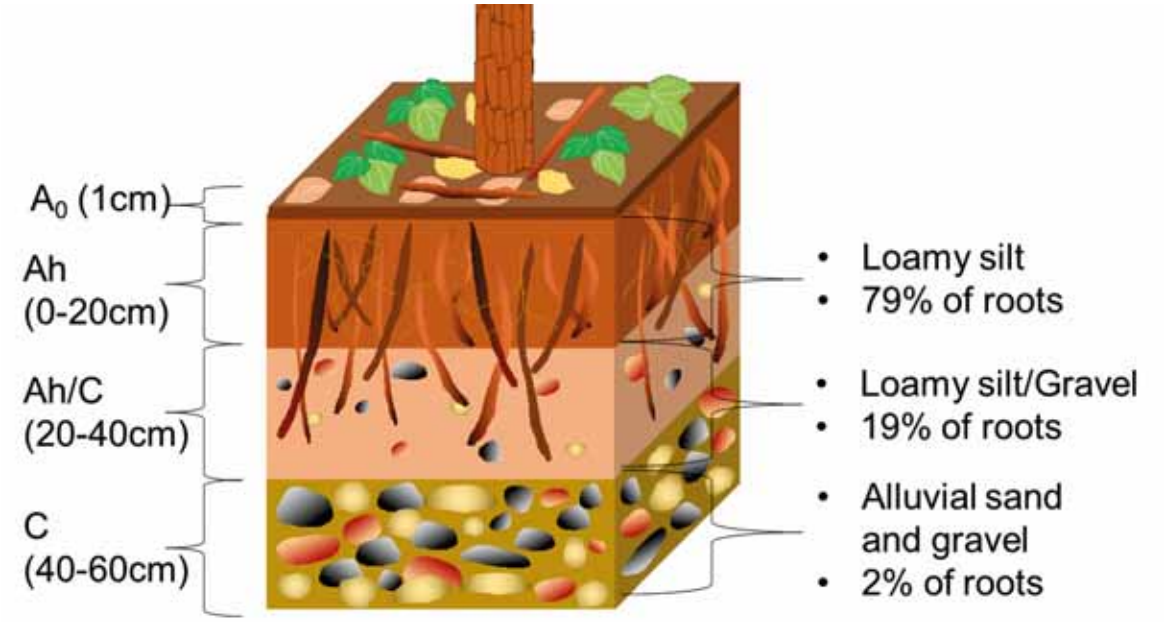

Figure 12. Schematic diagram of the typical soil profile at Hartheim forest. Following the shallow organic layer (A0; ca. 1 cm), densely rooted loamy silt layer (Ah; ca. 20 cm), transition layer from silt layer to gravel layer (Ah/C; ca. 20 cm), and sparsely rooted alluvial sand and gravel layer (C; > 20cm) are stratified. Vertical distribution of roots is based on Maier et al. (2011).

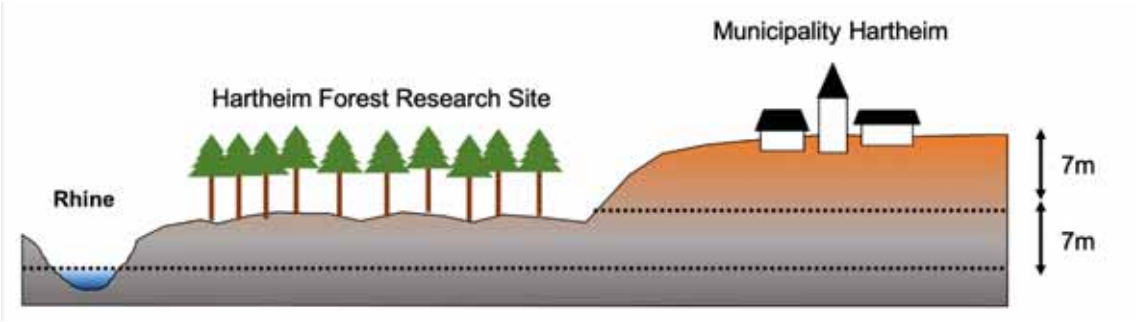

Figure 13. Schematic profile of the Hartheim Forest Research Site, showing elevation gaps of Municipality Hartheim, study site, and Rhine River (after Mayer et al., 2005). The groundwater table has been lowered to ~7 m below the surface, thus, tree roots are not able to reach and absorb water from the aquifer.

Warm and dry climatic conditions combined with the highly drainable underlying soil have made the study site prone to drought hazards (Sturm et al., 1996). Wellpott et al (2005) revealed that water deficiency (i.e., potential evapotranspiration > actual transpiration) has repeatedly occurred at Hartheim forest site during the period between 1978 and 2001, particularly severely during August 1983; Aug-Oct 1985; June 1989; Aug 1990; Jul-Aug 1991; Aug 1992; and Jul 1998. They also indicated that August is most likely to induce drought stress in the study site based on the historical trend. Due to the 2003 European heatwave, water availability of the study site was clearly lowered compared to previous years (i.e., 1978-2002), even reaching below the permanent wilting point in part (Schindler et al., 2004, 2006). Holst et al (2008) demonstrated that severe summer drought in 2006 resulted in carbon uptake of Hartheim forest approximately 40% lower than that of 2005. More recently, Hartheim forest has been suffered from drought events in 2014, 2015, and 2018, resulting in decreased vitality and partial die-off of the pine plantation forest (Figure 14 and Figure 15). Because of the drought-prone environment and long-term monitoring data (i.e., long-term meteorological, hydrological, and biological data), this study site provides desirable

conditions for studying drought impact on forest productivity. From the field observation on 2 May 2019, I detected only Scots pine trees were severely damaged by recent droughts, therefore, this study focused on the particular drought response of Scots pine trees and interspecies drought responses were not examined.

Figure 14. Canopy structure of the Hartheim forest on 7 February 2008 after Mayer et al. (2008). Forest canopy shows the homogeneously greenish crown of pine trees.

Figure 15. Canopy structure of the Hartheim forest on 2 May 2019. Forest canopy shows the partially brownish crown of pine trees, damaged by recent drought events (Photo by the author).

3.2 Soil, Plant, Water, and isotope Model (SPWisoM)

This study employed the Soil, Plant, Water, and isotope Model (SPWisoM). SPWisoM is a physically-based 1-dimensional hydrological model newly established by Mr. Stefan Seeger, a research assistant of the Chair of Hydrology, the University of Freiburg in 2019. SPWisoM was originally developed for simulating stable isotope transport, however, SPWisoM also obtained a noteworthy potential advantage for my research. That is, SPisoM is able to simulate the spatiotemporal distribution of soil moisture and PWU directly through modeling a stand-level soil water balance. Since SPWisoM has not been applied for any published research yet, it was novel to calibrate, validate, evaluate, and utilize SPWisoM in this study. Full script of the SPWisoM used in this study is available in
Appendix 3 and Appendix 4. In this study, Python 3.7.3 was used for running SPWisoM.

Firstly, input parameters were collected from the literature review, unpublished long-term monitoring data, and the field observation (Figure 3). Secondly, SPWisoM was executed over a short validation period (July 2003 - November 2004; see section 3.2.2) and the resultant soil moisture was compared to measured soil moisture (θ_{meas}) of the corresponding period for calibrating and validating the model. Furthermore, modeled PWU was validated based on actual evapotranspiration data (ET_{act}) of the Hartheim forest. Thirdly, validated and calibrated SPWisoM was applied for the entire study period (1978-2018) for simulating long-term soil moisture and PWU dynamics of the study site under the changing climate. Finally, obtained long-term soil moisture and PWU were analyzed against long-term forest productivity data, for discussing the effect of the intensified drought and associated hydrological modifications on the productivity of the Hartheim pine forest.

3.2.1 Input parameters

In this study, three different types of parameters were used to operate, validate, and calibrate the SPWisoM: meteorological, pedological, and biological parameters. Meteorological parameters were obtained from the unpublished long-term meteorological observation data of the Hartheim Forest Research Site. Missing meteorological parameters were interpolated based on the external meteorological data recorded by neighboring weather stations of the German Meteorological Service (see section 3.2.1.1.5). Pedological (soil) parameters were collected mainly by reviewing previous studies conducted at the Hartheim forest. Some of the pedological parameters were also measured based on the field observation by the author at the soil profile A and B (Figure 26 and Figure 27). In addition, long-term forest measurement data at the study site as well as field observation were employed for acquiring biological parameters. Each parameter is described in detail in the following sections.

3.2.1.1 Meteorological parameters

Meteorological parameters were prepared on a daily basis over the period of 1978 - 2018, mainly based on the long-term meteorological data recorded at the Hartheim forest. Missing parameters were interpolated by empirical relationships among two neighboring public weather stations (see section 3.2.1.1.5).

3.2.1.1.1 Precipitation

Since the water inflow of the study site is sorely dependent on precipitation (Mayer et al., 2008), precipitation should play a critically important role in determining the soil moisture and PWU of the study site. Total precipitation has been measured above the canopy layer by continuously raising the height of measurement tower from 7m (Jaeger & Kessler, 1997), and it is currently being measured at the top of the 30m tower (Mayer et al., 2008). During the validation period (1 July 2003 to 16 November 2004; 504 days), the total precipitation amounted to 979 mm. Daily precipitation ranged from 0 mm/day to 48.3 mm/day, with the mean value of 1.89 mm/day (SD: 4.96 mm/day). From 1978 to 2018 (entire modeling period), daily precipitation varied from 0 mm/day to 75.2 mm/day. The total precipitation and average daily precipitations were 26,817 mm and 1.79 mm/day (SD: 4.54 mm/day), respectively.

3.2.1.1.2 Potential Evapotranspiration (PET)

Potential Evapotranspiration (PET) is defined as "the total amount of water transpired in a given time by a short green crop, completely shading the ground, of uniform height and with adequate water status in the soil profile" (Irmak & Haman, 2003). PET is of importance when understanding hydrological budgets and associated drought as it indicates the demand for water from the atmosphere (Rind et al., 1990). While several formulae have been proposed to compute the PET (e.g., Lu et al., 2005), in this study PET was calculated by using FAO ETo Calculator (Appendix 5) (Hargreaves & Samani, 1985). The advantage of using this software is to enable interpolation of missing meteorological parameters automatically by built-in empirical relationships; this makes FAO ETo Calculator suitable for this research as format and continuity of the meteorological parameters vary depending on time-series. ETo Calculator requires four types of input parameters (i.e., air temperature, air humidity, wind speed, and sunshine and radiation) in addition to the geographical setting of the study site (i.e., coordinate and elevation of the study site); air temperature data can be either mean temperature or minimum and maximum temperature; air humidity data can be either mean relative humidity, minimum and maximum relative humidity, mean dew point temperature, or mean actual vapor pressure; sunshine and radiation data can be either hours of bright sunshine, relative sunshine hours, global radiation, or net radiation. Units of each input parameters also can be flexible and definable in FAO ETo Calculator. If at least one data from each input parameter is available, one can calculate PET by using FAO ETo calculator which works based on the following FAO Penman-Monteith equation:

$$PET = \frac{0.408\Delta(R_n - G) + \frac{900}{T + 273}u_2(e_s - e_a)}{\Delta + \gamma(1 + 0.34u_2)} \quad (1)$$

where

PET potential evapotranspiration [mm day^{-1}],
R_n net radiation at the crop surface [MJ m^{-2} day^{-1}],
G soil heat flux density [MJ m^{-2} day^{-1}],
T mean daily air temperature at 2 m height [°C],
u_2 wind speed at 2 m height [m s^{-1}],

e_s saturation vapour pressure [kPa],
e_a actual vapour pressure [kPa],
$e_s - e_a$ saturation vapour pressure deficit [kPa],
Δ slope vapour pressure curve [kPa °C^{-1}],
γ psychrometric constant [kPa °C^{-1}].

This study selected four meteorological parameters as input data of the ETo Calculator in reference to the accessibility and continuity of the data: daily mean temperature (°C; section 3.2.1.1.4), daily mean relative humidity (%; section 3.2.1.1.3), daily mean wind speed (m/sec), and global radiation (W/m^2). This study used horizontal wind speed (m/sec) which has been measured at 2.1 m of 30-m measuring tower (Mayer et al., 2008; Figure 25). Radiation flux has been also measured on the 30-m tower. As a result of the calculation, the total PET was 943 mm over the validation period (1 July 2003 to 16 November 2004). Daily PET ranged from 0 mm/day to 5.20 mm/day with the mean value of 1.82 mm/day (SD: 1.51 mm/day). From 1978 to 2018, daily PET ranged from 0 mm/day to 6.00 mm/day with the average of 1.65 mm/day (SD: 1.47 mm/day). Total PET between 1978 and 2018 was 24,746 mm.

3.2.1.1.3 Relative humidity

Relative humidity (RH) literally indicates the humidity and aridity of the atmosphere, determining the capacity of water which can be either transpired or evaporated. RH, therefore, has been incorporated by previous drought studies as one of the important drought indicators (e.g., Rebetez et al., 2006). In this study, I calculated RH based on Huang's (2013) formula:

$$\mathrm{RH} = \frac{6.112 * e^{\frac{17.502 * T_w}{240.97 + T_w}} - 0.00066 * (1 + 0.00115 * T_w) * P * (T_d - T_w)}{6.112 * e^{\frac{17.502 * T_d}{240.97 + T_d}}} \quad (2)$$

where

RH relative humidity [%],
T_w wet-bulb temperature [°C],
T_d dry-bulb temperature [°C],
P mean atmospheric pressure.

During the validation period (1 July 2003 to 16 November 2004), daily mean relative humidity ranged from 48.13 % to 100 %, with the mean value of 81.29 % (SD: 12.72 %). In addition, daily relative humidity varied from 40.8 % to 100 % from 1978 to 2018. The mean daily relative humidity between 1978 and 2018 was 81.1 % (SD: 10.7 %).

3.2.1.1.4 Temperature

Air temperature affects evaporation and water transport in the plant body. For instance, absorption and transport of water are regulated under lower temperature due to increased viscosity of water and lowered transmissivity of root layers (Jensen & Taylor, 1961). In the study site, the temperature (both dry temperature and wet-bulb temperature) has been

measured at eight different heights: 2.0 m; 6.1 m; 9.9 m; 12.1 m; 15.5 m; 19.1 m; 23.4 m; and 29.3 m (Mayer et al., 2008). PT100 platinum resistance thermometers have been used to survey the air temperature (Jaeger et al., 1986). During the validation period (1 July 2003 to 16 November 2004), the daily mean temperature ranged from -3.24 °C to 27.41 °C, with an average value of 12.37 °C (SD: 7.19 °C). Over the full modeling period (1978-2018), the daily mean temperature ranged from -14.08 °C to 28.89 °C. The average temperature from 1978 to 2018 was 11.05 °C (SD: 7.31 °C).

3.2.1.1.5 Interpolation of missing meteorological parameters

In the study site, some of the meteorological parameters were not originally available (Table 1) therefore, missing meteorological parameters were interpolated based on the meteorological data recorded by the German Meteorological Service (*Deutscher Wetterdienst*: DWD). The closest DWD's weather station, Freiburg (48.023276 °N, E7.834441 °E), was selected for the primal procedure. The Freiburg weather station is located approximately 20 km northeast from the study site. The elevation of the Freiburg weather station is 236.3 m. DWD-based meteorological parameters were compared to existing meteorological parameters of the Hartheim study site, conducting regression analysis between two different data sources. The resultant empirical relationships were then used for estimating missing meteorological parameters of the study site. When both study site-based meteorological data and Freiburg DWD station-based meteorological data were unavailable, the second closest DWD station, Feldberg/Schwarzwald (8.003817 °N, 47.874893 °E; 1489.6m a.s.l.) was used for the compensation. Feldberg/Schwarzwald DWD station is located approximately 30 km southeast of the study site.

Table 1. The number of days without values over the period of 1978-2018 (14,975 days).

Parameters	Unit	Days without data
Precipitation	mm/day	327
Mean temperature	°C	15
Relative humidity	%	9185
PET	mm/day	9642

3.2.1.2 Pedological parameters

Pedological (soil) parameters were collected mainly from the literature review. Soil profile and root distribution were also observed by the author on 2 May 2019 at the soil profile A (Figure 26). A photograph of the soil profile B (Figure 27) was also used for interpreting the vertical structure of the soil layers. Although the spatial location (Figure 25) of soil profiles excavated and used by previous studies were not constant, the variabilities of each soil profile at the study site was assumed to be almost identical.

3.2.1.2.1 Soil profile

Soil profile information refers to both the vertical and horizontal structure of different soil layers, determining sub-surface hydrological properties of the study site. As described in section 3.1, the soil profile of the study site is homogenous and, therefore, the soil profile of the study site was assumed to be constant in this study. Three different layers were examined

in this research: Ah horizon (0-20 cm), Ah/C horizon (20-40 cm), and C horizon (>40 cm) (see section 3.1).

3.2.1.2.2 Soil texture and structure

Soil texture, the amount content of different sized-particles, affects the mobility of soil water including water-holding capacity and hydraulic conductivity. Soil texture, on the other hand, represents how those particles are spatially arranged, also influencing soil water movement and plant root penetration. SPWisoM requires to define clay volume (m^3/m^3), gravel (skeleton) volume (m^3/m^3) and bulk density (kg/m^3). The volumetric content of clay and gravel, as well as bulk density at different depths, were acquired from Jung (2005) (Figure 16 and Table 2).

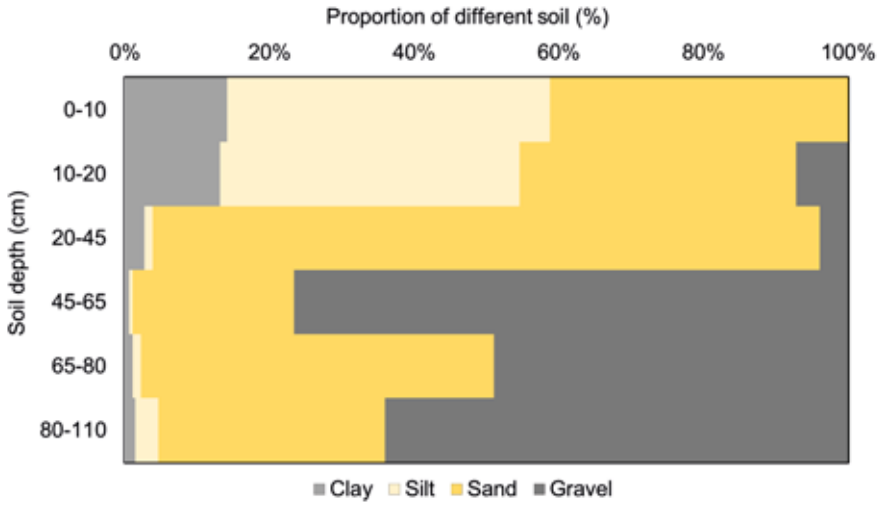

Figure 16. Vertical distribution of different soil particles from Jung (2005).

3.2.1.2.3 Soil temperature

The initial state of the soil temperature at each depth (0-20 cm; 20-40 cm; and 40-60 cm) needs to be pre-defined for processing SPWisoM. Soil temperature affects the efficiency of PWU; the lowered temperature of the roots zone generally results in declined PWU due to increased viscosity of water at the roots zone (Kuiper, 1964). This study used averaged soil temperature values from unpublished monitoring data.

3.2.1.2.4 Hydraulic soil properties

In addition to physical soil properties explained in section 3.2.1.2.2, hydraulic soil properties also play an important role in determining soil moisture and PWU dynamics. Saturated hydraulic conductivity (K_{sat}) and soil water retention curve (SWRC) are the main hydraulic soil properties of the soil (Wösten & van Genuchten, 2010). Saturated hydraulic conductivity (K_{sat}) indicates how easy water can be transported through the saturated soil. K_{sat} is normally estimated based on laboratory or field measurement (Jabro, 2013). Additionally, SWRC is the empirical relationship between soil moisture (θ) and soil water potential (ψ). van Genuchten (1980) presented θ as a function of ψ (Figure 17):

$$\theta = \theta_r + \frac{(\theta_s - \theta_r)}{[1 + (\alpha\psi)^n]^m} \quad (3)$$

$$m = 1 - \frac{1}{n} \quad (4)$$

where

θ soil water content [m^3/m^3],
θ_s saturated water content [m^3/m^3],
θ_r residual water content [m^3/m^3],
α scale parameter inversely proportional to mean pore diameter [m^{-1}],
ψ soil water potential [MPa], and
n and m shape parameters of soil water characteristics (Yang & You, 2013).

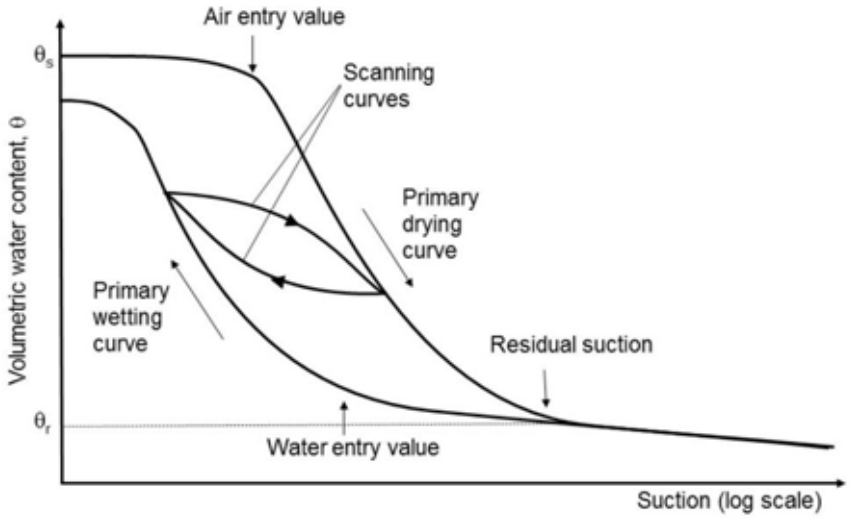

Figure 17. Schematic diagram of typical soil water retention curve (SWRC) from Toll et al. (2015).

This study applied saturated hydraulic conductivity (K_{sat}) and SWRC parameters by Jung (2005), in which K_{sat} and SWRC parameters of the study site (soil profile J in Figure 28) were experimentally estimated by means of the pedotransfer functions (Table 6-3 in Jung, 2005). Those soil hydraulic parameters applied to my study are summarized in Table 2.

Table 2. Summary of pedological parameters at three different soil layers (Ah, Ah/C, and C).

Variables	units	Horizon			Sources
		Ah	Ah/C	C	
Depth	cm	0-20	20-40	40-60	Wedler et al. (1996); Sturn et al. (1996); Wellpot et al.(2005)
Bulk density	kg/m^3	1150	1740	1900	Jung, 2005
Θ_r	m^3/m^3	0.06	0.05	0.05	Jung, 2005
Θ_s	m^3/m^3	0.44	0.32	0.37	Jung, 2005
alpha	cm^{-1}	0.0065	0.0315	0.0328	Jung, 2005
n		1.61	3.23	3.44	Jung, 2005
K_{sat}	cm/d	65.2	478.7	778.0	Jung, 2005
Clay	Vol%	13.6	2.7	0.6	Jung, 2005
Silt	Vol%	43.0	1.2	0.5	Jung, 2005
Sand	Vol%	39.7	92.1	22.2	Jung, 2005
Gravel	Vol%	3.6	4.0	77.0	Jung, 2005
Organic carbon	mg/g	134	32	3	Goffin et al. (2014)

3.2.1.2.5 Soil Organic Matter (SOM)

Soil organic matter (SOM) from plant residues decompositions modifies soil structure, altering hydrological properties of the soil. SPWisoM demands the volumetric amount of SOM (m^3/m^3) as one of the input parameters. Goffin et al. (2014) studied the vertical distribution of SOM (m^3/m^3) at two different soil pits of the Hartheim forest (Figure 18). Therefore, my study used the averaged values of the two soil pits from Goffin et al. (2014).

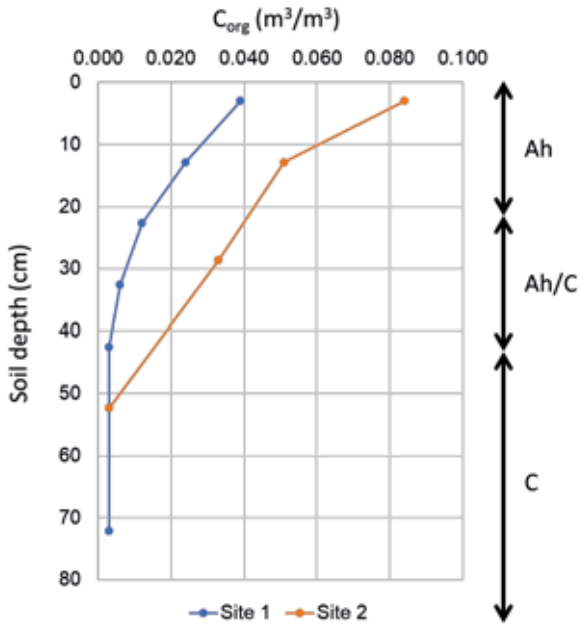

Figure 18. Vertical distribution of soil organic matter (SOM: m^3/m^3) at two soil profiles of the Hartheim, measured by Goffin et al., 2014.

3.2.1.3 Biological parameters

3.2.1.3.1 Feddes parameters

To compensate difficulties associated with the field-based PWU measurement, Feddes parameters were introduced by Feddes et al. (1976). Feddes parameters simply express the empirical relationship between the root zone water potential and the sufficiency of PWU, influenced by potential transpiration rate (Figure 19). Because species-specific Feddes parameters for Scots pine (*Pinus sylvestris*) were not available, I referred to Feddes parameters of general coniferous tree species from Lv (2014) (Table 3).

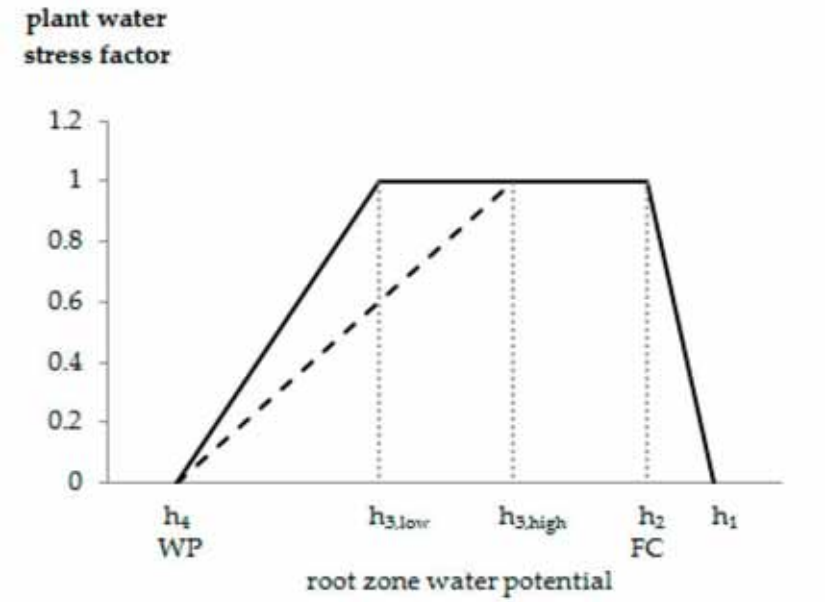

Figure 19. Schematic diagram of the Feddes plant water stress function from Rabbel et al. (2018). PWU occurs when root zone water potential = h < h_1 (anoxic condition); PWU continues to increase when h is between h_2 (field capacity, FC) and h_1; Optimal PWU occurs when h_3 (beginning of drought stress) < h < h_2. The timing of h_3 is determined by the potential transpiration rate (T_P), i.e., the higher T_P is (T_{Phigh}), the faster the drought stress may commence (h_{3high}), and vice versa; PWU declines from h_3 to h_4 due to increasing drought stress; PWU finally ceases when h drops below h_4 (permanent wilting point, WP).

Table 3. Summary of the measured Feddes parameters for different vegetation types from Lv (2014). My study employed Feddes parameters for coniferous vegetation because species-specific values for Scots pine (Pinus sylvestris) were not available.

Vegetation	h1 [cm]	h2 [cm]	h3h [cm]	h3l [cm]	h4 [cm]	T_{Plow} [cm/d]	T_{Phigh} [cm/d]
Aspen	0	0	-330	-2000	-15000	0.5	0.1
Conifer	0	0	-5100	-12800	-21500	0.5	0.1
Grass/forbs	0	0	-300	-1000	-15000	0.5	0.1
sagebrush	0	0	-400	-5100	-33000	0.95	0.1

3.2.1.3.2 Leaf Area Index (LAI) and Woody Area Index (WAI)

Leaf Area Index (LAI: m^2/m^2) represents the summed one-sided leaf area of photosynthetic tissue per given ground surface area (Watson, 1947; Bréda, 2003; Weiss et al., 2004). LAI plays an important role in forest hydrology; LAI influences the amount of canopy interception and transpiration, altering plant water uptake and subsequent dynamics (Bréda & Granier, 1996). LAI values at the study site varied dynamically from time to time and from data source

to data source, presumably owing to the inconsistency of measurement methodologies (i.e., destructive or non-destructive; Jaeger & Kessler, 1996) and/or historical thinning operations (Mayer et al., 2012). For instance, biomass harvest-based LAI value increased from 3.71 m^2/m^2 (April 1988) to 3.78 m^2/m^2 (April 1989) (Jaeger & Kessler, 1996). LAI ranged from 2.6 to 2.8 based on non-destructive optical measurement in May 1992 (Jaeger & Kessler, 1996). Thinning in 1993 reduced LAI from 3.28 m^2/m^2 to 2.07 m^2/m^2 based on destructive measurement (Mayer et al., 2012).

In addition to LAI, woody area index (WAI: m^2/m^2) refers to the total area of woody plant tissues per unit of ground surface area. Large WAI, particularly large sapwood area generally leads to a larger amount of sap flow and consequently greater transpiration (Granier, 1987). WAI can be measured either by a destructive way (e.g., Köstner et al., 2002) or non-destructive way (e.g., Bieker & Rust, 2010). At the Hartheim forest, pre- and post-thinning WAI were measured by a destructive method (Mayer et al., 2012); WAI was decreased from 0.65 m^2/m^2 in 1992 to 0.40 m^2/m^2 in 1994 due to thinning operation in 1993.

In the study site, unfortunately, LAI and WAI values have incompletely been reported; one study measured and reported both LAI and WAI based on a destructive method (Mayer et al., 2012), while other studies exhibited only LAI mostly by optical methods (Jaeger & Kessler, 1996). Additionally, some other studies at the Hartheim forest used constant LAI = 2.8 (e.g., Wedler et al., 1996). Therefore, in order to interpolate missing LAI and WAI during the study period, the ratio of woody area to total area was assumed to be constant over the study period as 0.65/(3.28+0.65) = 0.17 (Walter et al., 2003; Mayer et al., 2012). This value was used to estimate LAI and WAI in case they were absent. LAI and WAI values between measurement dates were linearly interpolated automatically by SPWisoM. Figure 20 summarizes interpolated LAI and WAI of the study site from different resources.

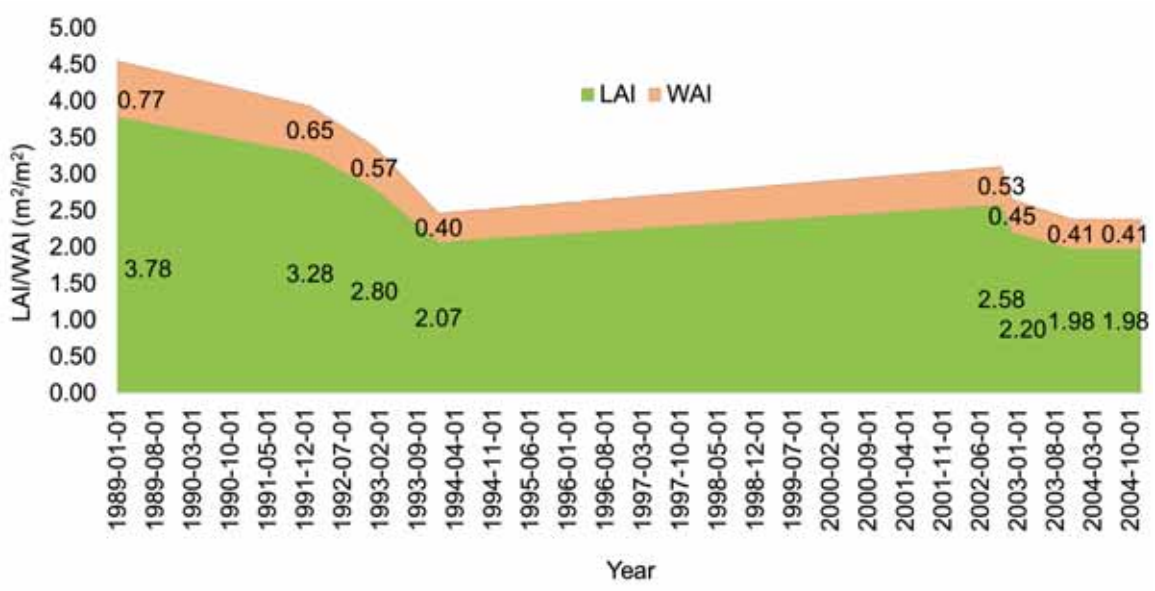

Figure 20. Development of leaf area index (LAI: m^2/m^2) and woody area index (WAI: m^2/m^2) of the Hartheim forest. LAI and WAI between measurements were linearly interpolated with SPWisoM (source: Welder et al., 1996; Jaeger & Kessler, 1996; Mayer et al., 2012; unpublished monitoring data).

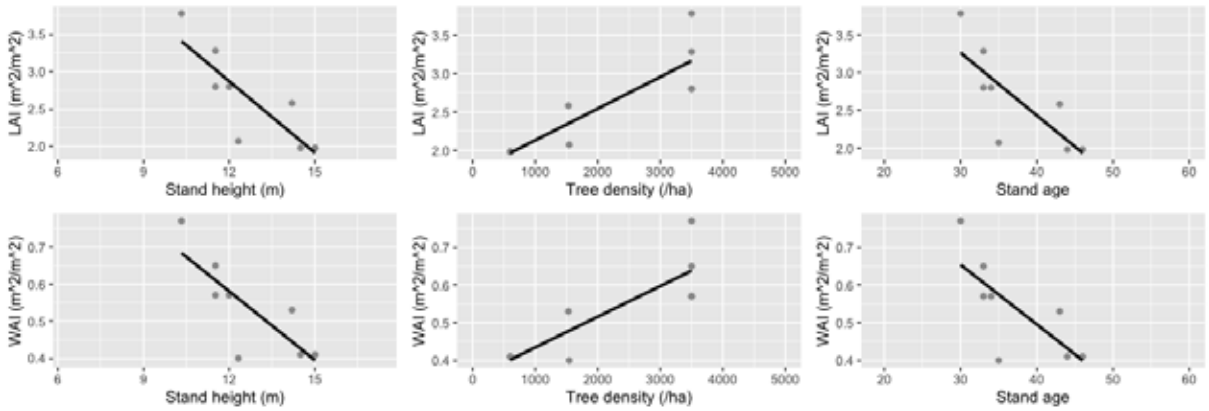

Figure 21. Regression analyses between stand characteristics (stand height, tree density, and stand age) and biological parameters (LAI and WAI).

In addition, SPWisoM requires to define LAI and WAI for the first and last date of the modeling period, i.e., 1 January 1978 and 31 December 2018. Therefore, regression analyses among stand characteristics (stand height, tree density, and stand age), LAI, and WAI were conducted in accordance with Jagodziński & Kałucka (2008) (Figure 21). As a result of the regression analyses, the following allometric equations were acquired (R^2 = 0.7321, p = 0.006734 for LAI: Equation 5; R^2 = 0.7018, p = 0.009421 for WAI; Equation 6) and applied for estimating initial and final LAI and WAI (i.e., 1 January 1978 and 31 December 2018).

$$LAI = 1.7159392 + 0.0004128 * Tree\ density \quad (5)$$

$$WAI = 0.3526 + 0.00008151 * Tree\ density \quad (6)$$

3.2.1.3.3 Stand height

Stand height is required in SPWisoM as one of the biological parameters. Stand height is one of the best well-measured biological parameters at the study site according to Jaeger & Kessler (1997). Stand height of the pine plantation has been measured from 1969 to 2019. The mean stand height has been determined by measuring heights of eight pilot trees twice a year (Jaeger and Kessler, 1997). Full description of the stand height at Hartheim forest can be found in section 3.1.

3.2.1.3.4 Roots distribution

In SPWisoM, vertical distribution of the roots is expressed as a percentage of roots at different depths, possibly measured either volumetrically or gravimetrically. Roots distribution influences the capacity and efficiency of plant water uptake, as well as upward redistribution of water from deeper soil layers (Jackson et al., 2000; Feddes et al., 2001) Based on the literature review and field observation, the maximum rooting depth of the study area is approximately 40 cm (Figure 12 and Figure 22). Quantitative root distribution data of Hartheim forest was derived from Maier et al. (2011).

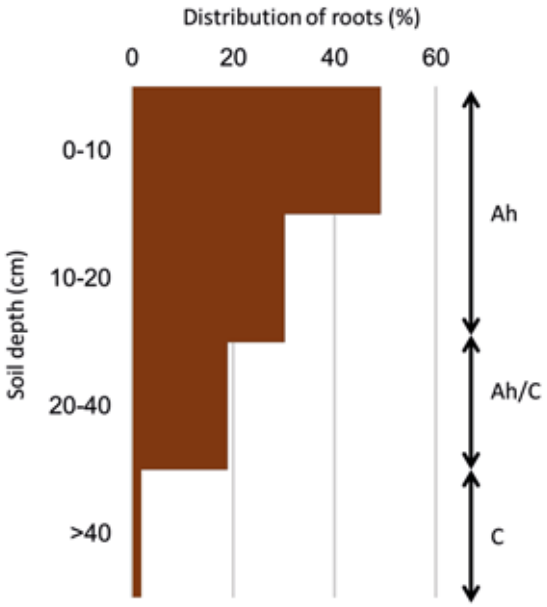

Figure 22. Vertical distribution of roots at Hartheim Forest Research Site based on organic carbon contents measured by Maier et al. (2011).

3.2.1.3.5 Tree ring widths

Tree ring width data was used for analyzing drought-induced forest growth reduction at Hartheim Scots pine forest. Tree ring data of Hartheim forest was provided by the Chair of Silviculture, University of Freiburg. Eighty Scots pine trees were randomly selected from even-aged plantation forest around the fenced area (Figure 7). The temporal coverage of tree ring data ranges from 1952 to 2016, depending on individual samples trees. Sampled Scots pine trees were classified into 4 groups depending on tree health conditions; Scots pine tree were categorized based on the proportion of damaged crown which was determined by visual estimation: health class1 (hc_1; 0-20%), class 2 (hc_2; 20-50%), class 3 (hc_3; 50-80%), and class 4 (hc_4; 80-100%). Raw tree ring width data of individual trees (Figure 23) was firstly de-trended with "detrend" function of R. This de-trending was executed in reference to long-term growth changes over 30-years, in order to remove the age-affected long-term growth trends. The average chronology of Scots pine trees was then computed by averaging the de-trended tree ring data (Figure 24). Standardized tree ring width was indicated as ring width index (RWI). From 1978 and 2016, the mean value of RWI was 0.994089 with the standard deviation of 0.14763.

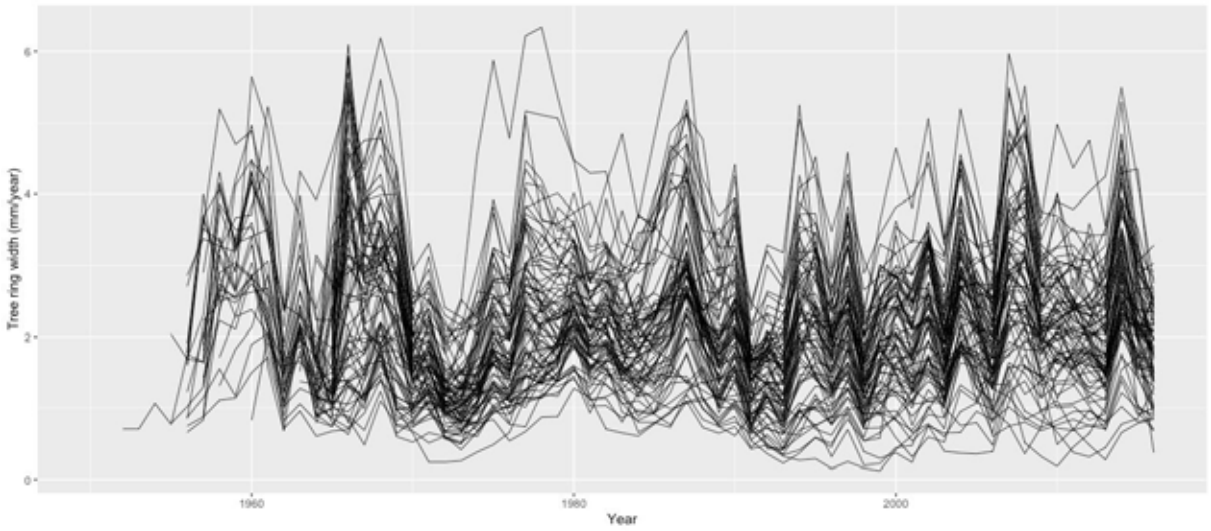

Figure 23. Pre-detrended and pre-averaged tree ring width data of Scots pine trees (n = 80).

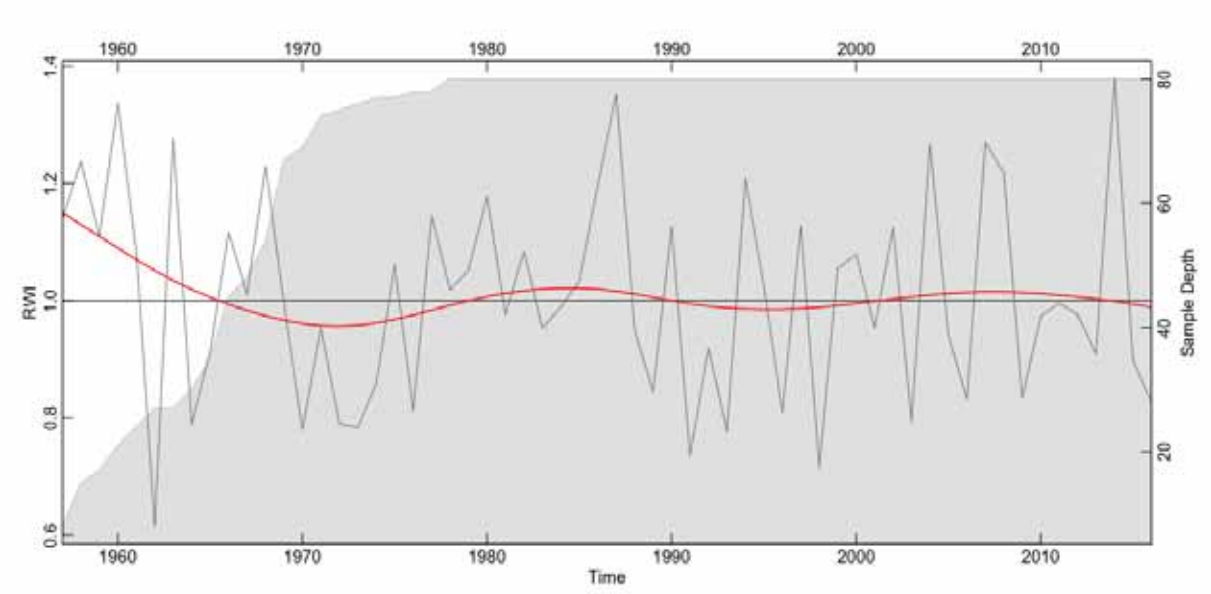

Figure 24. Average chronology of n = 80 Scots pine trees detrended over 30 years. Red line and shaded area indicate Spline and total number of sampled trees, respectively.

3.2.2 Model calibration and validation

SPWisoM was calibrated and validated before modeling the long-term soil moisture and PWU dynamics. For the calibration and validation, measured soil moisture data (θ_{meas}) and actual evapotranspiration data (ET_{act}) at the Hartheim forest were employed. Following sections describe the properties of the used datasets.

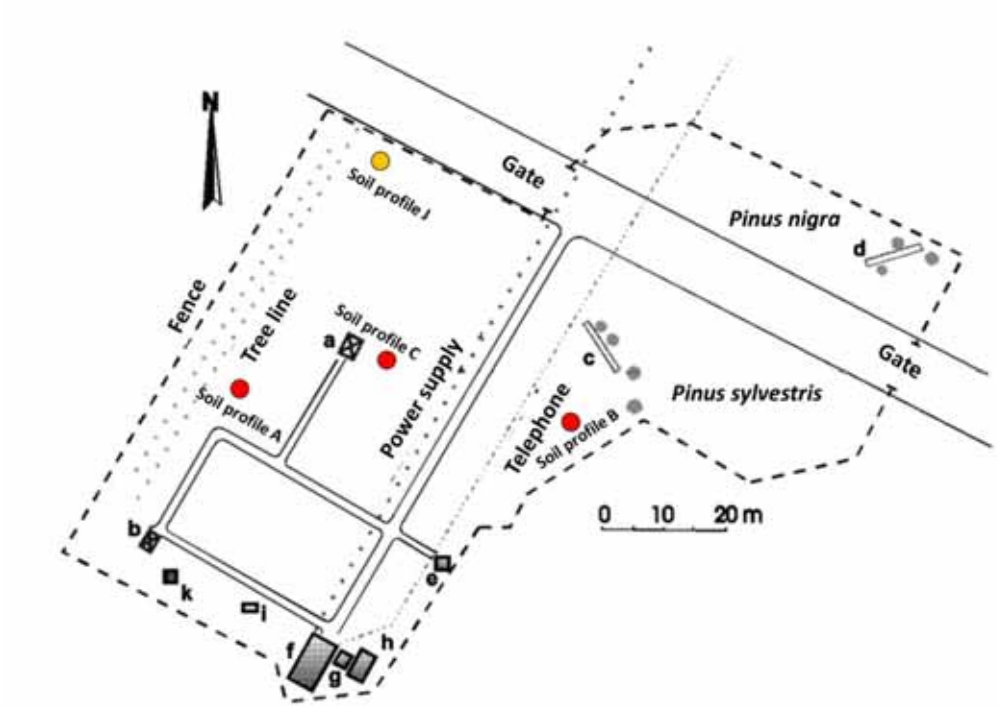

Figure 25. Schematic diagram of the Hartheim Forest Research Site, after Jaeger & Kessler (1996) and Mayer et al. (2012). Small letters represent measurement equipment: (a) 30m measuring tower; (b) 18m measuring tower; (c) crown interception and stem flow measurement for Scots pine (Pinus sylvestris); (d) crown interception and stem flow measurement for Black pine (Pinus nigra); (e) large weather hut; (f) wooden hut for recording; (g) battery power supply; (h) material storage; (i) soil moisture measurement; and (k) soil temperature measurement. Soil profile A (100cm), B (0-100cm), and C (0-10cm) were excavated for installing soil moisture sensors in 2019. Soil profile J is the location of soil pit used by Jung (2005), for the purpose of soil moisture measurement from 2003 to 2004.

Figure 26. Soil profile A: soil moisture sensors were newly installed at 5cm, 10cm, 20cm, 50cm, and 100cm on 2 May 2019 (Photo by the author).

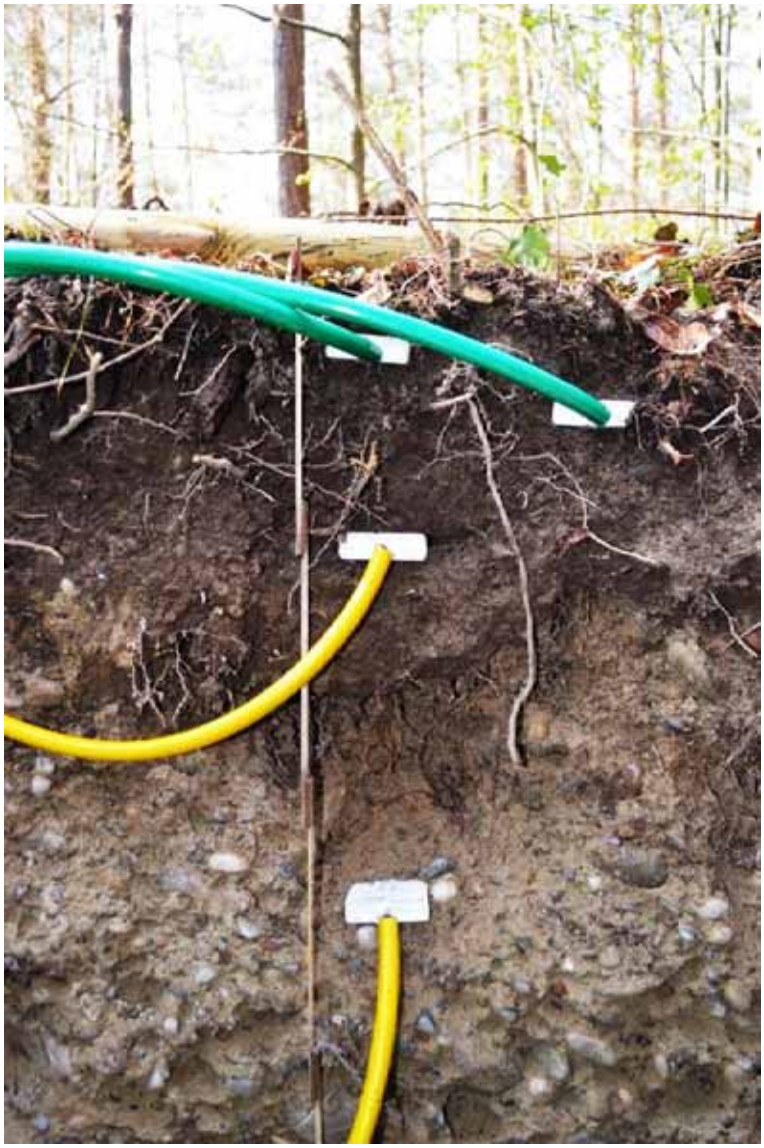

Figure 27. Soil profile B: Each segment of the scale represents 20 cm. The first segment from the ground surface (0-20 cm) shows densely rooted silty sand layer (A layer). The second segment from above (20-40 cm) exhibits less rooted transition layer from Ah to C (Ah/C layer). The third segment (40-60 cm) displays alluvial sand gravel layer (C layer) (Photo by Prof. Andreas Christen on 11 April 2019).

Figure 28. Soil profile J: 120-cm depth soil pit was used by Jung (2005) for measuring in-situ soil moisture at 5 cm, 15 cm, 35 cm, 65 cm, and 110 cm from 1 July 2003 to 17 November 2004 (Filming date: 1 July 2003).

3.2.2.1 Measured soil moisture data (θ_{meas})

3.2.2.1.1 θ_{meas} from Jung (2005)

SPWisoM was firstly validated and calibrated based on continuously measured soil moisture by Jung (2005). Soil moisture was measured at five different depths (5cm, 15cm, 35cm, 65cm, and 110cm) of soil pit J (Figure 25 and Figure 28). Jung (2005) employed ECH2O soil moisture sensors for this measurement between 1 July 2003 and 17 November 2004 with the temporal resolution of every 10 minutes.

3.2.2.1.2 θ_{meas} from Königer (2003)

Additionally, soil moisture measurement data by Königer (2003) was also used for validating the SPWisoM. At the Hartheim forest, Königer (2003) measured soil moisture destructively with soil core samples. Soil samples were collected from three different depths: 0-2 cm, 2-20cm, 20-40 cm. At the laboratory, soil moisture of each sample was determined gravimetrically. The temporal resolution of the soil core samples ranges from weekly to triweekly, covering from 29 April 1998 to 13 January 2000 (Sprenger et al., 2015). The exact location of the soil profile used for soil core sampling was not specified.

3.2.2.2 Actual evapotranspiration data (ET_{act})

Plant water uptake (PWU) was validated based on actual evapotranspiration (ET_{act}) measured at the Hartheim forest. ET_{act} was measured by eddy covariance and processed using "Smart Flux" with 30-minutes temporal resolution. ET_{act} covers from 15 February 2019 to 16 July 2019. Because some of 30-min ET_{act} data were missing, total daily ET_{act} was not available. Thus, daily mean 30-min ET_{act} was compared to modeled PWU. Furthermore, interpolated meteorological data in section 3.2.1.1.5 was used to compute PWU from 15 February 2019 to 16 July 2019.

3.2.2.3 Model scenarios

Two different spatial resolutions and two different modeling depths were developed for examining optimal setting of SPWisoM (Table 4): scenario 1 consists of coarser spatial resolution = 10 cm down to 40 cm; scenario 2 consists of coarser spatial resolution = 10 cm down to 60 cm; scenario 3 consists of finer spatial resolution = 2 cm down to 40 cm; and scenario 4 consists of finer spatial resolution = 2cm down to 60 cm, respectively.

Table 4. Four different scenarios prepared for the model validation.

Scenario	Spatial resolution [cm]	Modeling depth [cm]
1	10	40
2	10	60
3	2	40
4	2	60

3.2.2.4 Kling-Gupta efficiency (KGE)

Kling-Gupta efficiency (KGE; Gupta et al., 2009) was used to quantify the goodness of fitting between θ_{meas} and θ_{mod}. One hydrological model fits well to actual hydrological values when the KGE is close to 1, while it deviates from actual values when the KGE is smaller. The KGE was computed by using R as below:

$$KGE = 1 - \sqrt{(r-1)^2 + (\alpha-1)^2 + (\beta-1)^2} \quad (-\infty < KGE \leq 1) \qquad (7)$$

where

r Pearson coefficient value,
α the ratio between SD of simulated values and SD of observed ones,
β the ratio between mean of simulated values and mean of observed ones.

3.2.2.5 Model calibration

Based on the KGE values of different scenarios, one scenario was selected for the further calibration. During the calibration process, input skeleton value (m^3/m^3) of each layer was modified and subsequent KGE values were compared. Skeleton parameter was selected as a modifying factor since the skeleton component might be highly soil profile-dependent as well as soil sampling method-dependent. Once KGE values of 5cm, 15cm, and 35cm became

satisfactory, SPWisoM was assumed to have been calibrated in this study. Then, calibrated SPWisoM was applied for the entire period, i.e., 1 January 1978 – 31 December 2018.

4 Results

4.1 Interpolation of missing meteorological data

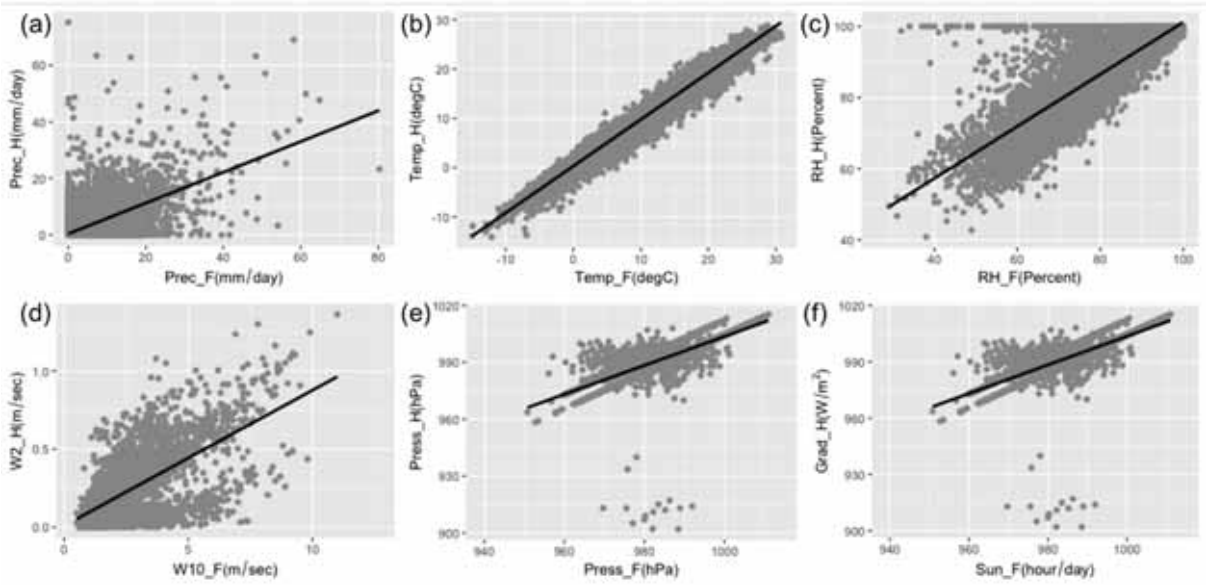

Figure 29. The scatter plots between meteorological data from Hartheim forest and German Meteorological Service weather station (Freiburg): (a) Daily precipitation of Freiburg ($Prec_F$: mm/day) and Hartheim ($Prec_H$: mm/day) (R^2 = 0.4027; p <0.001); (b) Mean daily temperature of Freiburg ($Temp_F$: °C) and Hartheim ($Temp_H$: °C) (R^2 = 0.9664; p < 0.001); (c) Daily mean relative humidity of Freiburg (RH_F: %) and Hartheim (RH_H: %) (R^2 = 0.5927; p < 0.001); (d) Daily mean wind speed of Freiburg ($W10_F$: m/sec at 10m a.g.l.) and Hartheim ($W2_H$: m/sec at 2m a.g.l.) (R^2 = 0.4036; p < 0.001); (e) Daily mean atmospheric pressure of Freiburg ($Press_H$: hPa) and Hartheim ($Press_H$: hPa) (R^2 = 0.5889; p < 0.001); (f) Relative sunshine hours of Freiburg (Sun_F: hours/day) and global radiation of Hartheim ($Grad_H$: W/m²) (R^2 = 0.6629; p < 0.001).

$$Prec_H = 0.421791 + 0.543657 * Prec_F \quad (8)$$

$$Temp_H = 0.291269 + 0.947974 * Temp_H \quad (9)$$

$$RH_H = 28.024940 + 0.731018 * RH_F \quad (10)$$

$$W2_H = 0.008082 + 0.086904 * W10_F \quad (11)$$

$$Press_H = 241.0 + 0.7627 * Press_F \quad (12)$$

$$Grad_H = 43.3382 + 18.9958 * Sun_F \quad (13)$$

Figure 29 and Equations 8 – 13 indicate the results of the regression analyses between meteorological data from the Hartheim forest and German Meteorological Service weather station (Freiburg). Following the first interpolation based on Freiburg weather station data, twenty-one meteorological data were still missed, i.e., five days for relative humidity, nine days for wind speed, and seven days for atmospheric pressure. Thus, the supplemental interpolation was implemented based on the meteorological data of Feldberg/Schwarzwald

(Figure 30; Equations 14 – 16). Likely due to the relatively more differentiated geographic setting from the Hartheim forest, DWD data from Feldberg/Schwarzwald station was less strongly correlated to Hartheim data. Those above mentioned twenty-one meteorological data were interpolated based on this correlation.

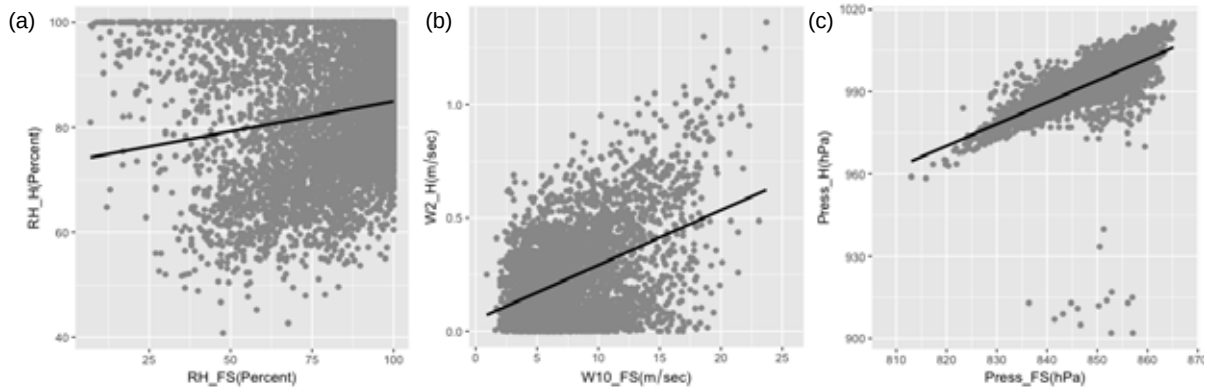

Figure 30. The scatter plots between meteorological data from Hartheim forest and German Meteorological Service weather station (Feldberg/Schwarzwald): (a) Daily mean relative humidity of Feldberg/Schwarzwald (RH_{FS}: %) and Hartheim (RH_H: %) (R^2 = 0.03296; $p < 0.001$); (b) Daily mean wind speed of Feldberg/Schwarzwald ($W10_{FS}$: m/sec at 10m a.g.l.) and Hartheim ($W2_H$: m/sec at 2m a.g.l.) (R^2 = 0.1963; $p < 0.001$); (c) Daily mean atmospheric pressure of Feldberg/Schwarzwald ($Press_{FS}$: hPa) and Hartheim ($Press_H$: hPa) (R^2 = 0.5054; $p < 0.001$).

$$RH_H = 73.49266 + 0.11466 * RH_{FS} \quad (14)$$

$$W2_H = 0.0500258 + 0.0241939 * W10_{FS} \quad (15)$$

$$Press_H = 320.1 + 0.7928 * Press_{FS} \quad (16)$$

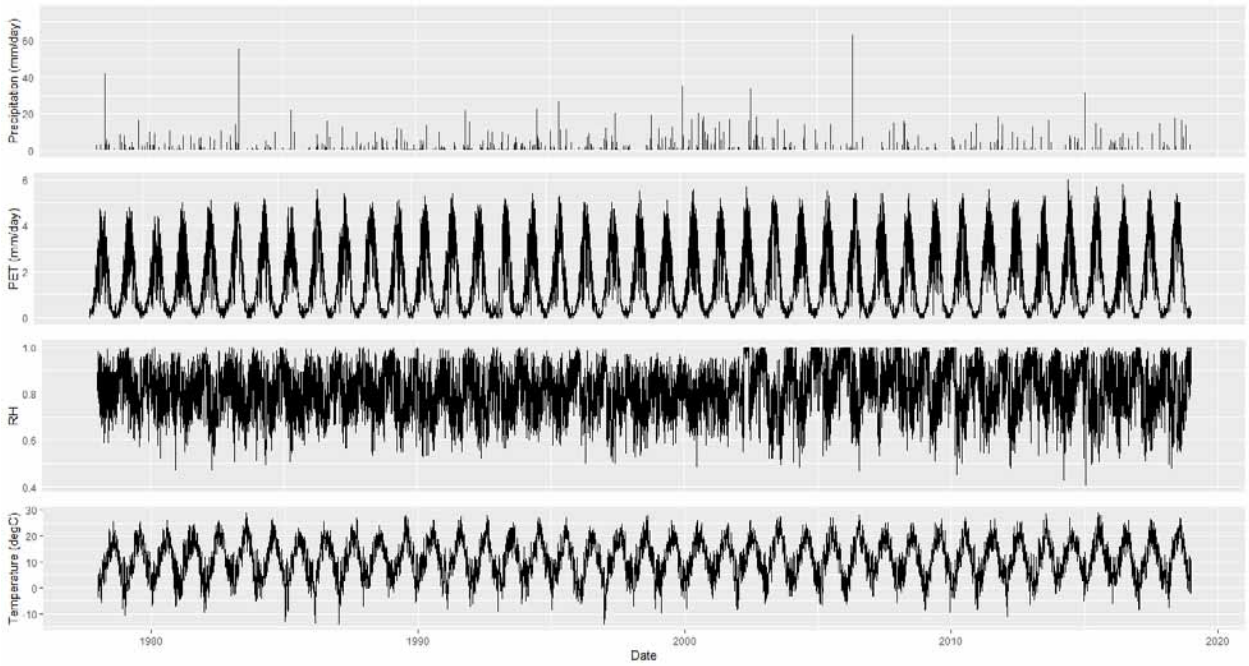

Figure 31. Time series plot of input meteorological parameters: precipitation (mm/day); potential evapotranspiration (PET, mm/day); relative humidity (RH); and Temperature (ºC).

4.2 Calibration and validation of SPWisoM

After running SPWisoM with four different scenarios, scenario 1, 2, 3 generated rational values (Figure 32a, Figure 32b, Figure 32c, Figure 33a, Figure 33b, and Figure 33c) while scenario 4 provoked an error (Figure 32d and Figure 33d). An error of scenario 4 was likely attributed to the original script of SPWisoM, however, I was not able to detect the particular reasons for the error. Then, instead, I decided to calibrate SPWisoM based on scenario 3 which showed the highest KGE at 15 and 35 cm (Table 5). Table 6 explains the input skeleton values (m^3/m^3) and resultant KGE values, whereas Table 7 shows the relative change in skeleton and KGE values for eleven different attempts. Finally, KGE at 5 cm, 15 cm, and 35 cm were improved to 0.211, 0.253, and 0.014, respectively. Figure 34 indicates the time-series plot of θ_{meas} and calibrated θ_{mod}.

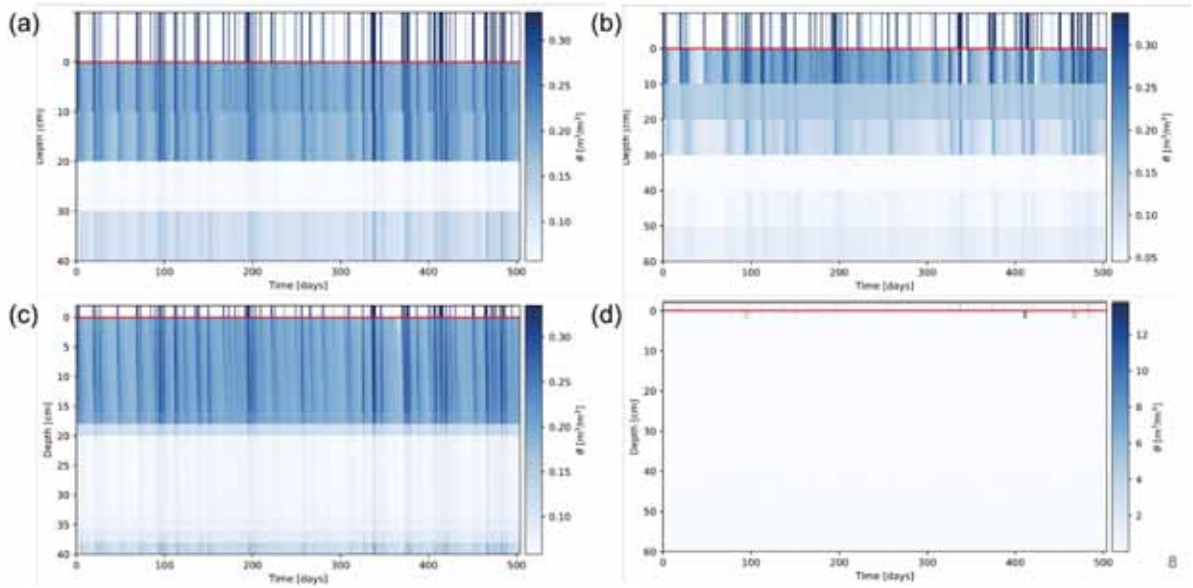

Figure 32. Results of SPWisoM-based soil moisture (θ_{mod}) from (a) scenario1 (10cm spatial resolution until 40cm); (b) scenario2 (10cm spatial resolution until 60cm); (c) scenario3 (2cm spatial resolution until 40cm), and (d) scenario4 (2cm spatial resolution until 60cm). Scenario4 generated error. Bars above red horizontal line indicate daily accumulated values.

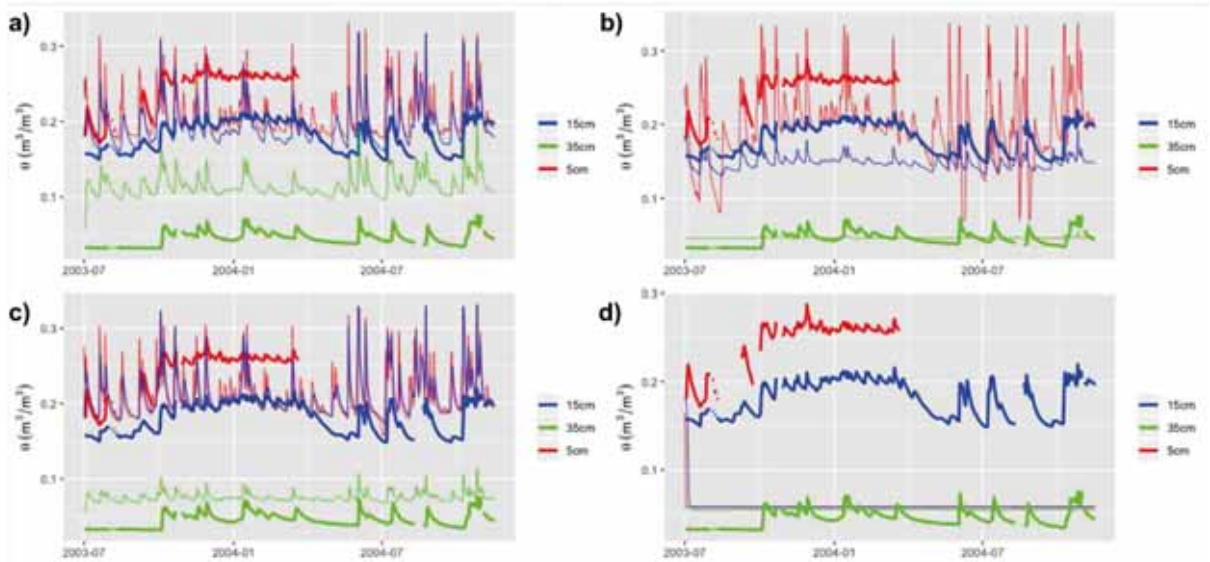

Figure 33. Time series plots of modeled soil moisture (thin line) and measured soil moisture data (thick line) for (a) scenario1 (10cm spatial resolution until 40cm); (b) scenario2 (10cm spatial resolution until 60cm); (c) scenario3 (2cm spatial resolution until 40cm), and (d) scenario4 (2cm spatial resolution until 60cm). Scenario4 generated error.

Table 5. Results of KGE values for three different depths, based on four different scenarios.

Scenario	Depth [cm]		
	5	15	35
1	0.097	0.250	-0.755
2	0.205	0.233	-0.162
3	0.181	0.263	-0.010
4	-0.705	-0.405	-0.398

Table 6. Modified input skeleton values of two layers (Ah and Ah/C) and resultant KGE values at three different depths. KGE values at 35cm turned to be positive when skeleton value (m^3/m^3) was increased to more than 0.060.

Values (m^3/m^3)	Ah	Ah/C	KGE_5cm	KGE_15cm	KGE_35cm
Reference	0.036	0.040	0.181	0.263	-0.010
cal1	0.000	0.000	0.185	0.234	-0.040
cal2	0.000	0.026	0.183	0.234	-0.040
cal3	0.000	0.060	0.185	0.236	0.000
cal4	0.024	0.000	0.179	0.252	-0.040
cal5	0.024	0.026	0.181	0.252	-0.021
cal6	0.024	0.060	0.181	0.254	-0.001
cal7	0.054	0.000	0.181	0.275	-0.035
cal8	0.054	0.026	0.177	0.275	-0.018
cal9	0.054	0.060	0.180	0.275	0.002
cal10	0.000	0.100	0.183	0.235	0.016
cal11	0.000	0.500	0.211	0.253	0.014

Table 7. Relative changes in input skeleton values and consequent KGE values expressed as percentage.

Change (%)	Ah	Ah/C	KGE_5cm	KGE_15cm	KGE_35cm
Reference	-	-	-	-	-
cal1	-100.000	-100.000	+2.088	-11.313	-280.466
cal2	-100.000	-35.000	+0.967	-11.313	-280.466
cal3	-100.000	+50.000	+2.184	-10.403	+103.854
cal4	-33.333	-100.000	-1.080	-4.140	-278.354
cal5	-33.333	-35.000	-0.171	-4.152	-102.143
cal6	-33.333	+50.000	+0.157	-3.694	+89.876
cal7	+50.000	-100.000	+0.207	+4.416	-237.271
cal8	+50.000	-35.000	-2.382	+4.409	-70.584
cal9	+50.000	+50.000	-0.707	+4.442	+116.632
cal10	-100.000	+150.000	+1.057	-10.924	+248.500
cal11	-100.000	+1150.000	+16.424	-4.006	+238.085

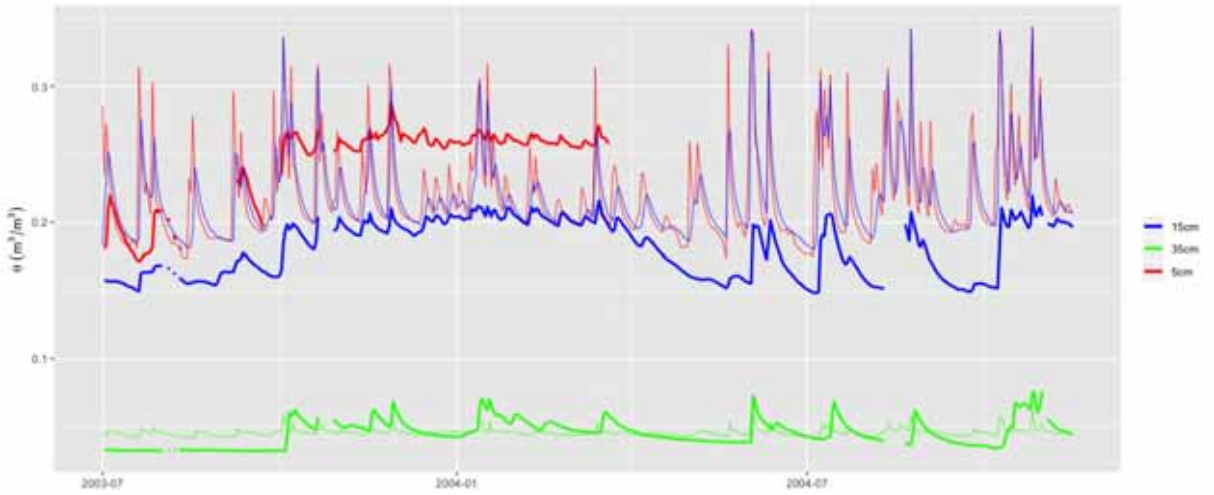

Figure 34. Time series plot of modeled soil moisture (θ_{mod}; thin lines) based on calibrated SPWisoM, compared to the measured soil moisture (θ_{meas}; thick lines) from Jung (2005).

Additional validation of SPWisoM was conducted based on discontinuously measured soil moisture data (θ_{meas}) and actual evapotranspiration data (ET_{act}). Calibrated SPWisoM was applied for the period of 29 April 1998 - 13 January 2000 when Königer (2003) measured soil moisture data at the Hartheim forest on a weekly to triweekly basis. When accumulated soil moisture between 0 and 30 cm was compared, a strong correlation between SPWisoM-based θ_{mod} and θ_{meas} were found (Figure 35). Besides, calibrated SPWisoM was implemented for 15 February 2019 - 16 July 2019 when ET_{act} is available, also observing a significant correlation between SPWisoM-based PWU and mean 30-min ET_{act} (Figure 36).

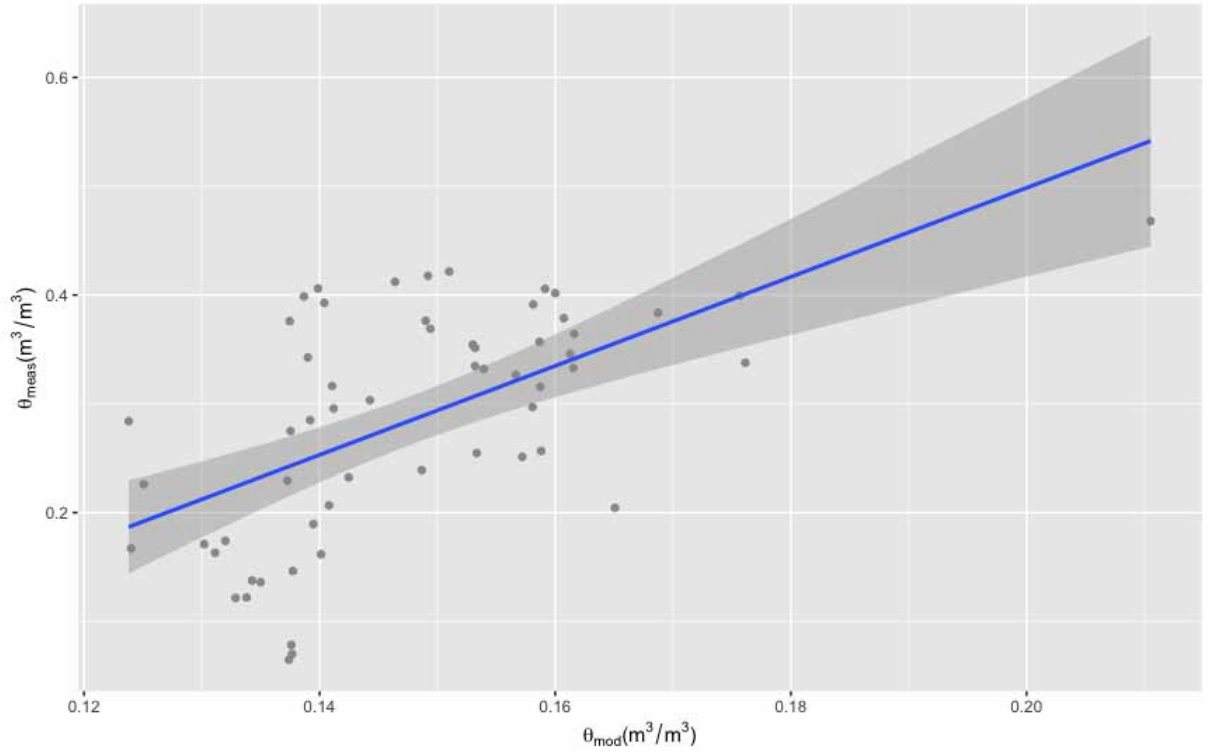

Figure 35. Scatter plot of mean θ_{mod} (0-30cm) and mean θ_{meas} (0-30cm) from Königer (2003) (R^2 = 0.3458; $p < 0.001$). Königer's (2003) soil moisture was measured discontinuously between 29 April 1998 and 13 January 2000 at Hartheim forest, with the total measured days = 58. The blue line and shaded area indicate a regression line and 95% confidence interval.

$$Mean\ \theta_{meas} = -0.3198 + 4.0916 * Mean\ \theta_{mod} \quad (17)$$

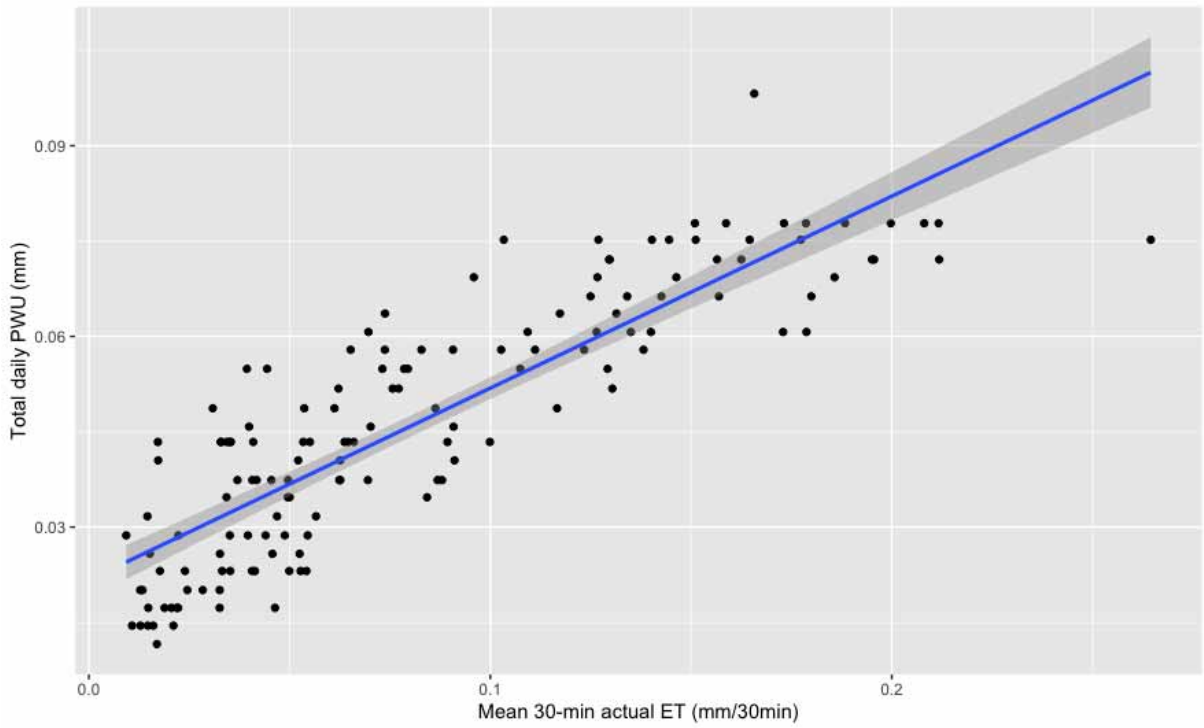

Figure 36. Scatter plot of mean 30-min actual evapotranspiration (ET_{act}: mm/30min) and modeled total daily PWU (mm/day) between 15 February 2019 and 16 July 2019 (197 days) (R^2 = 0.7494; p < 0.001). Actual evapotranspiration was measured by using eddy covariance and newly installed Smart Flux system. Total daily PWU was calculated based on SPWisoM. Input meteorological data between 15 February 2019 and 16 July 2019 was interpolated from the closest weather station of German Meteorological Service Freiburg) by using Equations 8 – 13. The blue line and shaded area indicate a regression line and 95% confidence interval.

$$Total\ daily\ PWU = 0.02168 + 0.30183 * Mean30\ \text{min}\ ET_{act} \quad (18)$$

4.3 Spatiotemporal distribution of soil moisture (θ_{mod})

As a result of the modeling of soil moisture (θ_{mod}) for the period of 1978 – 2018, total daily soil moisture (0-40 cm) ranged from 1.97 m^3/m^3/day (25 July 2006) to 3.96 m^3/m^3/day (24 April 1982), with the mean value of 2.56 m^3/m^3/day (SD: 0.28 m^3/m^3/day) (Figure 37). Mean daily soil moisture of 20 different layers with 2cm depth each varied from 0.10m^3/m^3/day (25 July 2006; SD: 0.06 m^3/m^3/day) to 0.20 m^3/m^3/day (24 July 1982; SD: 0.13 m^3/m^3/day). The minimum total soil moisture between 1978 and 2018 occurred at the layer between 22-24 cm (527.98 m^3/m^3), followed by 20-22 cm (528.10 m^3/m^3) and 24-26 cm (528.10 m^3/m^3). On the other hand, the maximum total soil moisture between 1978 and 2018 was observed at 8-10 cm (3347.08 m^3/m^3), followed by 10-12 cm (3344.88 m^3/m^3) and 6-8 cm (3341.00 m^3/m^3). The mean daily soil moisture was the smallest at 22-24 cm (0.04 m^3/m^3/day; SD: 0.004 m^3/m^3/day), while it was the largest at 8-10 cm (0.22 m^3/m^3/day; SD: 0.03 m^3/m^3/day). Overall, 81.7 % of total soil moisture existed at soil layer 0-20 cm, while 18.3 % of total soil moisture was at layer 20-40 cm over the modeling period.

When the total daily soil moisture was averaged based on the day of the year (DOY) (Figure 38), the maximum value marked 2.72 m^3/m^3/day (SD: 0.41 m^3/m^3/day) when DOY = 133, followed by DOY = 155 (2.70 m^3/m^3/day; SD: 0.40 m^3/m^3/day) and DOY = 151 (2.69 m^3/m^3/day; 0.45 m^3/m^3/day). In contrast, DOY-based total daily soil moisture was the

smallest when DOY = 72 (2.45 m^3/m^3/day; SD: 0.17 m^3/m^3/day), followed by DOY = 214 (2.45 m^3/m^3/day; 0.17 m^3/m^3/day) and DOY = 18Y (2.45 m^3/m^3/day; SD: 0.22 m^3/m^3/day).

On a monthly basis, total monthly soil moisture (0-40cm) ranged from 64.13 m^3/m^3/month in February 2014 to 93.18 m^3/m^3/month in May 1983, with the mean value of 77.89 m^3/m^3/month (SD: 4.76 m^3/m^3/month). The mean total soil moisture (0-40 cm) became the minimum in June 2010 (mean: 2.16 m^3/m^3month; SD: 0.03 m^3/m^3/month) and it became the maximum in May 1983 (mean: 3.01 m^3/m^3/month; SD: 0.39 m^3/m^3/month).

From yearly perspective, 2018 was found to be the most water limited year between 1978 and 2018, with the annual total soil moisture (0-40 cm) of 896.14 m^3/m^3/year. The other recent water limited years were 2010 (896.47 m^3/m^3/year), 2009 (900.80 m^3/m^3/year), 2003 (901.57 m^3/m^3/year), 2008 (917.35 m^3/m^3/year), and 2014 (918.97 m^3/m^3/year). Meanwhile, the annual total soil moisture marked the largest value in 2000 (966.544 m^3/m^3/year), followed by 1987 (961.29 m^3/m^3/year) and 2002 (960.07 m^3/m^3/year). The average of the annual total soil moisture from 1978 to 2018 resulted in 934.62 m^3/m^3/year (SD: 17.46 m^3/m^3/year).

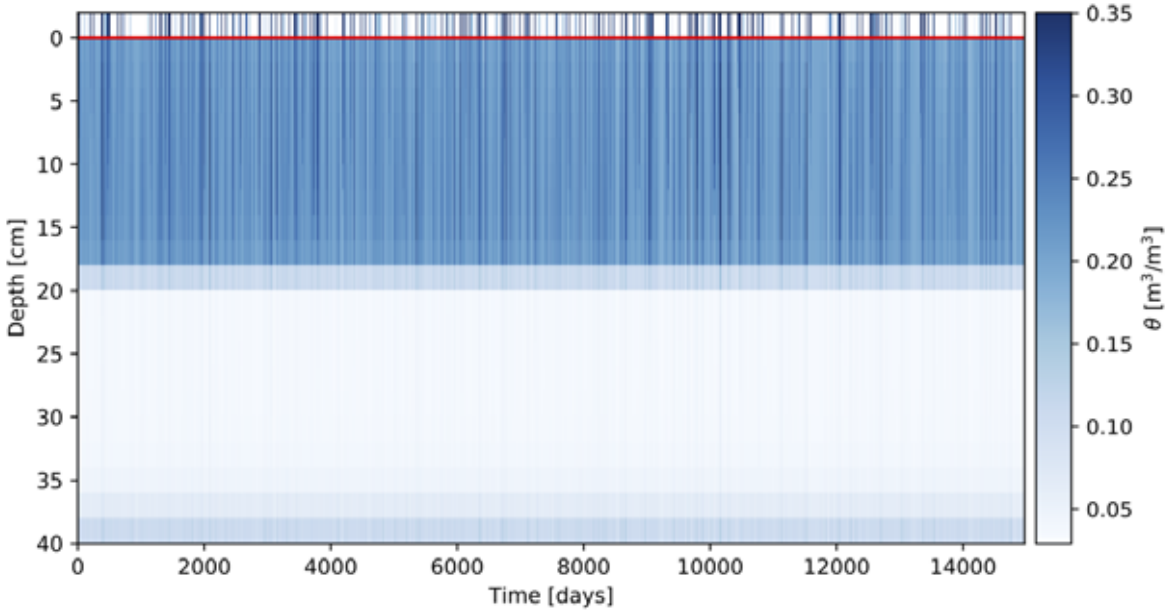

Figure 37. SPWisoM-based spatiotemporal distribution of soil moisture over the period from 1978 to 2018 (14,974 days). Bars above the horizontal red line indicates the accumulated daily soil moisture between 0 and 40 cm.

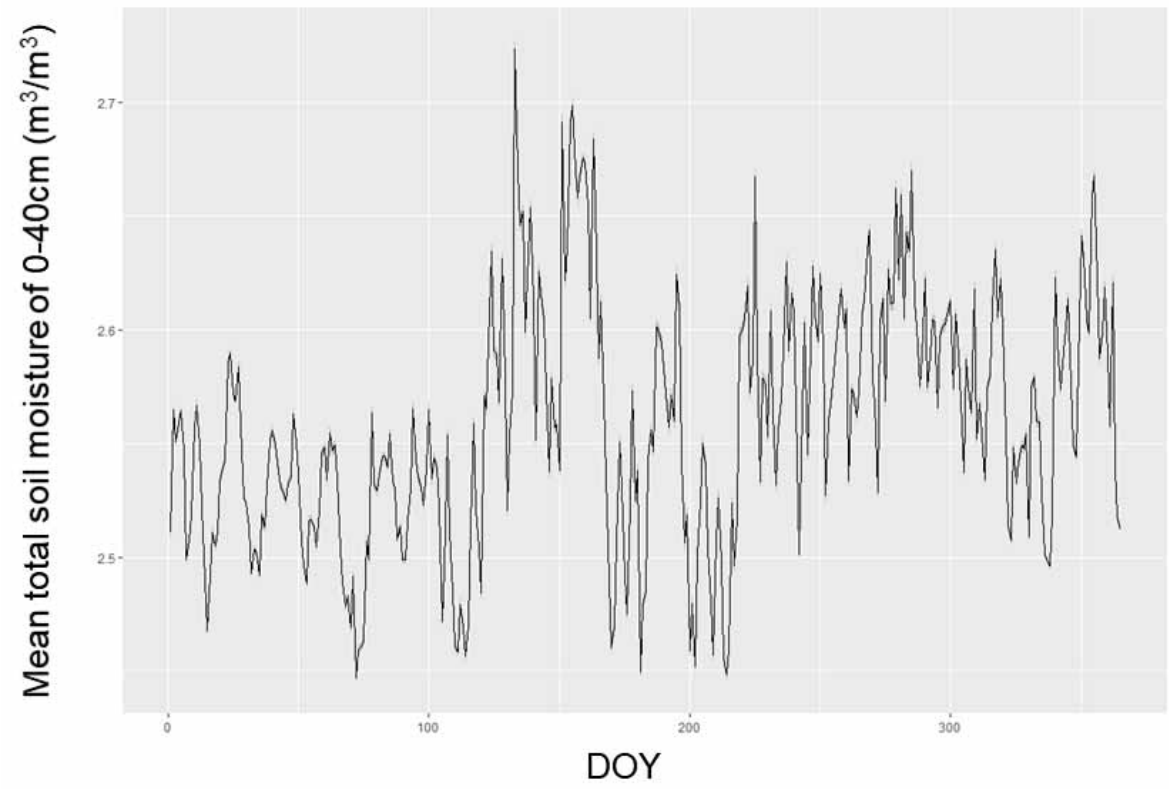

Figure 38. Mean total daily soil moisture (m^3/m^3/day) at 0-40 cm for the period of 1978-2018, based on the day of the year (DOY).

4.4 Spatial temporal distribution of plant water uptake (PWU)

Total daily PWU between 0 and 40 cm ranged from 0 cm/day to 0.0219 cm/day (22 June 1986) with the average value of 0.0054 cm/day (SD: 0.0049 cm/day) (Figure 39). As indicated in DOY-based total daily PWU (Figure 40), total daily PWU generally became smaller (ca. 0 cm/day) during winter and larger (ca. 0.02 cm/day) during summer. The mean daily PWU of each layer was the smallest at the vertical depth of 38-40 cm (ca. 0 cm/day; SD: ca. 0 cm/day), while it was the largest at the vertical depth of 0-2 cm (0.0004 cm/day; SD: 0.0004 cm/day). The PWU modeling showed the tendency that the shallower the soil layer is located, the larger the mean daily PWU becomes. Overall, 64.8 % of total PWU from 1978 and 2018 occurred at a soil depth of 0-20 cm, while 35.2 % happened at soil layer of 20-40 cm.

From monthly point of view, the total monthly PWU (0-40 cm) ranged from 0.0070 cm/month (December 2016) to 0.5570 cm/month (July 1983), with the average value of 0.1663 cm/month (SD: 0.1331 cm/month). Likewise, December 2016 indicated the minimum mean daily PWU of 0.0002 cm/day (SD: 0.0002 cm/day) and July 1983 showed the maximum mean daily PWU (mean: 0.0180 cm/day; SD: 0.0018 cm/day). As mentioned already, summer season including growing period of the Hartheim forest (April – September) normally contributed to higher PWU (Figure 40); from 1987 to 2018, 84.7 % of total PWU occurred during the summer period (April-September), while 15.3 % of total PWU resulted from the rest of the year.

Additionally, from 1978 to 2018, the annual total PWU ranged from 1.5897 cm/year in 2012 to 2.4810 cm/year in 2010, with the mean value of 1.9953 cm/year (SD: 0.2495 cm/year). Other examples of PWU-limited years were 1988 (1.5942 cm/year), 2017 (1.5942 cm/year), and 1978 (1.7232 cm/year). Also, examples of other PWU-abundant years were 2008 (2.4212 cm/year), 2004 (2.3661 cm/year), and 1999 (2.3621 cm/year).

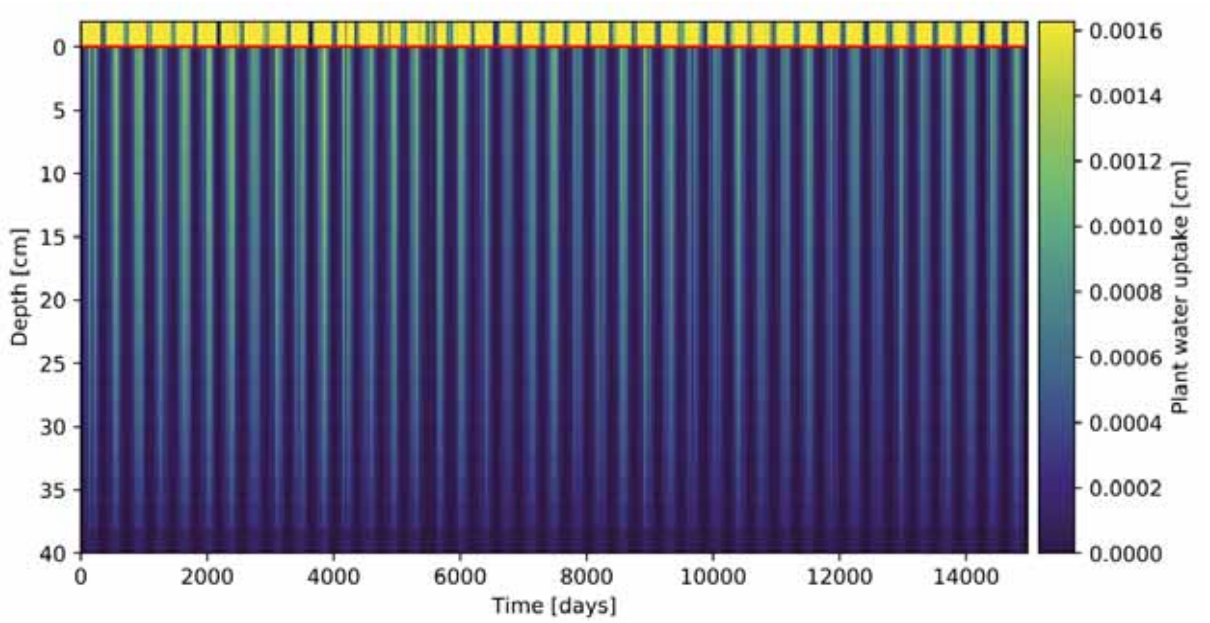

Figure 39. SPWisoM-based spatiotemporal distribution of plant water uptake (PWU) over the period from 1978 to 2018 (14,974 days). Bars above the horizontal red line indicates the accumulated daily soil moisture between 0 and 40 cm.

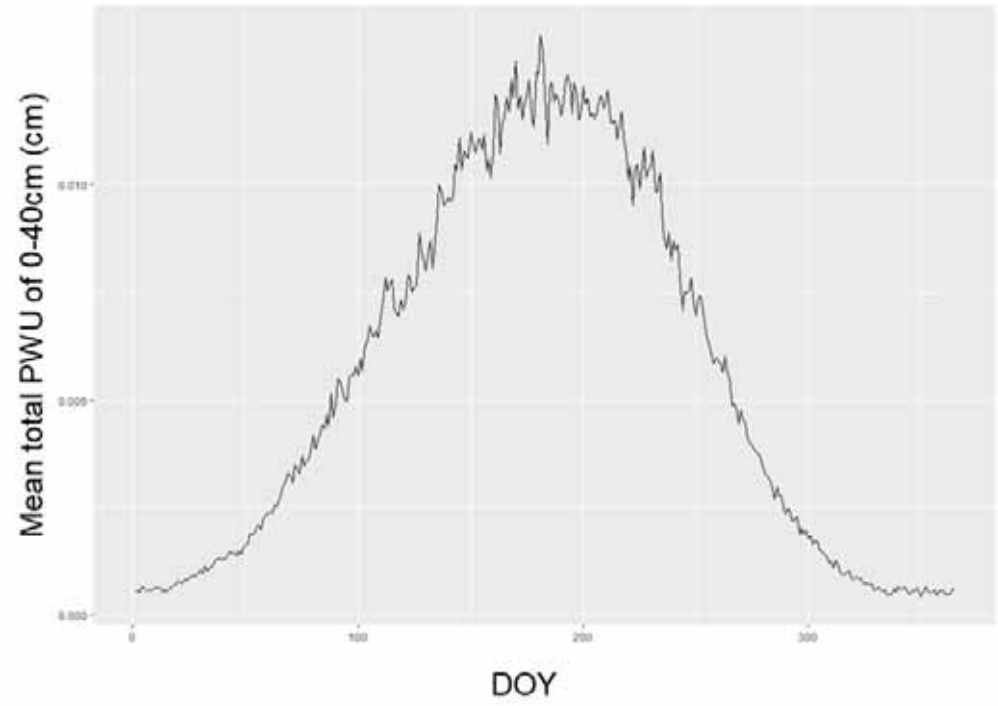

Figure 40. Mean total plant water uptake (cm/day) from 0-40cm for the period of 1978-2018, based on the day of the year (DOY).

Based on SPWisoM, I also observed that both soil moisture and PWU have been significantly declining from 1978 to 2018 (Equations 19 – 22). Figure 41a and Figure 41b demonstrated that both annual total soil moisture (m^3/m^3/year) and annual total PWU (cm/year) between 0 and 40 cm have been decreased during the modeling period. Similarly, both mean daily total soil moisture (m^3/m^3/day: Figure 41c) and mean daily PWU (cm/day: Figure 41d) also

significantly decreased from 1978 to 2018. From a seasonal perspective, both soil moisture and PWU suggested strong declining trends (Equation 23 – 24; Figure 42a and Figure 42b) during the summer season (June – August). During the winter period (December – February), on the other hand, only PWU showed a significant decreasing trend (Figure 42d; Equation 25) and soil moisture did not appear to have a trend (Figure 42c).

$$Annual\ total\ \theta = 2339.3409 - 0.7031 * Year \quad (19)$$

$$Mean\ daily\ \theta = 0.6849 - 0.0002343 * Year \quad (20)$$

$$Annual\ total\ PWU = 32.554348 - 0.015295 * Year \quad (21)$$

$$Mean\ daily\ PWU = 0.08913 - 0.0004188 * Year \quad (22)$$

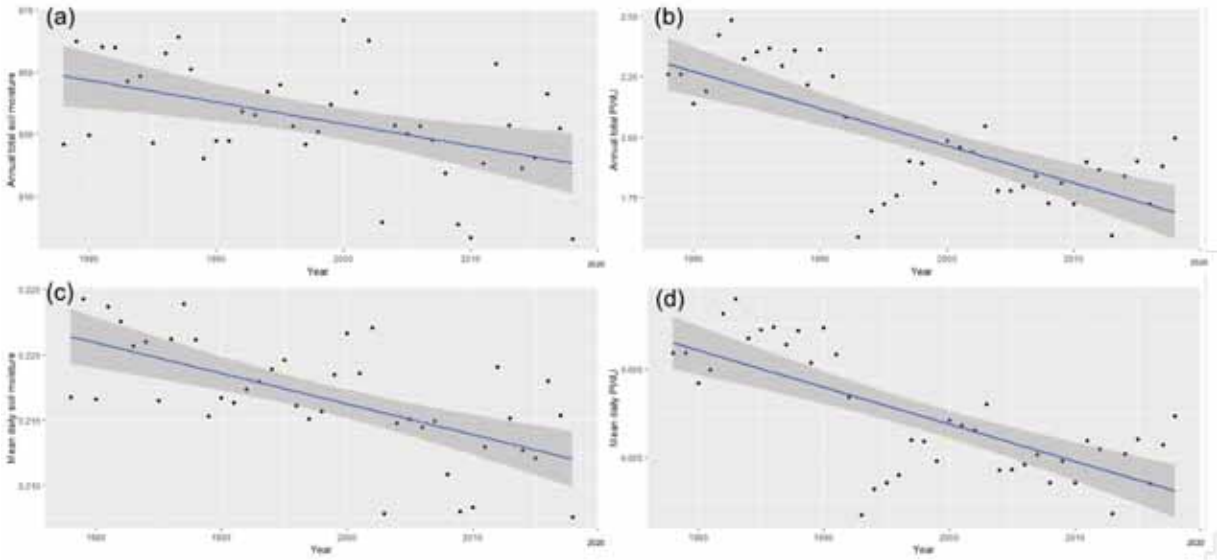

Figure 41. Scatter plots between year and (a) annual total soil moisture (m^3/m^3/year; $R^2 = 0.2271$; $p = 0.002$); (b) annual total PWU (cm/year; $R^2 = 0.4108$; $p < 0.001$); (c) mean daily total soil moisture (m^3/m^3/day; $R^2 = 0.5263$; $p < 0.001$); and (d) mean daily total PWU (cm/day; $R^2 = 0.5257$; $p < 0.001$) from 1978 to 2018 (n = 40). Blue line and shaded area indicate regression line and 95% confidence interval, respectively.

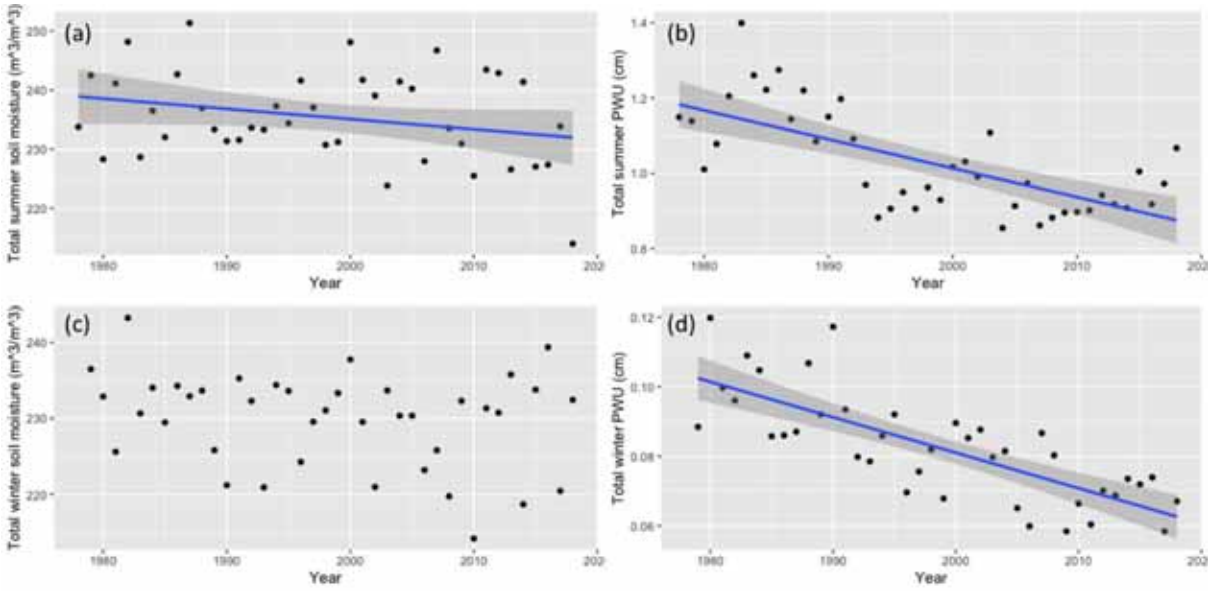

Figure 42. Season-based change of (a) total summer soil moisture (June-August; m^3/m^3; $R^2 = 0.07355$; $p = 0.086$); (b) total summer PWU (June-August; m^3/m^3); (c) total winter soil moisture (December-February; cm; $R^2 = 0.4633$; $p < 0.001$); and (d) total winter PWU (December-February; cm; $R^2 = 0.5917$; $p < 0.001$). Blue line and shaded area indicate regression line and 95% confidence interval, respectively.

$$Total\ summer\ \theta = 580.99451 - 0.17295 * Year \quad (23)$$

$$Total\ summer\ PWU = 16.375314 - 0.007681 * Year \quad (24)$$

$$Total\ winter\ PWU = 2.1248866 - 0.0010219 * Year \quad (25)$$

5 Discussion

5.1 Performance and applicability of SPWisoM

It is important to understand the credibility and uncertainty associated with SPWisoM before discussing the effect of the modeled soil moisture (θ_{mod}) and the modeled plant water uptake (PWU) on forest growth reduction. In this section, I, therefore, evaluated the performance and applicability of SPWisoM regarding the simulation of soil moisture and PWU dynamics. This model evaluation was conducted in reference to previous studies which were mainly carried out also at the Hartheim forest site.

Kling-Gupta efficiency (KGE) values of calibrated SPWisoM (Table 6) indicated that soil moisture dynamics of the study site was more or less satisfactorily simulated by SPWisoM. Sprenger et al. (2015) employed HYDRUS-1D and 4 different inverse models to simulate water transport at Hartheim forest, resulting in KGE values ranging from 0.10 to 0.43 in reference to the time-series soil moisture data. Their measured soil moisture data was provided from Königer (2003) explained in section 3.2.2.1.2. Although KGE at 35 cm in my study (0.014) was one order smaller than those of Sprenger et al. (2015), SPWisoM-based KGEs at shallower depths (i.e., KGE = 0.211 at 5 cm; KGE = 0.253 at 15 cm) fitted into the value range of Sprenger et al. (2015). SPWisoM-based soil moisture relatively deviated from measured soil moisture data at deeper depths, likely due to comparatively higher spatial

variability of gravel layer at deeper depths (Figure 12); although the Hartheim forest exhibits relatively gentle terrain (< 3°; Sprenger et al., 2015; Figure 8), distribution of gravel and subsequent hydrological properties possibly differ dynamically within small distances in floodplains such as the Hartheim forest (Asselman & Middelkoop, 1995). Thus, SPWisoM assumedly performed comparatively better at shallower depths than deeper gravel layers.

Modeled soil moisture (θ_{mod}) was also plotted against measured soil moisture (θ_{meas}) to analyze the correlation between two soil moisture datasets. When compared to θ_{meas} data by Königer (2003), SPWisoM tended to magnify the total soil moisture between 0 and 30 cm by a factor of 4 (Equation 17). Scatter plot between θ_{meas} and θ_{mod} (Figure 35), on the other hand, showed a significant correlation ($R^2 = 0.3458$; $p < 0.001$). These results implied that SPWisoM was able to simulate general soil moisture dynamics of the Hartheim forest to some extent, however, the actual soil water content may vary largely depending on the position of measured soil pits. Unfortunately, it was impossible to discuss the spatial variability between soil pits used in my research (Figure 13) and a soil pit used by Königer (2003) as the location of Königer' (2003) soil pit was not specified. Moreover, Wellpot et al. (2005) hired another physically-based hydrological model (BROOK90) to examine soil moisture dynamics (0 – 40 cm) of the Hartheim forest from 1978 to 1982, resulting in a stronger correlation between θ_{meas} and θ_{mod} ($R^2 = 0.811$) with a gentler slope of 1.031. While SPWisoM seemed less credible compared to BROOK90 at least for the soil moisture modeling, it was also seemingly that SPWisoM had room for improvement, especially if calibrated with the vertical distribution of the actual soil water content measured by recently installed soil moisture sensors (Figure 26).

In addition to soil moisture, modeled PWU was also validated in comparison to actual evapotranspiration data (ET_{act}). As a result of the regression analysis (Figure 36), modeled PWU was strongly correlated to mean 30-min ET_{act} ($R^2 = 0.7494$; $p < 0.001$), suggesting SPWisoM was capable of modeling general trends of PWU. However, Equation 18 implied that total daily PWU (0 – 40 cm) was potentially underestimated compared to the actual PWU. Assuming mean 30-min ET_{act} was constant for a given day, modeled daily PWU was estimated to be approximately 1/159 of daily ET_{act} (e.g., 0.30183/48 = 1/159). Even though Wedler et al. (1996) suggested understory and unvegetated areas of the Hartheim forest contributed to about 20 % of ET_{act}, SPWisoM-based annual PWU (21.1 ± 2.6 mm/year) between 1978 and 2001 was still one order smaller than actual transpiration (365 mm/year) over the same period (Wellpott et al., 2005). Sap flow measurement (11 May to 24 May 1992) by Granier et al. (1996) also confirmed that corresponding SPWisoM-based daily PWU (0.1 to 1.2 mm/day) was possibly one order smaller than actual daily cumulated sap flow (2.0 to 2.7 mm/day). This means that while SPWisoM was able to simulate the spatiotemporal distribution of PWU more or less precisely in a relative manner, SPWisoM tended to underestimate the spatiotemporal distribution of PWU in an absolute manner. Because the main focus of this research was to evaluate the effect of time-series PWU trend on forest productivity, I assumed that underestimation of absolute PWU values was negligible given relative distribution of PWU was valid.

This study also revealed clear declining trends of both soil moisture and PWU from 1978 to 2018 (Figure 41 and Figure 42). The declining trend of the soil moisture was consistent with

findings of Holsten et al. (2009), in which available soil water content was revealed to have been decreased from 1951 to 2003 in northeastern Germany. It was also understandable that PWU has been declined as the availability of soil water and subsequent actual transpiration have been declined over the modeling period (Denmead & Shaw, 2010). Moreover, Figure 43 showed long-term trends of 4 different input meteorological parameters, indicating that annual mean temperature (°C), annual total PET (mm/year), and annual mean humidity have also been increasing since 1978 at the Hartheim forest. In particularly, annual mean temperature (Figure 43b) and annual total PET (Figure 43c) demonstrated stronger increasing trends compared to that of annual mean humidity (Figure 43d). These increasing mean temperature and annual total PET are the commonly observed and/or predicted climate change-related phenomena across Europe (Eckhardt & Ulbrich, 2003; Luterbacher et al., 2004; Spinoni et al., 2015; Appendix 6). Increased temperature and PET potentially trigger water deficit given PWU is regulated by a limited amount of available soil water content, intensifying drought and consequent forest growth reduction (Teuling et al., 2013). Thus, I presumed that soil moisture and PWU of the Hartheim forest have been decreased since 1978, owing to changing stand-level climatic conditions and subsequently intensified drought conditions.

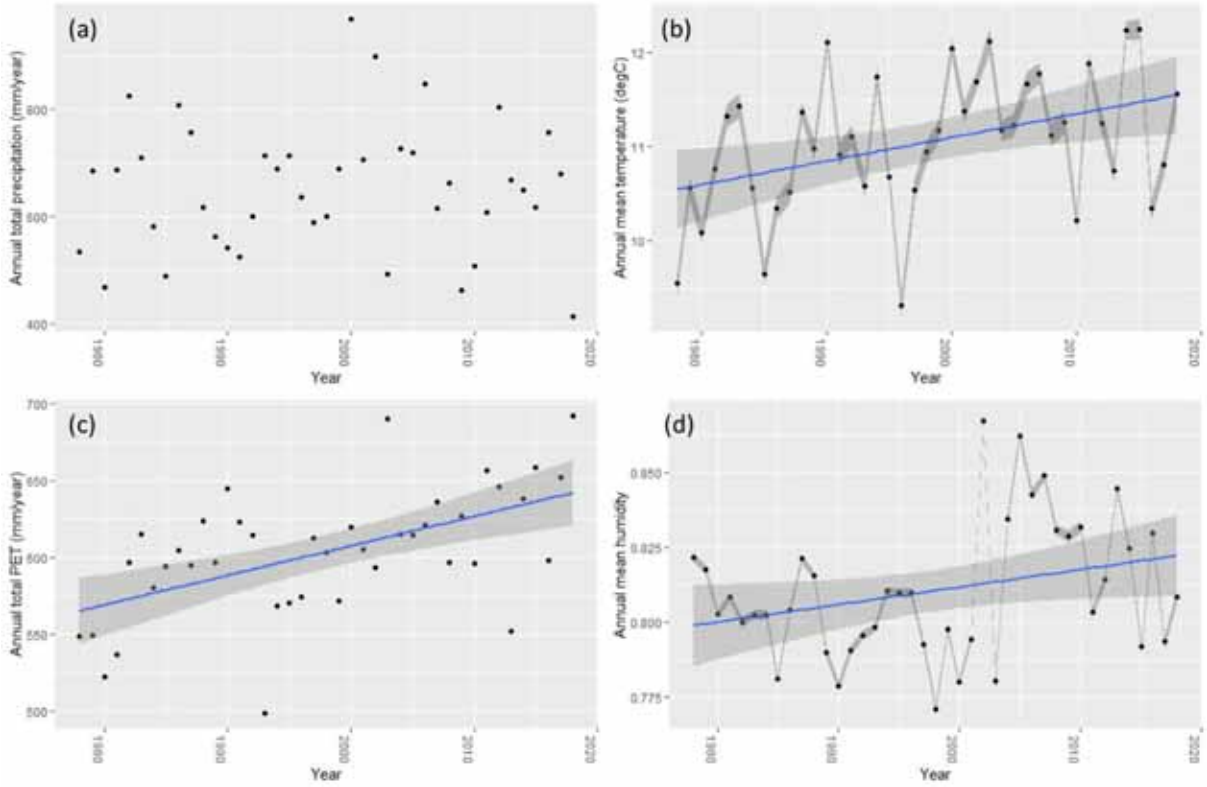

Figure 43. Long-term trends of input meteorological parameters from 1978 to 2018: (a) annual total precipitation (mm/year) showed no significant trend; (b) annual mean temperature (°C) showed increasing trends (Equation 26; $R^2 = 0.1717$; $p = 0.007$); (c) annual total potential evapotranspiration (PET: mm/year) showed increasing trend (Equation 27; $R^2 = 0.3117$; $p < 0.001$); and (d) annual mean humidity showed slightly increasing trend (Equation 28; $R^2 = 0.09545$; $p = 0.049$). Shaded area around blue regression lines are 95 % confidence interval regarding the long-term trends. Other shaded area between dots of (b) and (d) are 95 % confidence interval of intra-annual values.

$$Annual\ mean\ temperature\ =\ -38.957181\ +\ 0.025029 * Year \quad (26)$$

$$Annual\ total\ PET\ =\ -3222.7232\ +\ 1.9151 * Year \quad (27)$$

$$Annual\ mean\ RH\ =\ -0.3555175\ +\ 0.0005837 * Year \quad (28)$$

5.2 Effects of changing soil moisture and PWU on the tree productivity

After computing soil moisture (θ_{mod}) and plant water uptake (PWU) based on SPWisoM, drought-induced forest growth reduction at Hartheim forest was investigated. Forest productivity data was represented by ring width index (RWI: section 3.2.1.3.5) from 1978 to 2016. In the beginning, I assessed the tree response to drought at yearly-scale, followed by monthly- and seasonal-scales. Finally, stand-level drought-induced forest growth reduction was discussed by investigating intra-species, single tree-level variabilities.

5.2.1 Impacts of annual soil moisture and plant water uptake

Firstly, the effect of drought on forest productivity was investigated on a yearly basis. Figure 44 shows the temporal distribution of soil moisture and plant water uptake between 1978 and 2016. Total annual soil moisture (Figure 44a) and mean daily total soil moisture (Figure 44c) shows identical behavior, while total annual PWU (Figure 44b) and mean daily total PWU (Figure 44d) exhibits similar trends over the same period. Those annual values were plotted against annual radial growth (RWI) of Scots pine trees at Hartheim forest (Figure 45). However, no significant relationships were found neither between yearly soil moisture and RWI nor between yearly PWU and RWI.

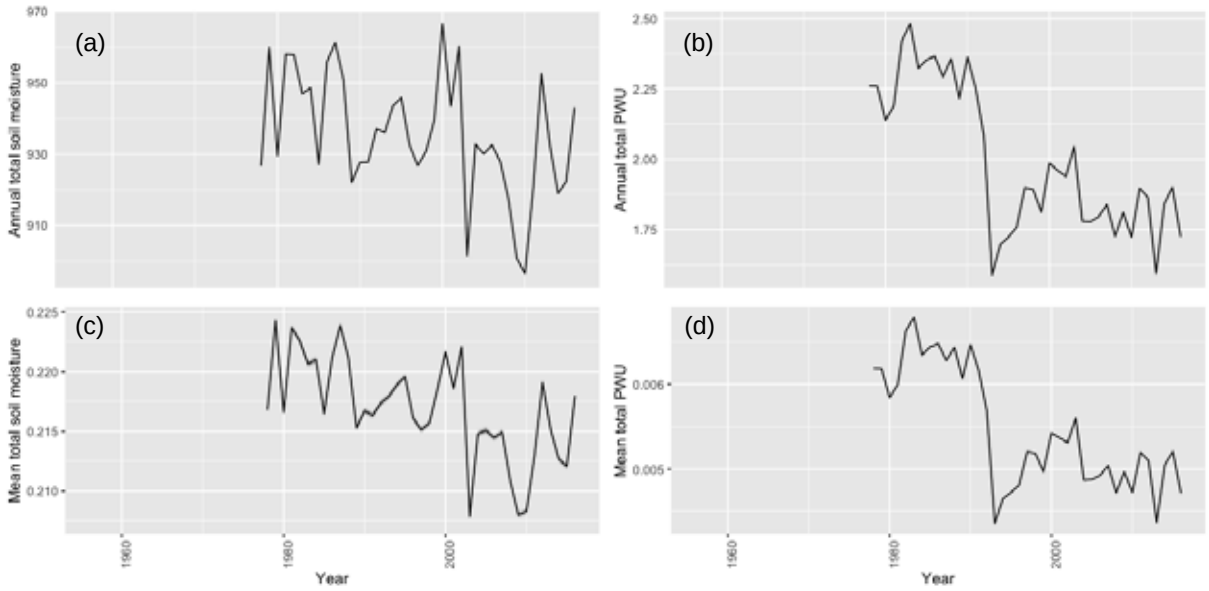

Figure 44. (a) Total annual soil moisture (m^3/m^3/year), (b) total annual plant water uptake (cm/year), (c) mean daily total soil moisture (m^3/m^3/day), and (d) mean daily total plant water uptake (cm/day) over the period of 1978 - 2016.

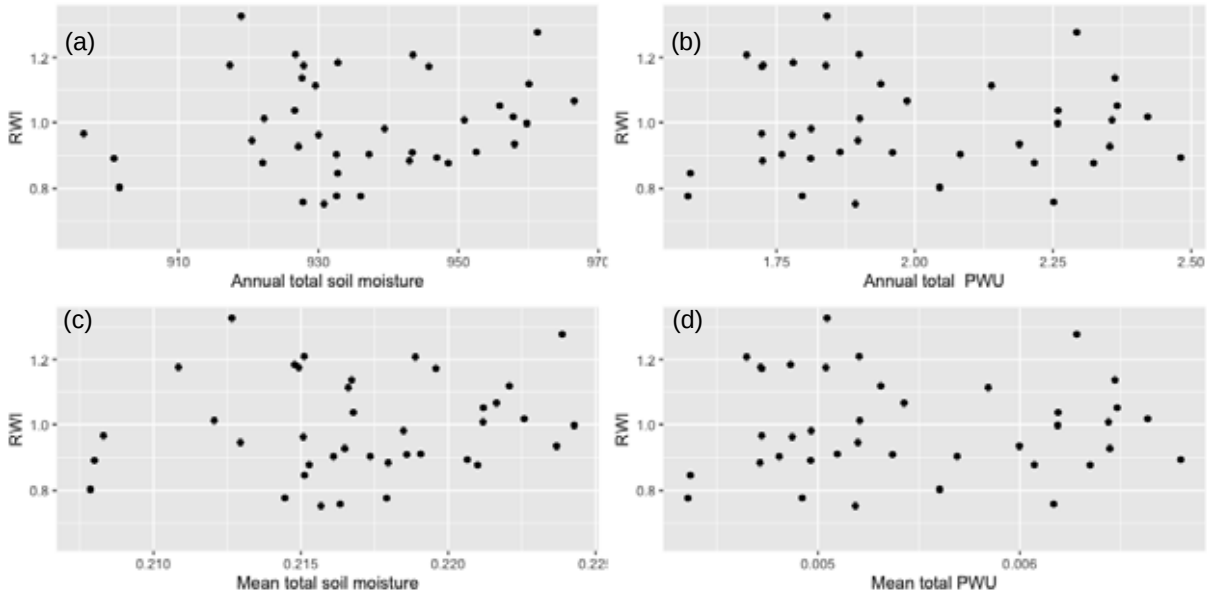

Figure 45. Scatter plots of tree ring width (Ring width index: RWI) and (a) annual total soil moisture (m^3/m^3/year); (b) annual total PWU (cm/year); (c) mean total soil moisture (m^3/m^3/day); and (d) mean total PWU (cm/day) from 1978 to 2016 (n = 38). No significant relationships were identified.

Additionally, I assessed the depth-based distribution of soil moisture and PWU to examine the role of different layers in providing soil water to Scots pine trees. Figure 46 and Figure 47 show vertical distribution of soil moisture (annual total soil moisture: m^3/m^3/year) and PWU (annual total PWU: cm/year) with a spatial resolution of 2 cm. Here, I only used annual values because Figure 44 suggested annual values and mean daily values were almost identical both for soil moisture and PWU. From 1978 to 2016, both soil moisture (Figure 46) and PWU (Figure 47) indicated synchronized trends regardless of soil depths. The correlations between RWI was analyzed for soil moisture (Figure 48) and for PWU (Figure 49) at different depths, resulting in no significant correlation observed.

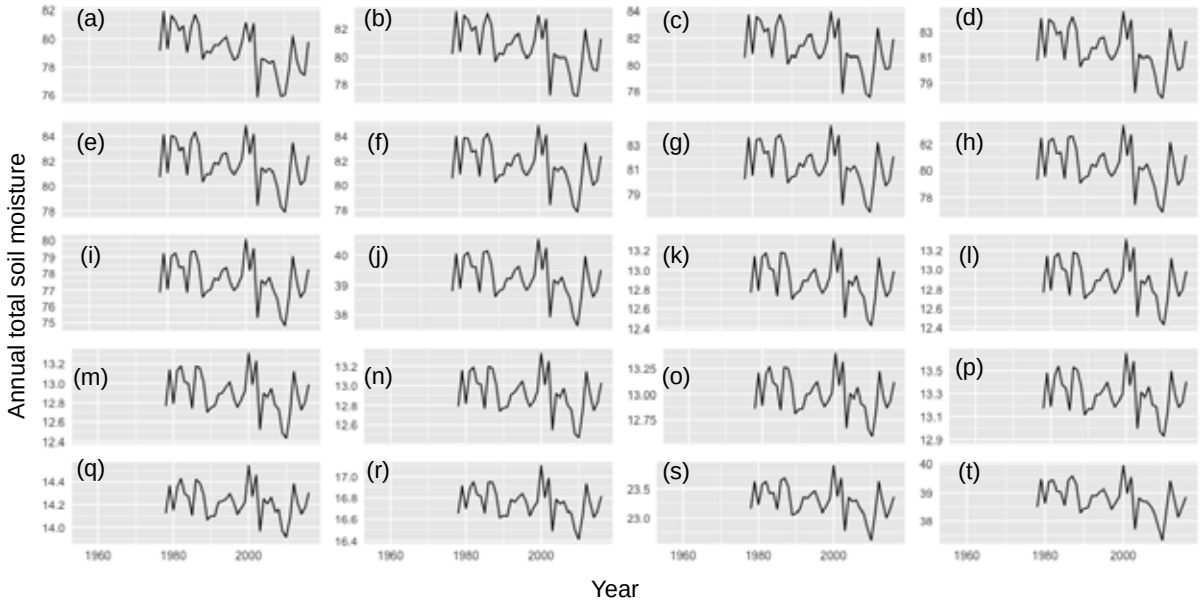

Figure 46. Annual total soil moisture (m^3/m^3/year) of (a) 0-2 cm; (b) 2-4 cm; (c) 4-6 cm; (d) 6-8 cm; (e) 8-10 cm; (f) 10-12 cm; (g) 12-14 cm; (h) 14-16 cm; (i) 16-18 cm; (j) 18-20 cm; (k) 20-22 cm; (l) 22-24 cm; (m) 24-26 cm; (n) 26-28 cm; (o) 28-30 cm; (p) 30-32 cm; (q) 32-34 cm; (r) 34-36 cm; (s) 36-38 cm; (t) 38-40 cm between 1978 and 2016.

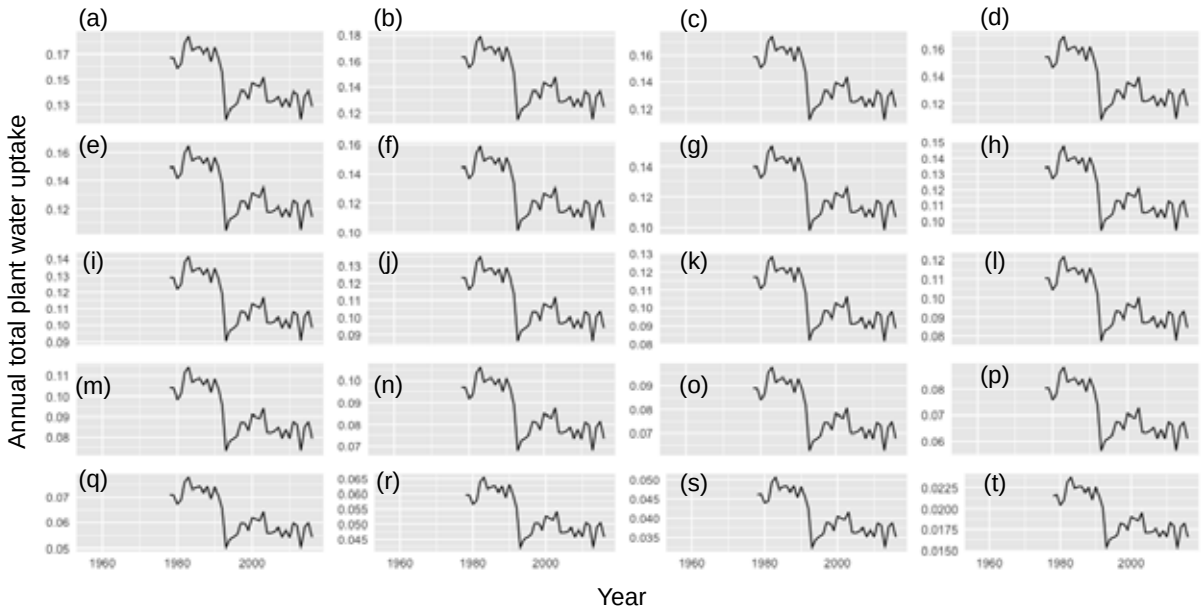

Figure 47. Annual total plant water uptake (cm/year) of (a) 0-2 cm; (b) 2-4 cm; (c) 4-6 cm; (d) 6-8 cm; (e) 8-10 cm; (f) 10-12 cm; (g) 12-14 cm; (h) 14-16 cm; (i) 16-18 cm; (j) 18-20 cm; (k) 20-22 cm; (l) 22-24 cm; (m) 24-26 cm; (n) 26-28 cm; (o) 28-30 cm; (p) 30-32 cm; (q) 32-34 cm; (r) 34-36 cm; (s) 36-38 cm; (t) 38-40 cm from 1978 to 2016.

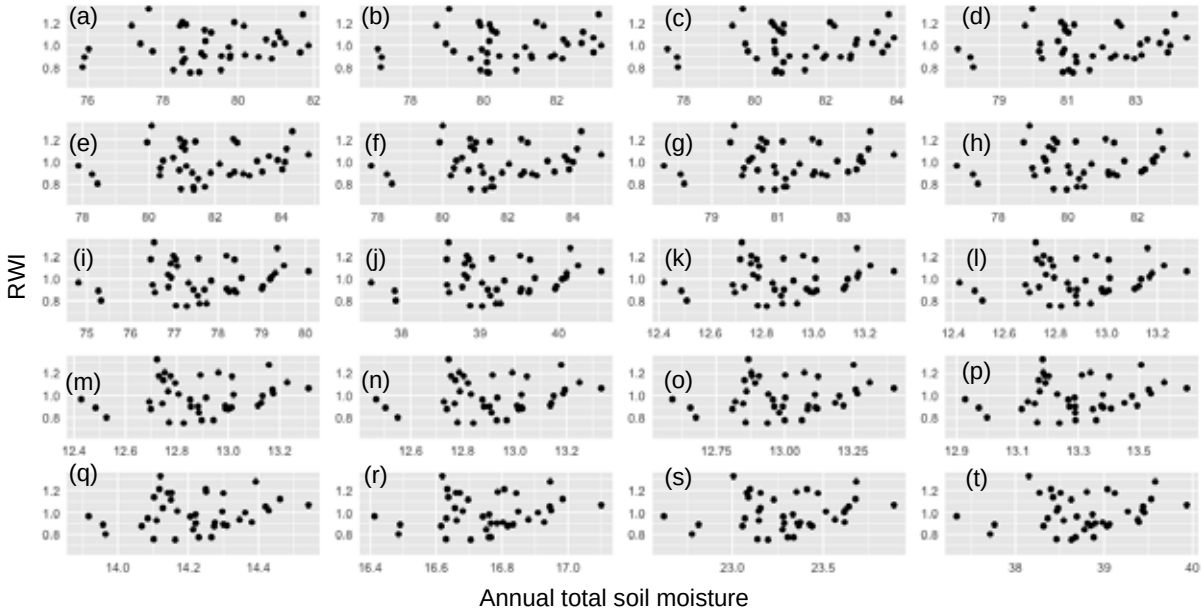

Figure 48. Scatter plots of tree ring width (Ring width index: RWI) and annual total soil moisture (m^3/m^3/year) of (a) 0-2 cm; (b) 2-4 cm; (c) 4-6 cm; (d) 6-8 cm; (e) 8-10 cm; (f) 10-12 cm; (g) 12-14 cm; (h) 14-16 cm; (i) 16-18 cm; (j) 18-20 cm; (k) 20-22 cm; (l) 22-24 cm; (m) 24-26 cm; (n) 26-28 cm; (o) 28-30 cm; (p) 30-32 cm; (q) 32-34 cm; (r) 34-36 cm; (s) 36-38 cm; (t) 38-40 cm between 1978 and 2016 (n = 38). No significant correlation was identified.

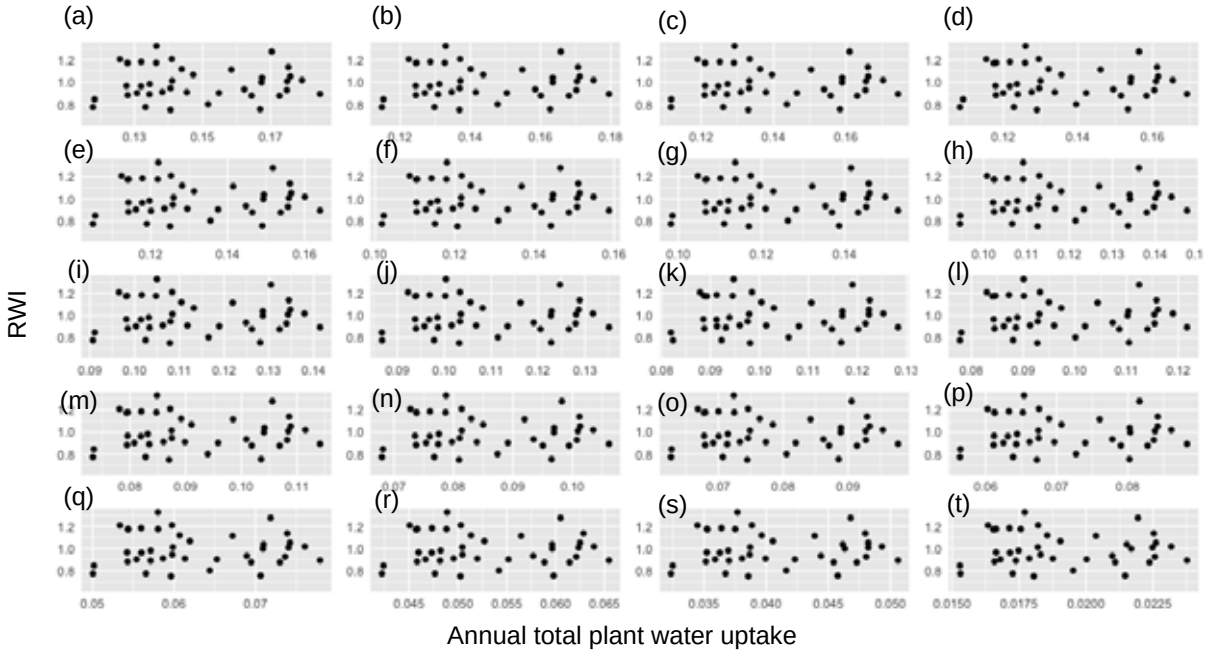

Figure 49. Scatter plots of tree ring width (Ring width index: RWI) and annual total plant water uptake (cm/year) of (a) 0-2 cm; (b) 2-4 cm; (c) 4-6 cm; (d) 6-8 cm; (e) 8-10 cm; (f) 10-12 cm; (g) 12-14 cm; (h) 14-16 cm; (i) 16-18 cm; (j) 18-20 cm; (k) 20-22 cm; (l) 22-24 cm; (m) 24-26 cm; (n) 26-28 cm; (o) 28-30 cm; (p) 30-32 cm; (q) 32-34 cm; (r) 34-36 cm; (s) 36-38 cm; (t) 38-40 cm between 1978 – 2016 (n = 38). No significant correlation was identified.

This study could not find any significant correlation between annual water availability (i.e., soil moisture and PWU) and annual forest productivity (i.e., RWI), likely due to (1) the effect of short-term drought event on forest growth and (2) the effect of single tree-level variabilities in physiological responses to droughts. For instance, Weber et al. (2007) investigated the drought response patterns of *Pinus* and *Quercus* species in southwestern Switzerland, demonstrating species-specific response patterns to climatic conditions. Their study presented that growth rate of *Quercus* was mainly affected by the climate of the previous autumn and current spring, while *Pinus* growth strongly responded to climatic condition during the summer. Their findings implied that productivity of Hartheim Scots pine trees might have been strongly affected by climatic conditions of particular months and/or seasons. Moreover, Miyazawa et al. (2014) measured sap flux of different tropical trees under drought conditions in Cambodia, revealing tree-level drought adaptation and transpiration at different microenvironments within same small stands caused intra-species inhomogeneous sap flux. Those results suggested that intra-species variabilities of Hartheim Scots pine trees might have possibly caused drought-induced growth reduction differently. Therefore, the drought effects on forest growth reduction were additionally analyzed based on a monthly and seasonal basis in section 5.2.2. Furthermore, I also discussed individual trees´ responses to droughts in section 5.2.3.

5.2.2 Effects of monthly and seasonal soil moisture and plant water uptake

In this section, I discussed the drought effects on forest growth reduction by focusing on particular months and/or seasons. Seven different months and seven different seasons were selected for this analysis. Seven different months were March, April, May, June, July, August, and September, covering the whole growing season of Hartheim forest (April – September; Brandes et al., 2007). In addition, seven different seasons consisted of autumn (September – November), winter (December – February), spring (March – May), summer

(June – August), vegetation period of the current year (current year March – current year September), vegetation period of the previous year (previous year March – previous year September), and whole previous year (previous year January – December). Those above-mentioned analyses employed mean monthly soil moisture (m^3/m^3/month) and mean monthly PWU (cm/month), while one analysis was additionally conducted based on the total summer soil moisture and the total summer PWU.

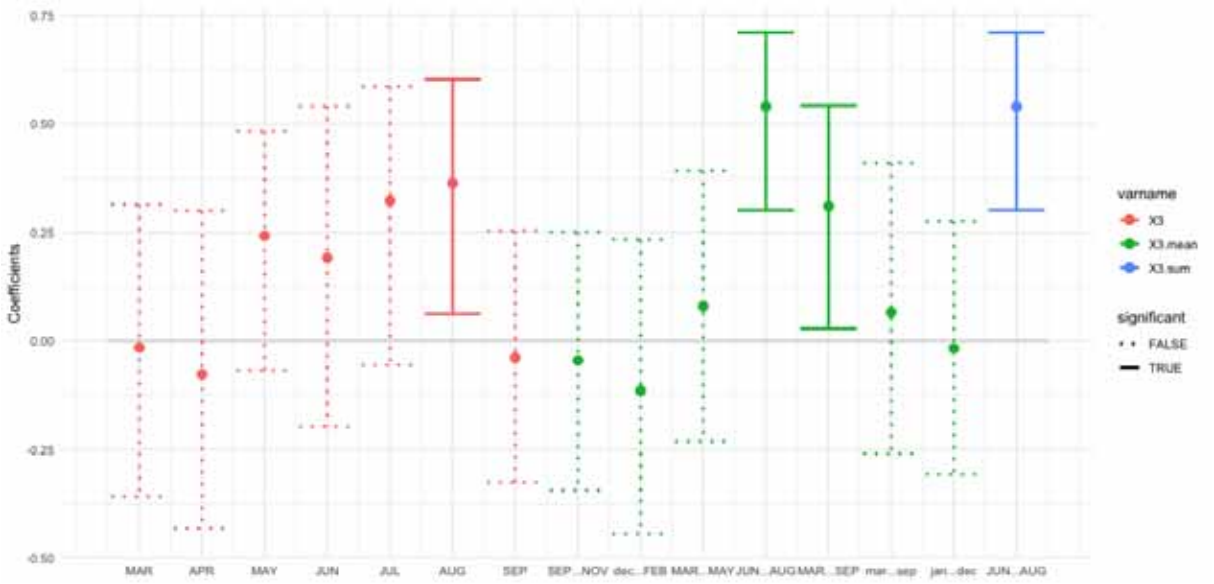

Figure 50. Pearson´s correlation coefficients (r) between monthly (seasonal) soil moisture and ring width index (RWI). Pink, green, and blue bars represent the mean value of each month, the mean value of different seasons, and the total value of summer season from 1978-2016, respectively. In X-axis, small letters and capital letters mean the values of current years and previous years. Dashed and solid bars are statistically false and true. Filled circles, lower and upper error lines are median, 5th and 95th percentile, respectively.

Figure 50 presented the correlation coefficients between monthly (seasonal) soil moisture and radial growth of Scots pine trees (RWI). According to Figure 50, four periods of soil moisture data were significantly correlated to RWI: monthly soil moisture of August, mean summer soil moisture, mean soil moisture of the current vegetation period, and total summer soil moisture. Among them, mean summer soil moisture and total summer soil moisture showed the equivalently strongest correlations to RWI (R^2 = 0.2844; p = 0.0004728), followed by soil moisture of August (R^2 = 0.1225; p = 0.02892) and mean soil moisture of the current vegetation period (R^2 = 0.09449; p = 0.05697).

Those results indicated that the stand-level productivity of Scots pine tree has been regulated, especially by available soil water during summer periods. This finding was consistent with previous researches regarding other Scots pine stands in Europe. For instance, Martínez-Vilalta et al. (2012) studied radial growth response of Scots pine trees to severe drought occurred in 1986 in northwest Spain, showing that warm and dry summer had caused reduced basal area increment of Scots pine trees. In southern Germany, Zang et al. (2012) also observed that radial growth of Scots pine trees was negatively correlated with water stress during summer periods. Based on tree ring width data from 1960 to 2007, Michelot et al. (2012) demonstrated that soil water deficits during the summer growing season were negatively correlated to Scots pine productivity in northern France. Therefore, it seemed that in accordance with other Scots pine stands in Europe, soil water availability during summer periods played an important role in determining radial growth of Scots pine trees at the Hartheim forest.

Contrary to soil moisture, PWU and RWI only indicated a weak correlation (R^2 = 0.05357; p = 0.1621) during the winter period (December – February; Figure 51). According to Figure 51, correlation coefficients generally decreased toward the end of the growing period. Correlation coefficients during autumn (September – November), winter (December – February), and spring (March – May) were also seemingly higher than that of the summer period (June – August). Therefore, although non-summer soil moisture seemed less important for tree productivity (Figure 50), non-summer PWU was likely essential for radial growth of Scots pine trees in Hartheim. This was presumably due to winter-generated carbohydrate storage and consequently promoted earlywood formation before summer season (Michelot et al., 2012); due to mild winter at the study site, I assumed soil water deficits during winter period is less intense than those of summer. Thus, winter soil moisture was not a growth-limiting factor at Hartheim forest. In contrast, due to relatively higher water availability combined with mild winter (Lévesque et al., 2013), winter PWU and photosynthesis might strongly have contributed to pre-summer radial growth at Hartheim forest.

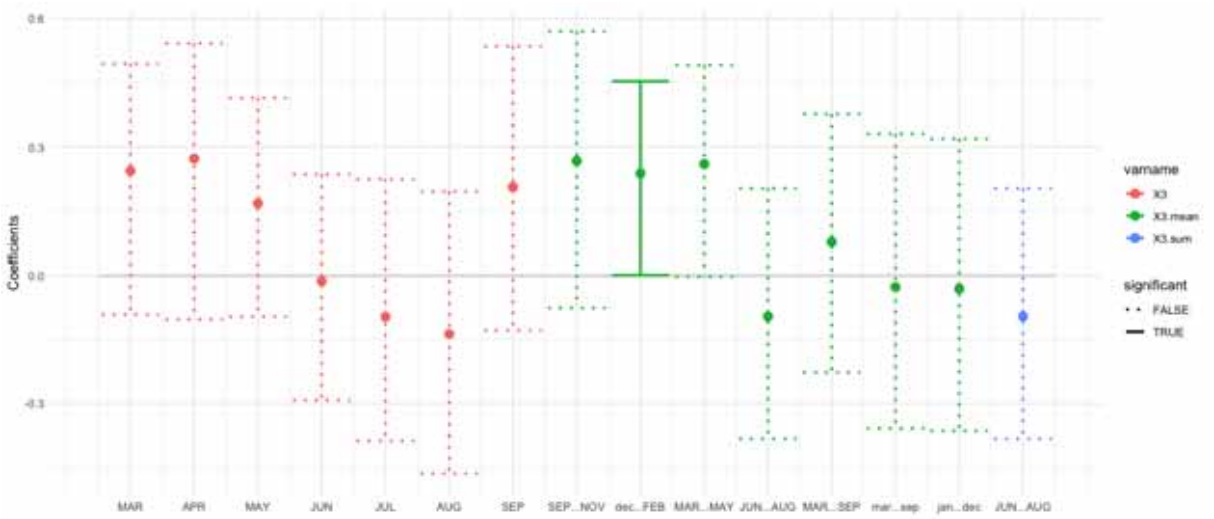

Figure 51. Pearson´s correlation coefficients (r) between monthly (seasonal) plant water uptake (PWU) and ring width index (RWI). Pink, green, and blue bars represent the mean value of each month, the mean value of different seasons, and the total value of summer season from 1978-2016, respectively. In X-axis, small letters and capital letters mean the values of current years and previous years. Dashed and solid bars are statistically false and true. Filled circles, lower and upper error lines are median, 5th and 95th percentile, respectively.

Moreover, I also assessed the effect of monthly and seasonal soil moisture and PWU on forest productivity based on health class of sampled trees. This health class-based analysis was conducted since Scots pine trees potentially have reacted differently to drought, depending on the vitality of individual trees (Dobbertin et al., 2007). For instance, decreased crown coverage (LAI) associated with defoliated needles would probably result in decreased transpiration and consequently declined radial growth (Sterck et al., 2008). Likewise, damaged Scots pine trees are also likely to be more susceptible to secondary bark beetle attack following summer droughts (Dobbertin et al., 2007), possibly altering radial growth rate depending on the vitality classes. Thus, by separating Scots pine trees based on health class, I aimed to investigate vitality-specific tree responses to drought events.

Figure 52 – Figure 59 displayed the results of health class-based tree responses to drought. Generally, summer soil moisture was significantly correlated to tree ring growth (RWI) of

Scots pine trees regardless of health classes (Figure 52, Figure 54, Figure 56, and Figure 58). The strongest correlation between summer soil moisture and RWI was observed for hc_3 (R^2 = 0.3027; $p < 0.001$), followed by hc_1 (R^2 = 0.2737; $p < 0.001$), hc_2 (R^2 = 0.2672; $p < 0.001$), and hc_4 (R^2 = 0.226; $p = 0.002$). In contrast to soil moisture, a weak correlation between PWU and RWI was observed only for hc_3 (R^2 = 0.06492; $p = 0.1227$; Figure 57), while overall trends were generally consistent across different health classes. Those results indicated that health classes had minor effects in determining the drought-induced growth reduction for a short-term, i.e., months to two years. Rather, as discussed later, health classes were presumably more important when looking at long-term growth trends at the Hartheim forest.

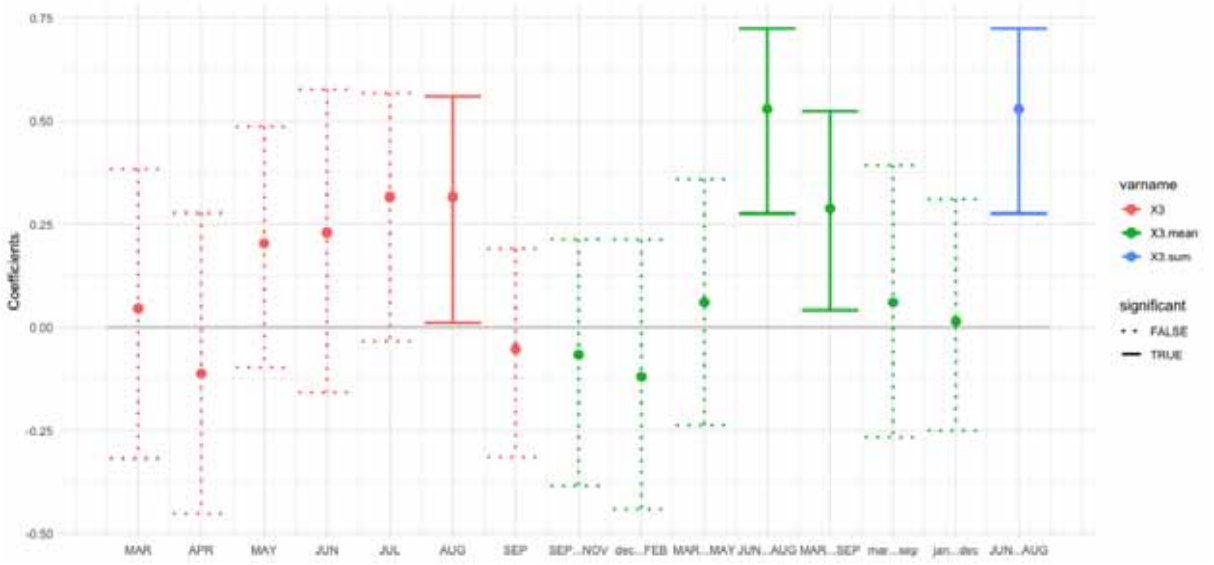

Figure 52. Pearson´s correlation coefficients (r) between monthly (seasonal) soil moisture and ring width index (RWI) for hc_1 (N = 20; damaged crown = 0-20%). Pink, green, and blue bars represent the mean value of each month, the mean value of different seasons, and the total value of summer season from 1978-2016, respectively. In X-axis, small letters and capital letters mean the values of current years and previous years. Dashed and solid bars are statistically false and true. Filled circles, lower and upper error lines are median, 5th and 95th percentile, respectively.

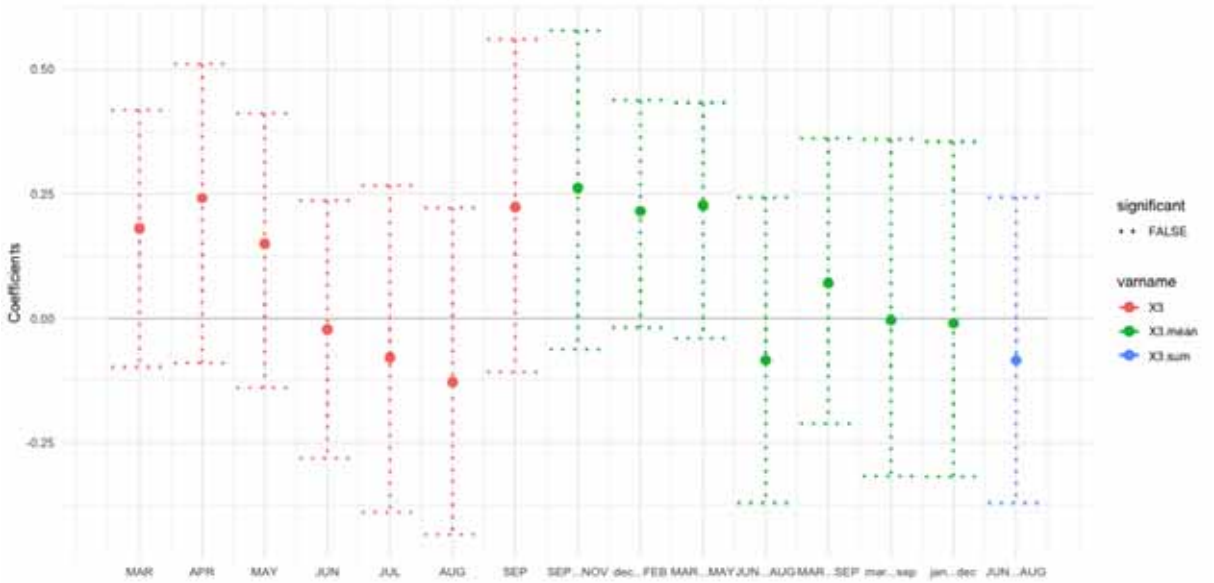

Figure 53. Pearson´s correlation coefficients (r) between monthly (seasonal) plant water uptake and ring width index (RWI) for hc_1 (N = 20; damaged crown = 0-20%). Pink, green, and blue bars represent the mean value of each month, the mean value of different seasons, and the total value of summer season from 1978-2016, respectively. In X-axis, small letters and capital letters mean the values of current years and previous years. Dashed and solid bars are statistically false and true. Filled circles, lower and upper error lines are median, 5th and 95th percentile, respectively. No significant relationship was found.

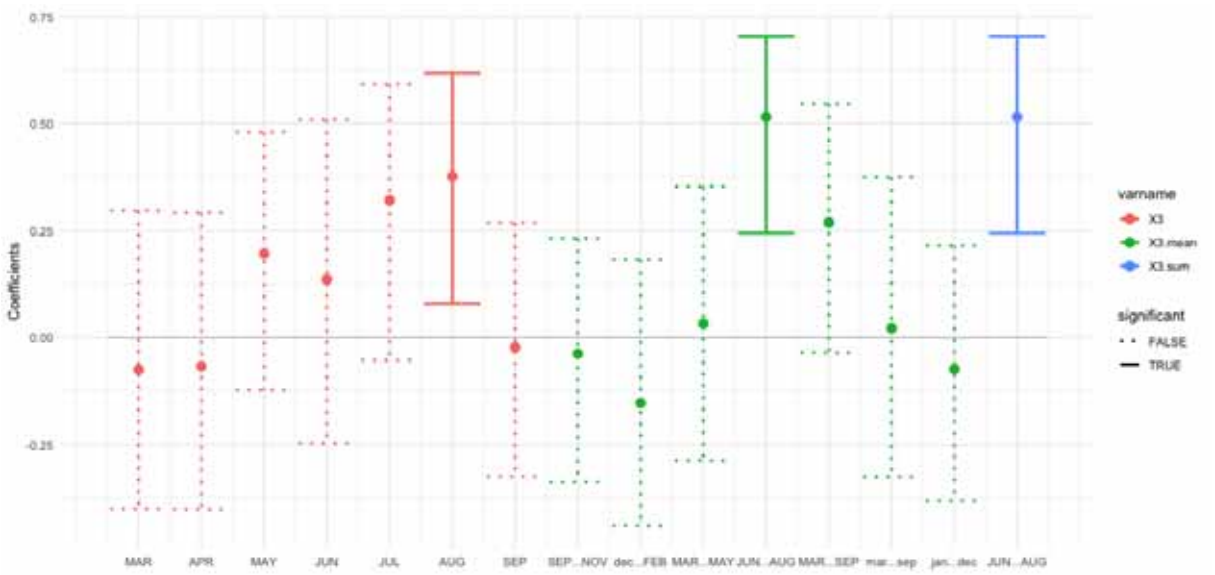

Figure 54. Pearson´s correlation coefficients (r) between monthly (seasonal) soil moisture and ring width index (RWI) for hc_2 (N = 20; damaged crown = 20-50%). Pink, green, and blue bars represent the mean value of each month, the mean value of different seasons, and the total value of summer season from 1978-2016, respectively. In X-axis, small letters and capital letters mean the values of current years and previous years. Dashed and solid bars are statistically false and true. Filled circles, lower and upper error lines are median, 5th and 95th percentile, respectively.

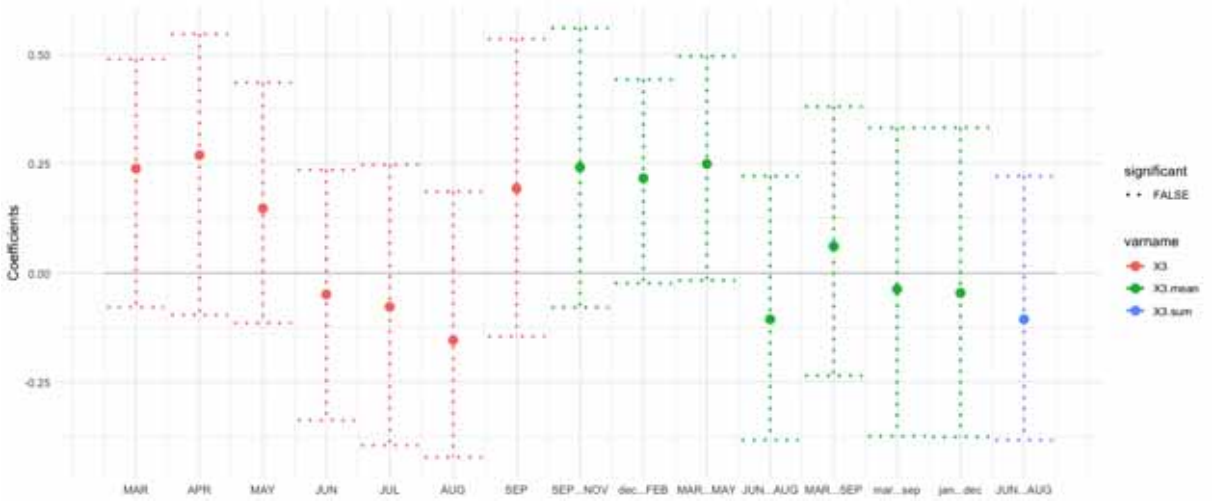

Figure 55. Pearson´s correlation coefficients (r) between monthly (seasonal) plant water uptake and ring width index (RWI) for hc_2 (N = 20; damaged crown = 20-50%). Pink, green, and blue bars represent the mean value of each month, the mean value of different seasons, and the total value of summer season from 1978-2016, respectively. In X-axis, small letters and capital letters mean the values of current years and previous years. Dashed and solid bars are statistically false and true. Filled circles, lower and upper error lines are median, 5th and 95th percentile, respectively. No significant relationship was found.

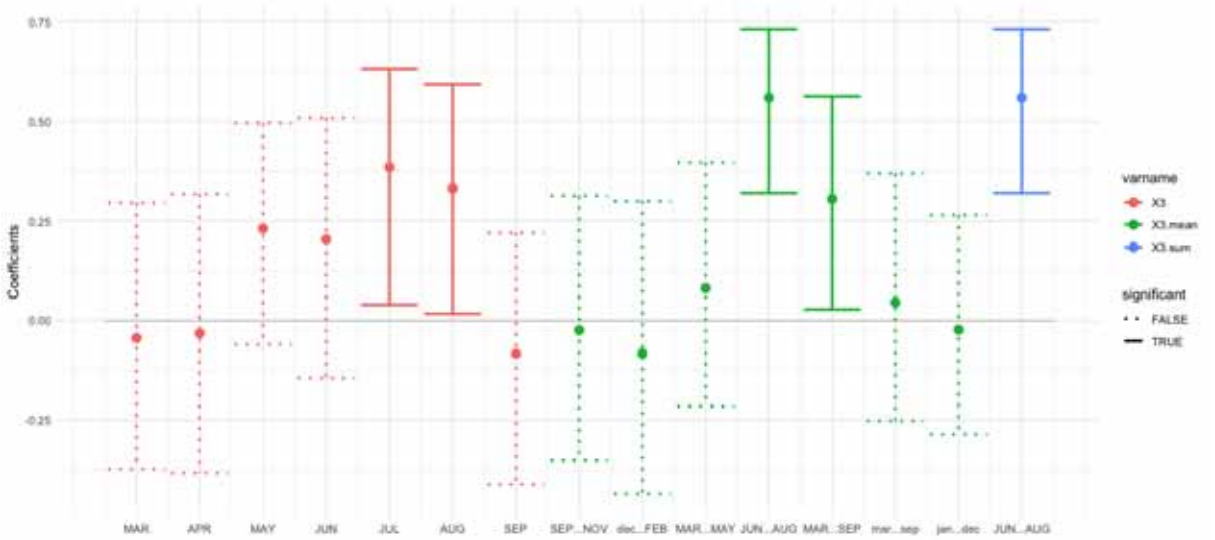

Figure 56. Pearson´s correlation coefficients (r) between monthly (seasonal) soil moisture and ring width index (RWI) for hc_3 (N = 20; damaged crown = 50-80%). Pink, green, and blue bars represent the mean value of each month, the mean value of different seasons, and the total value of summer season from 1978-2016, respectively. In X-axis, small letters and capital letters mean the values of current years and previous years. Dashed and solid bars are statistically false and true. Filled circles, lower and upper error lines are median, 5th and 95th percentile, respectively.

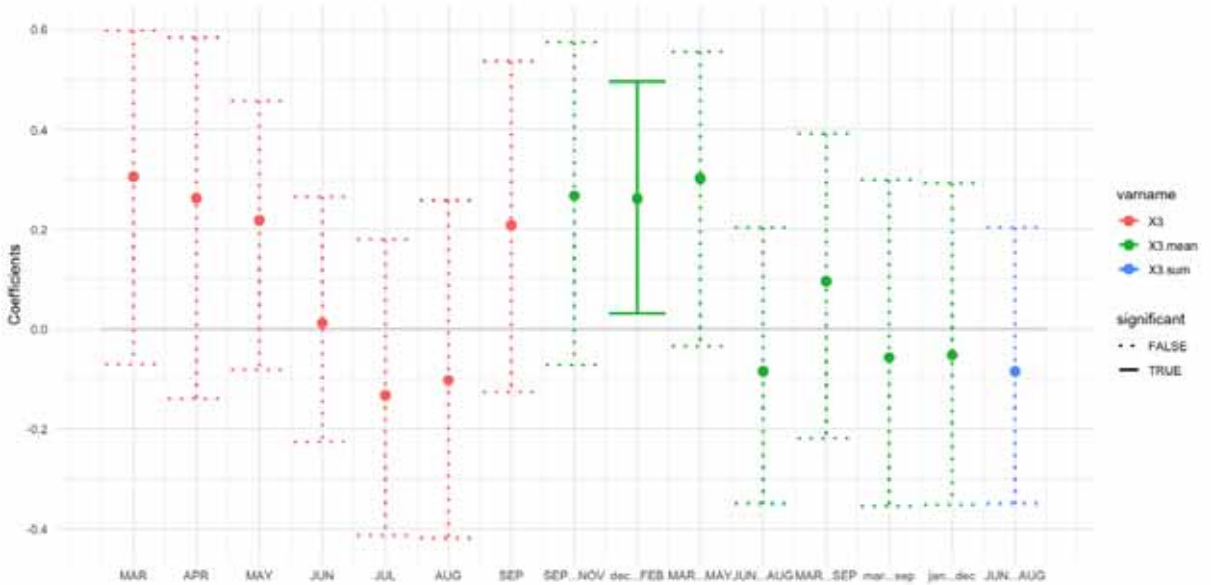

Figure 57. Pearson´s correlation coefficients (r) between monthly (seasonal) plant water uptake and ring width index (RWI) for hc_3 (N = 20; damaged crown = 50-80%). Pink, green, and blue bars represent the mean value of each month, the mean value of different seasons, and the total value of summer season from 1978-2016, respectively. In X-axis, small letters and capital letters mean the values of current years and previous years. Dashed and solid bars are statistically false and true. Filled circles, lower and upper error lines are median, 5th and 95th percentile, respectively.

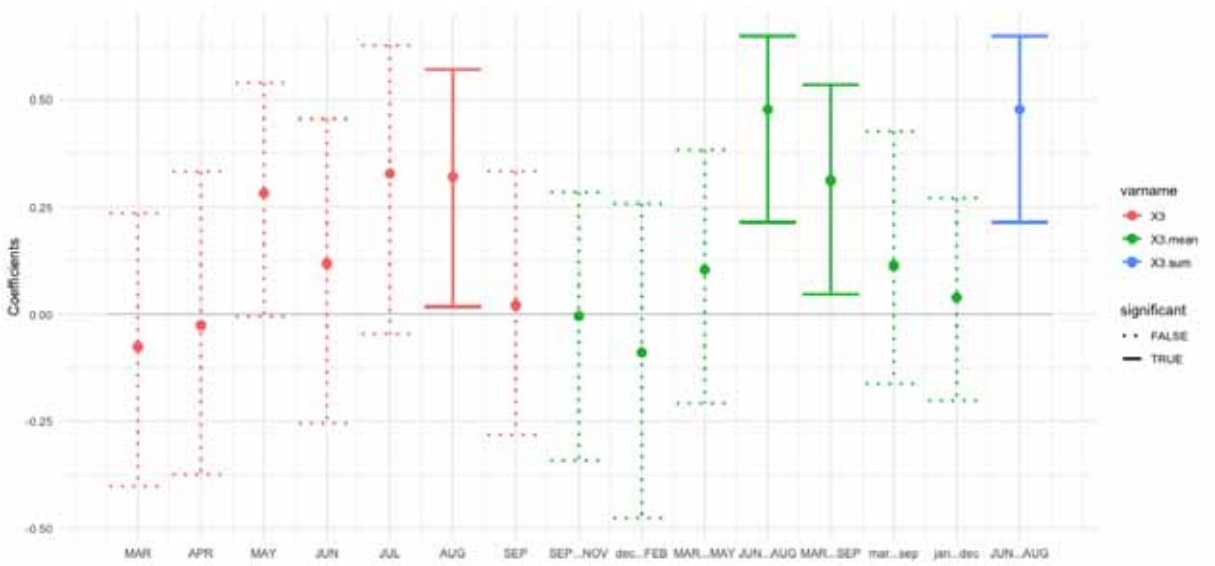

Figure 58. Pearson´s correlation coefficients (r) between monthly (seasonal) soil moisture and ring width index (RWI) for hc_4 (N = 20; damaged crown = 80-100%). Pink, green, and blue bars represent the mean value of each month, the mean value of different seasons, and the total value of summer season from 1978-2016, respectively. In X-axis, small letters and capital letters mean the values of current years and previous years. Dashed and solid bars are statistically false and true. Filled circles, lower and upper error lines are median, 5th and 95th percentile, respectively.

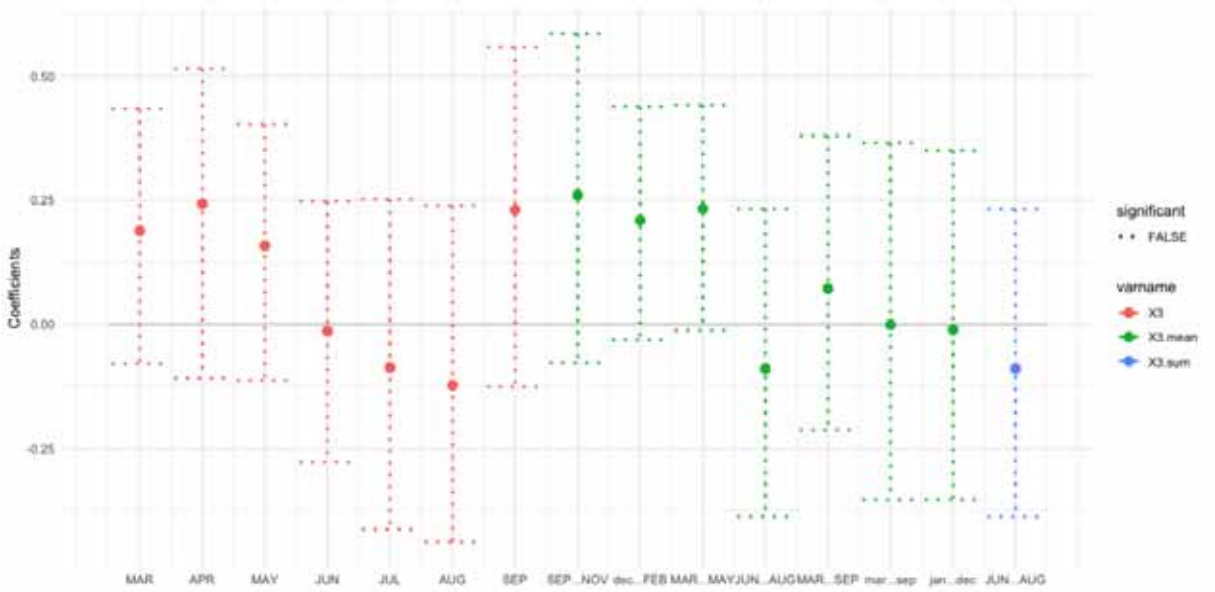

Figure 59. Pearson´s correlation coefficients (r) between monthly (seasonal) plant water uptake and ring width index (RWI) for hc_4 (N = 20; damaged crown = 80-100%). Pink, green, and blue bars represent the mean value of each month, the mean value of different seasons, and the total value of summer season from 1978-2016, respectively. In X-axis, small letters and capital letters mean the values of current years and previous years. Dashed and solid bars are statistically false and true. Filled circles, lower and upper error lines are median, 5th and 95th percentile, respectively. No significant relationship was found.

Moreover, I also assessed time-series radial growth of Scots pine trees with different health classes. Figure 60 expressed the mean values of raw annual ring widths data (mm/year) of four different health classes. Overall, annual ring widths have been showing similar trends among four health classes, however, I would emphasize that the relative productivities have been replaced among health classes over the decades; while lower health class trees definitely indicated smaller radial growth at the time of 2016, Scots pine of hc_4 used to growth at the fastest rate in 1961. The hc_4 trees were growing at the annual rate of approximately 4 mm/year, whereas hc_1 trees were growing only at the annual rate of approximately 2.5 mm/year. Figure 61 clearly indicated that relative productivity has been switched between hc_1 and hc_4 trees over the decades.

Those alternations of relative productivity occurred, likely due to different drought sensitivities associated with different growth rate among even-aged Scots pine trees at the Hartheim forest. In accordance with my research, Martínez-Vilalta et al. (2012) stated that fast-growing Scots pine trees in northeast Spain were relatively more sensitive to drought compared to slow-growing trees. Their study also suggested that fast-growing are more vulnerable to drought presumably owing to (1) amplified impacts on water and carbon use, (2) higher metabolic costs, or (3) heavier water deficits due to taller height. In terms of diameter, Zang et al. (2012) marked that Scots pine trees with larger diameter experienced greater growth reduction than that of smaller trees in drought years. At the Hartheim forest, the mean radial growth of hc_1 and hc_4 trees occurred similarly between 1997 and 2002 (Figure 61), however, the growth rate of hc_1 and hc_4 began to deviate from 2003 and hc_1 continued to grow faster than hc_4 since then. Interestingly, 2003 was the year of extreme drought in Europe (section 2.1). Therefore, it was seemingly that fast-growing hc_4 trees were more heavily damaged by the 2003 drought than slow-growing hc_1 trees, leading to less vital and less productive status. Those findings implied that intra-species characteristics, such as growth rate and subsequent tree size, might play an important role in determining physiological responses to drought events, even if tree age and forest structure are extremely homogeneous like the Harthiem forest.

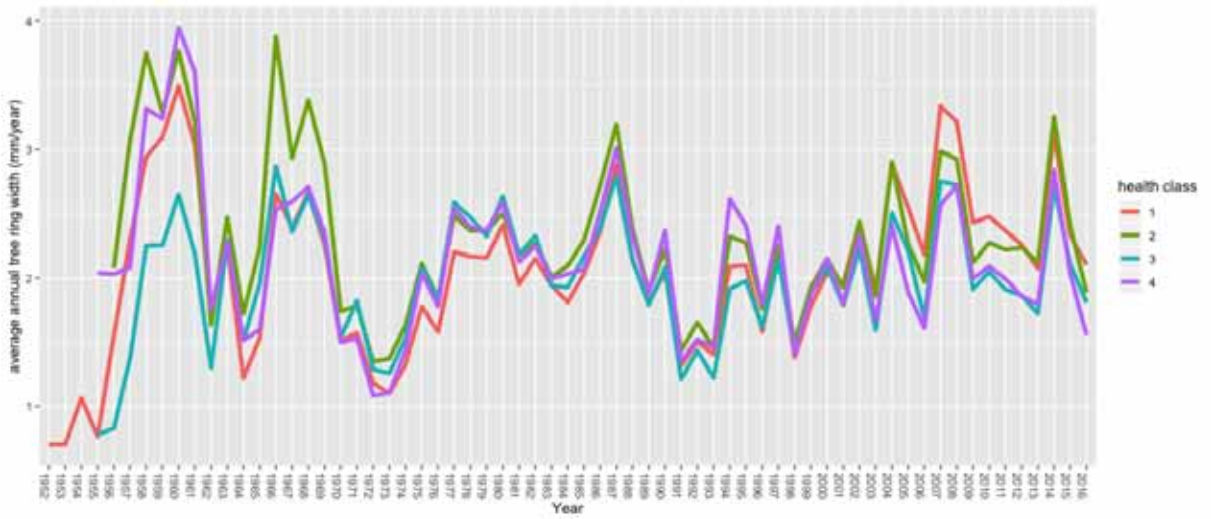

Figure 60. Time-series changes in average annual tree ring growth (mm/year) for different health classes (hc_1, hc_2, hc_3, and hc_4).

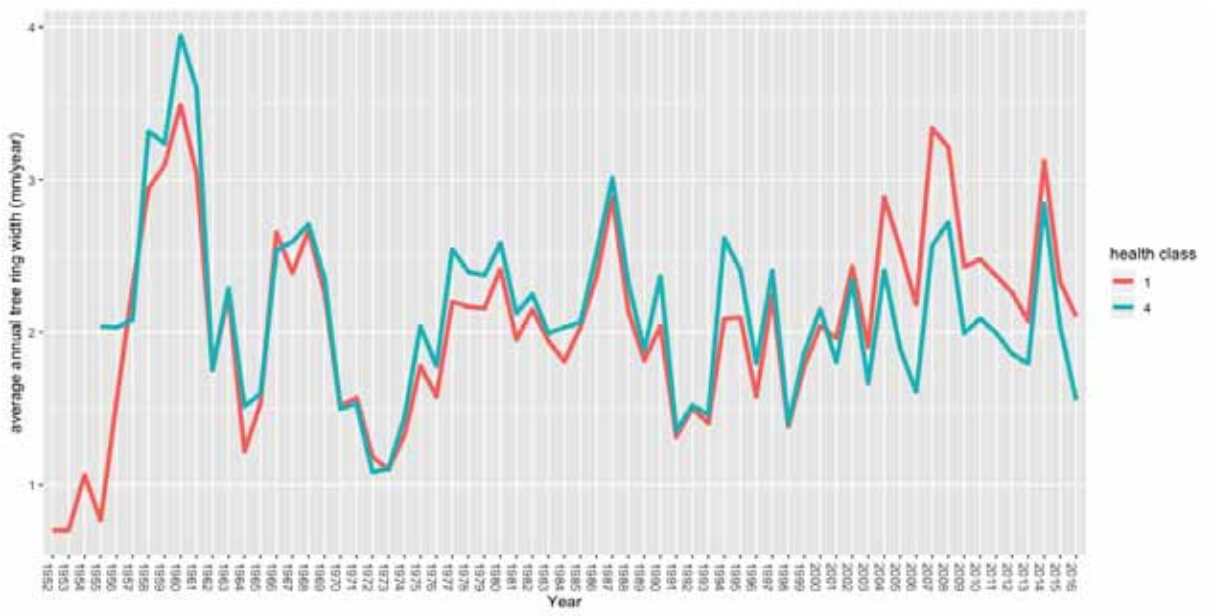

Figure 61. Time-series changes in average annual tree ring growth (mm/year) for hc_1 and hc_4 trees.

5.2.3 Effects of single tree-level variabilities

Finally, intra-species, single tree-level variability and its effects on drought-induced growth reduction at the Hartheim forest was investigated. Figure 62 showed the median *r* between monthly (seasonal) soil moisture and RWI for individual trees (n = 80). Additionally, Figure 63 represented the median *r* between monthly (seasonal) PWU and RWI for individual trees (n = 80). While monthly and seasonal trends of *r* were generally in accordance with those of Figure 50 and Figure 51, the median *r* of individual trees were widely distributed both for soil moisture (Figure 62) and PWU (Figure 63). Those findings seemingly supported the assumption that radial growth responses to drought at my study site were largely depending on intra-species, individual tree-level variabilities.

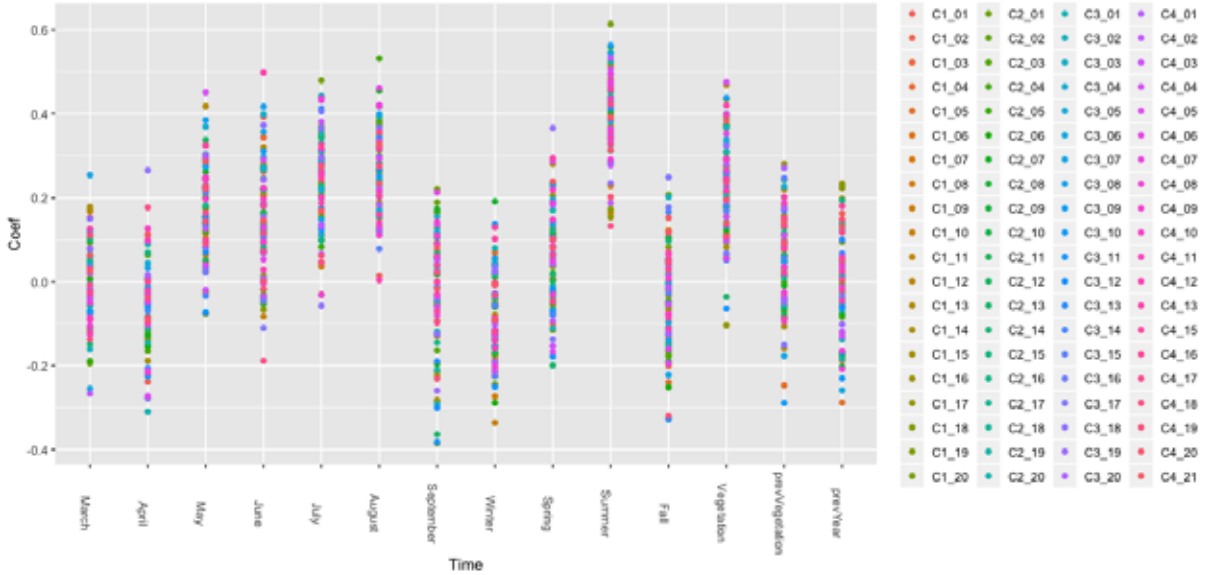

Figure 62. Median Pearson´s correlation coefficients (r) between monthly (seasonal) soil moisture and ring width index (RWI) for individual trees (n = 80).

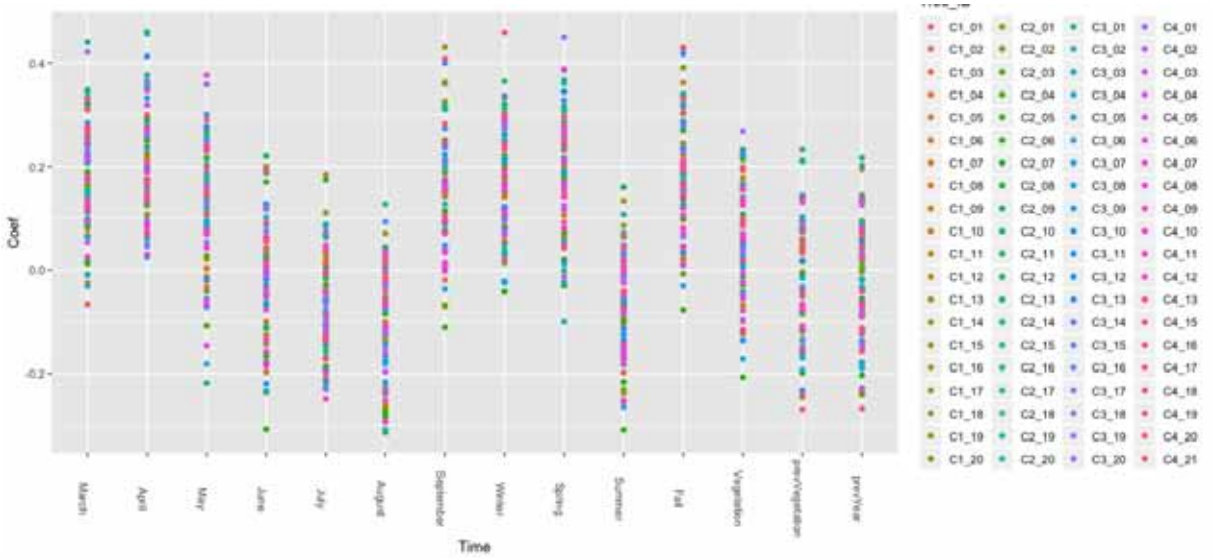

Figure 63. Median Pearson´s correlation coefficients (r) between monthly (seasonal) plant water uptake and ring width index (RWI) for individual trees (n = 80).

Similarly, Figure 64 – Figure 67 indicated that raw annual radial growth (mm/year) of individual Scots pine trees had diverse time-series trends regardless of health classes. From whole samples trees (n = 80), 23 Scots pine trees showed significantly increasing productivity, 23 Scots pine trees showed significantly decreasing productivity, and the rest of Scots pine trees did not exhibit statistically significant trends over the period of 1978-2016. It was also remarkable that some of the Scots pine trees have indicated even strongly increasing trends of diameter growth. Forty-five % of hc_4 trees showed significantly decreasing productivity, while trees with decreasing productivity accounted for only 10 % of hc_1 trees. Therefore, I expected that productivity of the Hartheim Scots pine forest under more frequent and prolonged drought would strongly be determined by growth condition of individual trees.

Those intra-species varied responses to drought were presumably due to the interaction between (1) tree-level drought resistance and resilience and (2) intra-stand microenvironment and resultant differentiated growing environments. Regarding the intra-species differences in drought tolerance, fast-growing Scots pine trees are generally more susceptible to drought due to low water use efficiency for growth, while slow-growing Scots pine trees may exhibit better resist against drought events (Martínez-Vilalta et al., 2012; Morán-López et al., 2014). My study at the Hartheim forest also supported the evidence that fast-growing Scots pine trees have been more severely damaged than slow-growing Scots pine trees (Figure 61). Merlin et al. (2015) also suggested that shorter Scots pine trees adapted better to summer drought compared to taller trees, supposedly attributed to more favorably shaded micro-environment at lower forest layers. A study in Franconia, Germany, indicated that Scots pine trees located at forest edges were more vulnerable to drought likely due to relatively harsh meteorological conditions combined with typically larger canopy volume at the forest edge, leading to less available soil water and higher PET (Buras et al., 2018). Other micro-environmental factors affecting the Hartheim Scots pine forest might be thinning-caused stratified light conditions (Giuggiola et al., 2013) and/or intra-stand dynamics in hydraulic soil properties (Gallardo, 2003) which could not be investigated in my research.

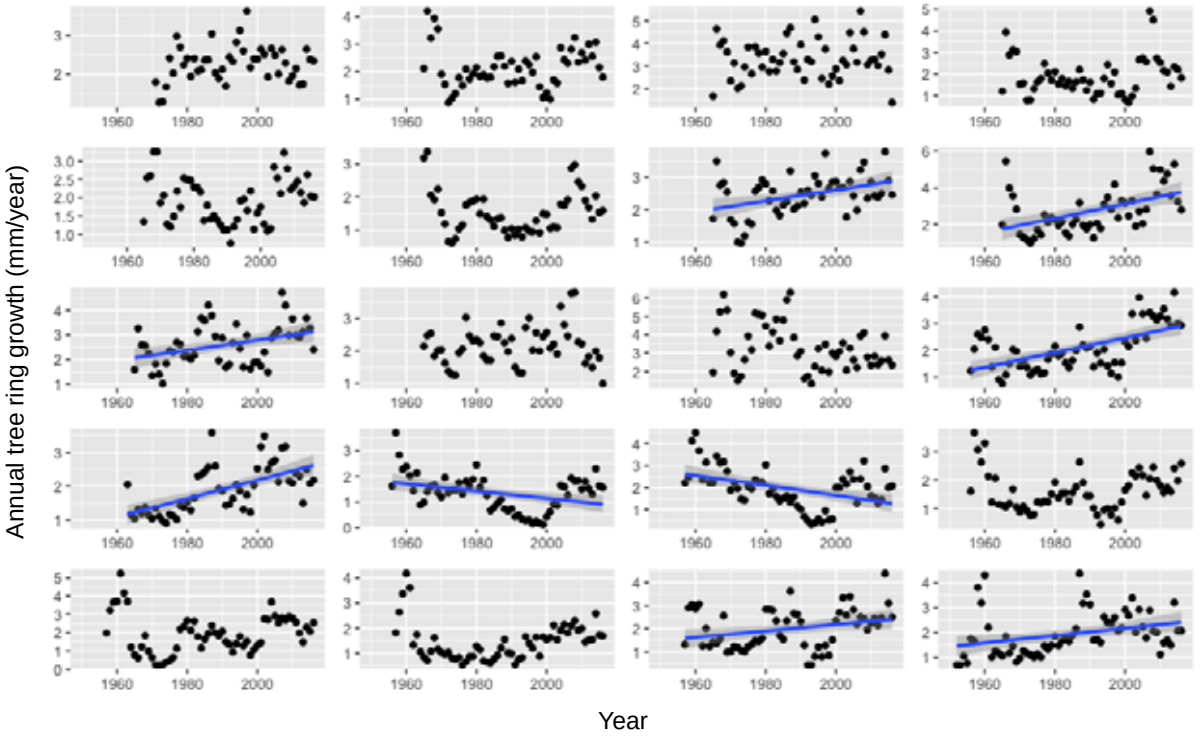

Figure 64. Scatter plots of the annual tree ring growth (mm/year) for hc_1 trees (n = 20). Blue line and shaded area are regression line and 95% confidence interval.

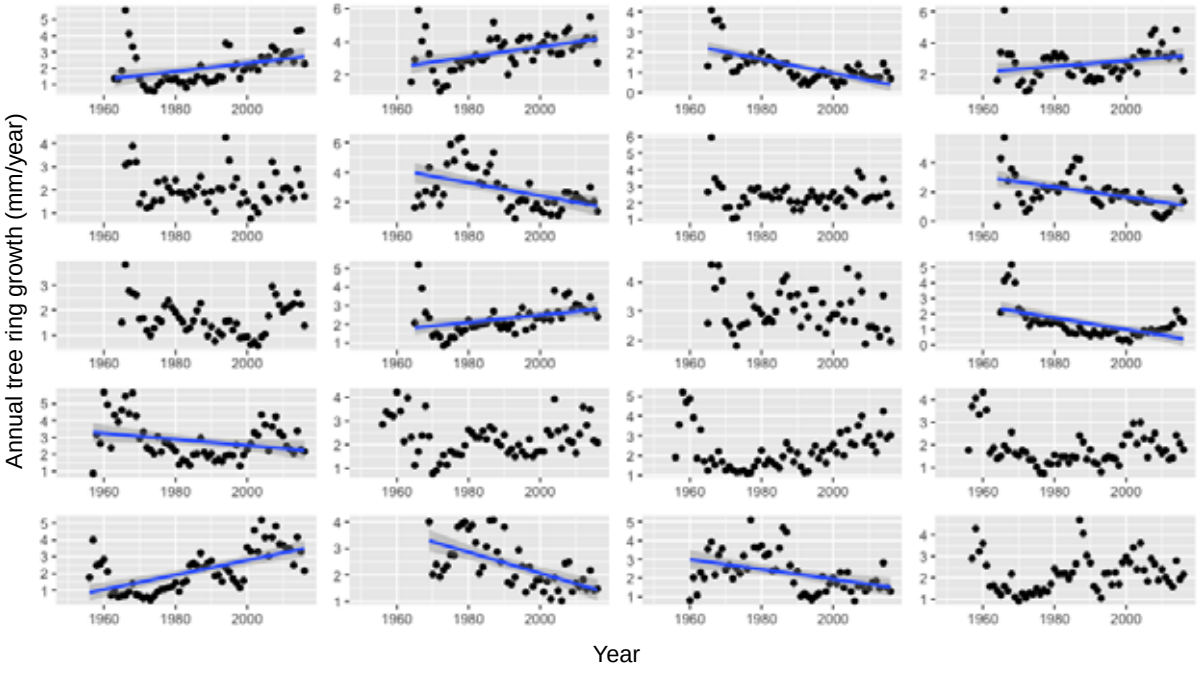

Figure 65. Scatter plots of the annual tree ring growth (mm/year) for hc_2 trees (n = 20). Blue line and shaded area are regression line and 95% confidence interval.

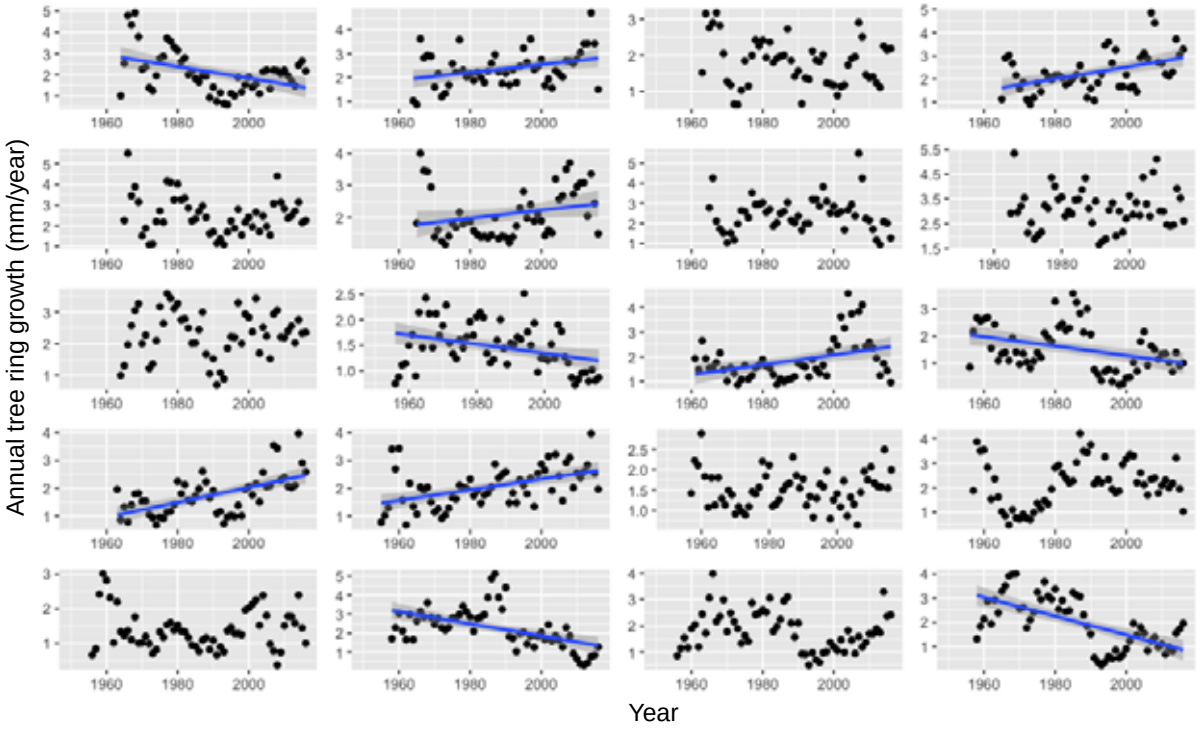

Figure 66. Scatter plots of the annual tree ring growth (mm/year) for hc_3 trees (n = 20). Blue line and shaded area are regression line and 95% confidence interval.

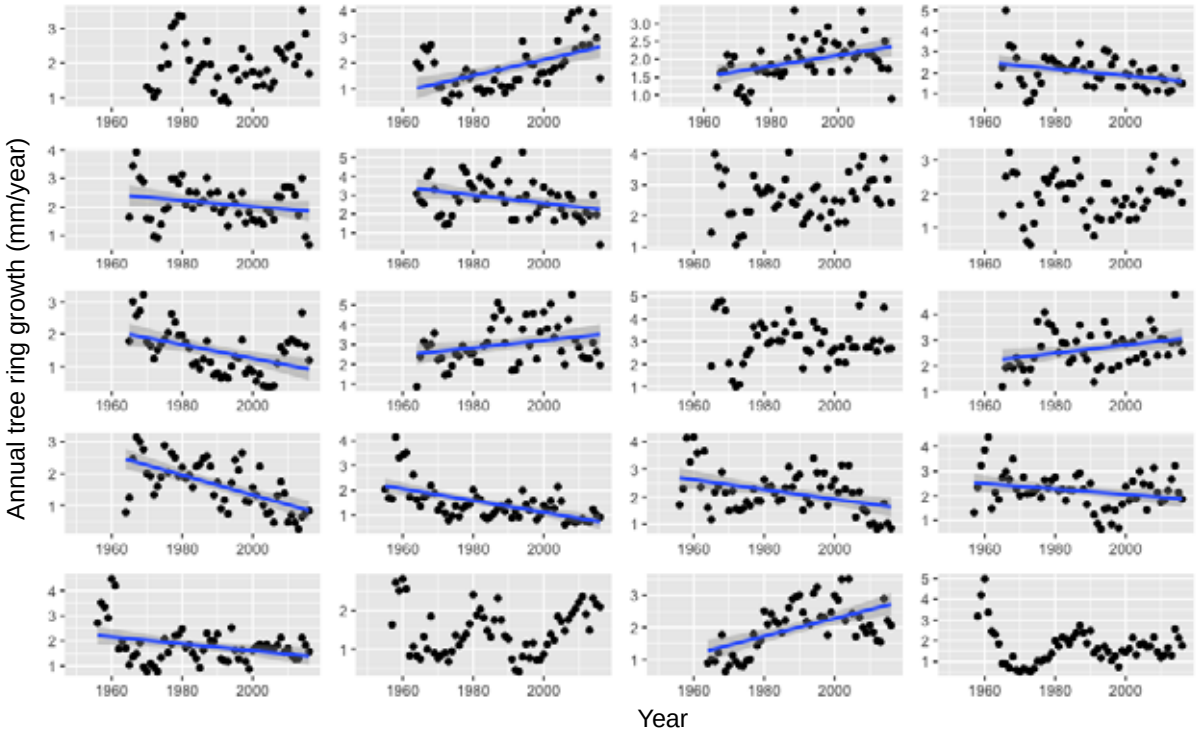

Figure 67. Scatter plots of the annual tree ring growth (mm/year) for hc_4 trees (n = 20). Blue line and shaded area are regression line and 95% confidence interval.

5.3 Implications and suggestions for future research

This master's thesis research offers several implications and suggestions for future research. Firstly, my research indicated that stand-level forest response to drought seemed strongly affected by intra-species and intra-stand variabilities. A future study may closely work on those variabilities because actual intra-species and intra-stand variabilities (e.g., growing

condition) of sampled Scots pine trees were not fully documented in my study. Secondly, this study also suggested that Scots pine, one of Europe´s most widely distributed species as well as one of Europe´s most commercially important species, would potentially be more and more threatened by intensified droughts in the future. As explained in section 2.1, it is expected that drought will be more frequent and prolonged in many regions of Europe. Distribution of Scots pine trees (Appendix 7) is widely overlapped with areas with high expectation of intensified droughts, indicating immediate forestry-based adaptation is crucially important. Thirdly, SPWisoM-based soil water and PWU modeling would be possibly improved given in-situ input parameters would be more applicable. For instance, this study interpolated LAI and WAI from discontinuously measured data (section 3.2.1.3.2), however, applying continuous LAI and WAI (e.g., Appendix 8) would probably enable more precise simulation (Wellpott et al., 2005). Likewise, recently installed sensors for soil moisture (section 3.2.1.2.1) and canopy transpiration (section 3.2.2.2) would strongly support the further calibration and improvement of SPWisoM.

Besides, this study had several limitations regarding data collection, modeling, and analysis. Input parameters were collected from different locations within the same stand (Figure 13), assuming stand-level spatial variabilities within the Hartheim forest was almost negligible. However, my findings implied that microenvironment within the stand possibly affected the growth reduction of Scots pine trees. As discussed already, micro-environmental factors associated with Scots pine growth, such as light and soil conditions, were not also traceable. Thus, the effect of intensive thinning at the study site (Figure 10) might have been underestimated. Furthermore, due to undetected errors, this study was not able to apply SPWisoM until 60 cm with 2 cm resolution (section 4.2); despite sparse distribution of roots below 40 cm (Figure 12), limited volume of deeper roots below 40 cm might possibly have largely contributed to PWU during drought as suggested by Matías et al. (2014). Additionally, this study focused on Scots pine trees which were dominated and was exclusively damaged by drought at the Hartheim forest, while partly mixed Black pine trees and their inter-species interactions with Scots pine trees were ignored. Thus, I might have missed some effects of inter-species interactions (e.g., resource competition or water redistribution; Anderegg, 2015) when assessing stand-level forest response to drought. Those were the main limitations regarding this master's thesis research.

6 Conclusion

This thesis research was implemented to investigate the effects of intensified drought on stand-level forest productivity reduction. A newly developed 1-D hydrological model (SPWisoM) was hired for simulating long-term soil moisture and PWU dynamics at 60-year-old Scots pine plantation forest in southwestern Germany. Tree ring width data was used for assessing time-series forest productivity. Followings are the main outcomes emerged from my study:

- SPWisoM was sufficiently capable of simulating 40-years soil moisture dynamics referring to measured soil moisture data (θ_{meas}) and Kling-Gupta efficiency (KGE). Modeled plant water uptake (PWU) was also strongly correlated to actual evapotranspiration (ET_{act}), however, the absolute amount of PWU seemed

approximately one order underestimated by SPWisoM. Accordingly, only the relative amount of PWU was regarded as valid.

- Based on calibrated SPWisoM, 82% of plant-available water was found at between 0 and 20 cm. Likewise, 65 % of PWU was originated from 0 – 20 cm. Thus, the shallower layer was seemingly critical in providing water resource to Scots pine trees at the study site where rooting depth is limited to ca.40 cm.
- Long-term modeling indicated that soil moisture and PWU have been significantly decreasing over the last 40 years. Particularly, soil moisture and PWU during the summer period showed strongly declining trends, implying climate change-driven intensification of summer drought at the study site.
- Soil moisture during the summer period and PWU during the winter period were positively correlated to radial growth of Scots pine trees, suggesting an important role of winter (pre-summer) water uptake for earlywood formation and subsequent radial growth of Scots pine trees.
- When sampled trees were classified by health classes, time-series growth rate suggested fast-growing trees were more susceptible to drought, showing relatively lowered productivity following recent drought events. It was in accordance with previous studies and assumingly owing to relatively lower water-use efficiency and drought-prone growing conditions.
- Because this study pointed out the relevance of intra-species and intra-stand variabilities in determining stand-level drought impacts, further studies should be carried out to quantitively investigate (1) single tree-level characteristics and (2) microenvironment surrounding individual trees.
- Micrometeorological parameters, modeled soil moisture, and modeled PWU over the past 40-years implied that the study site would provide additionally drought-prone unsuitable growing conditions for existing trees. I, therefore, propose an immediate action for forestry-based climate change adaptation at the study site, for instance by altering tree species to more drought-tolerant species.

Acknowledgment

My thesis research would not have been possible without the support of many people from interdisciplinary backgrounds. First and foremost, I would like to express my gratitude to Prof. Dr. Jens Lange (first supervisor, Chair of Hydrology) and Prof. Dr. Andreas Christen (second supervisor, Chair of Environmental Meteorology). I was honored to and excited to address this “hot” research issue under their supervision. Besides supervisors, it gives me great pleasure in acknowledging substantial technical supports from Mr. Stefan Seeger (Chair of Hydrology) and Mr. Georgios Skiadaresis (Chair of Silviculture). I also would like to thank Prof. Dr. Markus Weiler (Chair of Hydrology) for suggesting this research topic, Dr. Julia Annick Schwarz (Chair of Silviculture) for offering silvicultural insights, Prof. Dr. Dirk Schindler and Ms. Nora Bergner (Chair of Environmental Meteorology) for assisting meteorological data collection, and Mr. Felix Baab (Chair of Environmental Meteorology) for providing technical support during the fieldwork. A special thanks also go to Erasmus Mundus MSc European Forestry programme and people involved, by which realized my dream of studying in Europe. To my friends, thank you for your encouragement whenever I

had difficulties. Last but not least, I would like to express my deep and sincere gratitude to my family who has been always my greatest supporters.

References

Allen, C. D., Macalady, A. K., Chenchouni, H., Bachelet, D., McDowell, N., Vennetier, M., et al. (2010). A global overview of drought and heat-induced tree mortality reveals emerging climate change risks for forests. *Forest Ecology and Management*, *259*(4), 660–684. https://doi.org/10.1016/j.foreco.2009.09.001

Anderegg, W. R. L. (2015). Spatial and temporal variation in plant hydraulic traits and their relevance for climate change impacts on vegetation. *New Phytologist*, *205*(3), 1008-1014. https://doi.org/10.1111/nph.12907

Asselman, N. E. M., & Middelkoop, H. (1995). Floodplain Sedimentation: Quantities, Patterns and Processes. *Earth Surface Processes and Landforms*, *20*(6), 481–499.

Beven, K., & Germann, P. (2013). Macropores and water flow in soils revisited. *Water Resources Research*, *49*(6), 3071–3092. https://doi.org/10.1002/wrcr.20156

Bieker, D., & Rust, S. (2010). Non-destructive estimation of sapwood and heartwood width in scots pine (Pinus sylvestris L.). *Silva Fennica*, *44*(2), 267–273.

Brandes, E., Wenninger, J., Koeniger, P., Schindler, D., Rennenberg, H., Leibundgut, C., et al. (2007). Assessing environmental and physiological controls over water relations in a Scots pine (Pinus sylvestris L.) stand through analyses of stable isotope composition of water and organic matter. *Plant, Cell and Environment*, *30*(1), 113–127. https://doi.org/10.1111/j.1365-3040.2006.01609.x

Bréda, N. J. J. (2003, September 25). Ground-based measurements of leaf area index: A review of methods, instruments and current controversies. *Journal of Experimental Botany*, *54*(392), 2403-2417. https://doi.org/10.1093/jxb/erg263

Bréda, N., & Granier, A. (1996). Intra-and interannual variations of transpiration, leaf area index and radial growth of a sessile oak stand (Quercus petraea). *EDP Sciences*, *53*(2–3), 521–536.

Brodribb, T. J., & Cochard, H. (2009). Hydraulic Failure Defines the Recovery and Point of Death in Water-Stressed Conifers. *Plant Physiology*, *149*(1), 575–584. https://doi.org/10.1104/pp.108.129783

Buras, A., Schunk, C., Zeitrg, C., Herrmann, C., Kaiser, L., Lemme, H., et al. (2018). Are Scots pine forest edges particularly prone to drought-induced mortality? *Environmental Research Letters*, *13*(2), 025001. https://doi.org/10.1088/1748-9326/aaa0b4

Chen, M., Willgoose, G. R., & Saco, P. M. (2014). Spatial prediction of temporal soil moisture dynamics using HYDRUS-1D. *Hydrological Processes*, *28*(2), 171–185. https://doi.org/10.1002/hyp.9518

Choat, B., Jansen, S., Brodribb, T. J., Cochard, H., Delzon, S., Bhaskar, R., et al. (2012). Global convergence in the vulnerability of forests to drought. *Nature*, *491*(7426), 752–755. https://doi.org/10.1038/nature11688

Ciais, P., Reichstein, M., Viovy, N., Granier, A., Ogée, J., Allard, V., et al. (2005). Europe-wide reduction in primary productivity caused by the heat and drought in 2003. *Nature*, *437*(7058), 529–533. https://doi.org/10.1038/nature03972

Collatz, G. J., Ball, J., Grivet, C., & Berry, J. (1991). Physiological and environmental regulation of stomatal conductance, photosynthesis and transpiration. *Agricultural and Forest Meteorology*, *54*(1074), 107–136.

D'Amato, A. W., Bradford, J. B., Fraver, S., & Palik, B. J. (2013). Effects of thinning on drought vulnerability and climate response in north temperate forest ecosystems. *Ecological Applications*, *23*(8), 1735–1742. https://doi.org/10.1890/13-0677.1

Dale, V. H., Joyce, L. A., McNulty, S., Neilson, R. P., Ayres, M. P., Flannigan, M. D., & Hanson, P. J. et al. (2001). Climate change and forest disturbances: climate change can affect forests by altering the frequency, intensity, duration, and timing of fire, drought, introduced species, insect and pathogen outbreaks, hurricanes, windstorms, ice storms, or landslides. *BioScience*, *51*(9), 723–734. https://doi.org/10.1641/0006-3568(2001)051[0723:CCAFD]2.0.CO;2

Denmead, O. T., & Shaw, R. H. (2010). Availability of Soil Water to Plants as Affected by Soil Moisture Content and Meteorological Conditions1. *Agronomy Journal*, *54*(5), 385-390. https://doi.org/10.2134/agronj1962.00021962005400050005x

Ding, Y., Hayes, M. J., & Widhalm, M. (2011). Measuring economic impacts of drought: A review and discussion. *Disaster Prevention and Management: An International Journal*, *20*(4), 434-446. https://doi.org/10.1108/09653561111161752

Dobbertin, M. (2005). Tree growth as indicator of tree vitality and of tree reaction to environmental stress: A review. *European Journal of Forest Research*, *124*(4), 319-333. https://doi.org/10.1007/s10342-005-0085-3

Dobbertin, M., Wermelinger, B., Bigler, C., Bürgi, M., Carron, M., Forster, B., et al. (2007). Linking increasing drought stress to scots pine mortality and bark beetle infestations. *The Scientific World Journal*, *7*, 231-239. https://doi.org/10.1100/tsw.2007.58

Drake, B. G., Raschke, K., & Salisbury, F. B. (1970). Temperature and Transpiration Resistances of Xanthium Leaves as Affected by Air Temperature, Humidity, and Wind Speed. *Plant Physiology*, *46*(2), 324–330. https://doi.org/10.1104/pp.46.2.324

Eckhardt, K., & Ulbrich, U. (2003). Potential impacts of climate change on groundwater recharge and streamflow in a central European low mountain range. *Journal of Hydrology*, *284*(1–4), 244–252. https://doi.org/10.1016/j.jhydrol.2003.08.005

Elkin, C., Giuggiola, A., Rigling, A., & Bugmann, H. (2015). Short- and long-term efficacy of forest thinning to mitigate drought impacts in mountain forests in the European Alps. *Ecological Applications*, *25*(4), 1083–1098. https://doi.org/10.1890/14-0690.1

Feddes, R. A., Hoff, H., Bruen, M., Dawson, T., de Rosnay, P., Dirmeyer, P., et al. (2001). Modeling Root Water Uptake in Hydrological and Climate Models. *Bulletin of the American Meteorological Society*, *82*(12), 2797–2809. https://doi.org/10.1175/1520-0477(2001)082<2797:mrwuih>2.3.co;2

Feddes, R. A., Kowalik, P., Kolinska-Malinka, K., & Zaradny, H. (1976). Simulation of field water uptake by plants using a soil water dependent root extraction function. *Journal of Hydrology*, *31*(1–2), 13–26. https://doi.org/10.1016/0022-1694(76)90017-2

Franco, A. C., & Nobel, P. S. (1990). Influences of root distribution and growth on predicted water uptake and interspecific competition on predicted water uptake and interspecific competition. *Oecologia*, *82*(1990), 151–157.

Gallardo, A. (2003). Spatial Variability of Soil Properties in a Floodplain Forest in Northwest Spain. *Ecosystems*, *6*(6), 564–576. https://doi.org/10.1007/s10021-003-0198-9

George, E., & Marschner, H. (1996). Nutrient and water uptake by roots of forest trees. *Zeitschrift Für Pflanzenernährung Und Bodenkunde*, *159*(1), 11–21. https://doi.org/10.1002/jpln.1996.3581590103

Giuggiola, A., Bugmann, H., Zingg, A., Dobbertin, M., & Rigling, A. (2013). Reduction of stand density increases drought resistance in xeric Scots pine forests. *Forest Ecology and Management*, *310*, 827–835. https://doi.org/10.1016/j.foreco.2013.09.030

Goffin, S., Aubinet, M., Maier, M., Plain, C., Schack-Kirchner, H., & Longdoz, B. (2014). Characterization of the soil CO2 production and its carbon isotope composition in forest soil layers using the flux-gradient approach. *Agricultural and Forest Meteorology*, *188*, 45–57. https://doi.org/10.1016/j.agrformet.2013.11.005

Granier, A. (1987). Evaluation of transpiration in a Douglas-fir stand by means of sap flow measurements. *Tree Physiology*, *3*(4), 309–320. https://doi.org/10.1093/treephys/3.4.309

Granier, A., Biron, P., Bréda, N., Pontailler, J. Y., & Saugier, B. (1996). Transpiration of trees and forest stands: Short and long-term monitoring using sapflow methods. *Global Change Biology*, *2*(3), 265–274. https://doi.org/10.1111/j.1365-2486.1996.tb00078.x

Granier, A., Biron, P., Köstner, B., Gay, L. W., & Najjar, G. (1996). Comparisons of xylem sap flow and water vapour flux at the stand level and derivation of canopy conductance for Scots pine. *Theoretical and Applied Climatology*. *53*(1-3), 115-122. https://doi.org/10.1007/BF00866416

Granier, A., Reichstein, M., Bréda, N., Janssens, I. A., Falge, E., Ciais, P., et al. (2007). Evidence for soil water control on carbon and water dynamics in European forests during the extremely dry year: 2003. *Agricultural and Forest Meteorology*, *143*(1–2), 123–145. https://doi.org/10.1016/j.agrformet.2006.12.004

Gupta, H. V, Kling, H., Yilmaz, K. K., & Martinez, G. F. (2009). Decomposition of the mean squared error and NSE performance criteria: Implications for improving hydrological modelling. *Journal of Hydrology*, *377*(1–2), 80–91. https://doi.org/10.1016/j.jhydrol.2009.08.003

Hanel, M., Rakovec, O., Markonis, Y., Máca, P., Samaniego, L., Kyselý, J., & Kumar, R. (2018). Revisiting the recent European droughts from a long-term perspective. *Scientific Reports*, *8*(1), 9499. https://doi.org/10.1038/s41598-018-27464-4

Hanson, P. J., & Weltzin, J. F. (2000). Drought disturbance from climate change: Response of United States forests. *Science of the Total Environment*, *262*(3), 205–220. https://doi.org/10.1016/S0048-9697(00)00523-4

Hargreaves, G. H., & Samani, Z. A. (1985). Reference Crop Evapotranspiration from Temperature. *Applied Engineering in Agriculture*, *1*(2), 96–99. https://doi.org/10.13031/2013.26773

Hlásny, T., Mátyás, C., Seidl, R., Kulla, L., Merganičová, K., Trombik, J., et al. (2014). Climate change increases the drought risk in Central European forests: What are the options for adaptation? *Forestry Journal*, *60*(1), 5–18. https://doi.org/10.2478/forj-2014-0001

Holst, J., Barnard, R., Brandes, E., Buchmann, N., Gessler, A., & Jaeger, L. (2008). Impacts of summer water limitation on the carbon balance of a Scots pine forest in the southern upper Rhine plain. *Agricultural and Forest Meteorology*, *148*(11), 1815–1826. https://doi.org/10.1016/j.agrformet.2008.06.008

Holsten, A., Vetter, T., Vohland, K., & Krysanova, V. (2009). Impact of climate change on soil moisture dynamics in Brandenburg with a focus on nature conservation areas. *Ecological Modelling*, *220*(17), 2076–2087. https://doi.org/10.1016/j.ecolmodel.2009.04.038

Huang, Y., Zhang, K., Yang, S., & Jin, Y. (2013). A Method to Measure Humidity Based on Dry-Bulb and Wet-Bulb Temperatures. Research Journal of Applied Sciences, *Engineering and Technology*, *6*(16), 2984–2987.

Humphries, P., & Baldwin, D. S. (2003). Drought and aquatic ecosystems. *Freshwater Biology*, *48*(7), 1141–1146. https://doi.org/10.1002/9781444341812

Irmak, S., & Haman, D. Z. (2003). Evapotranspiration: Potential or Reference? *IFAS Extension*, *343(ABE 343)*, 1–2. Retrieved from http://edis.ifas.ufl.edu.

Jabro, J. D. (2013). Estimation of Saturated Hydraulic Conductivity of Soils From Particle Size Distribution and Bulk Density Data. *Transactions of the ASAE*, *35*(2), 557–560. https://doi.org/10.13031/2013.28633

Jackson, R. B., Sperry, J. S., & Dawson, T. E. (2000). Root water uptake and transport: Using physiological processes in global predictions. *Trends in Plant Science*. *5*(11), 482-488. https://doi.org/10.1016/S1360-1385(00)01766-0

Jaeger, L, & Kessler, A. (1996). The HartX period May 1992, seen against the background of twenty years of energy balance climatology at the Hartheim pine plantation. *Theoretical and Applied Climatology*, *53*(1–3), 9–21. https://doi.org/10.1007/BF00866407

Jaeger, L. (1978). Die klimatologischen Meßstation Hartheim des Meteorologischen Instituts der Universität Freiburg i.Br. [The climatological station Hartheim of the Meteorological Institute of the University of Freiburg i.Br] *Ber. Naturf. Ges. Freiburg*, *68*, 47–73.

Jaeger, Lutz, & Kessler, A. (1997). Twenty years of heat and water balance climatology at the Hartheim pine forest, Germany. *Agricultural and Forest Meteorology*, *84*, 25–36.

Jaeger, Lutz, Garthe, H.-J., & Kessler, A. (1986). The climatological site Hartheim Its philosophy, design and special measuring results. *International Symposium on Urban and Local Climatology Freiburg (Br.)*. 189–199.

Jagodziński, A. M., & Kałucka, I. (2008). Age-related changes in leaf area index of young Scots pine stands. *Dendrobiology*, *59*, 57–65.

Jensen, R. D., & Taylor, S. A. (1961). Effect of temperature on water transport through plants. *PLANT PHYSIOLOGY*, *36*(5), 639–642. https://doi.org/10.1104/pp.36.5.639

Jung, C. (2005). Numerische Modellierung des Bodenwassertransportes im Hinblick auf die Wasserverfügbarkeit an einem Trockenstandort [Numerical modeling of soil water transport with regard to water availability at a dry site]. Inst. für Hydrologie, Freiburg, Germany.

Kessler, A., & Jaeger, L. (1999). Long-Term Changes in Net Radiation and Its Components Above a Pine Forest and a Grass Surface in Germany. *International Journal of Climatology*, *19*, 211–226.

Kljun, N., Black, T. A., Griffis, T. J., Barr, A. G., Gaumont-Guay, D., Morgenstern, K., et al. (2007). Response of net ecosystem productivity of three boreal forest stands to drought. *Ecosystems*, *10*(6), 1039–1055. https://doi.org/10.1007/s10021-005-0082-x

Koeninger, P., & Leibundgut, C. (2001). Study of river water impacts on groundwater during flood events in a dry flood plain of the Upper Rhine Valley. *Groundwater ecology*. 369–374.

Königer, P. (2003). Tracerhydrologische Ansätze zur Bestimmung der Grundwasserneubildung [Tracer hydrological approaches for the determination of groundwater recharge]. Inst. für Hydrologie, Freiburg, Germany.

Köstner, B. (2001). Evaporation and transpiration from forests in Central Europe? relevance of patch-level studies for spatial scaling. *Meteorology and Atmospheric Physics. 76*(1-2), 69-82. https://doi.org/10.1007/s007030170040

Köstner, B., Falge, E., & Tenhunen, J. D. (2002). Age-related effects on leaf area/sapwood area relationships, canopy transpiration and carbon gain of Norway spruce stands (Picea abies) in the Fichtelgebirge, Germany. *Tree Physiology*, *22*(8), 567–574. https://doi.org/10.1093/treephys/22.8.567

Kuiper, P. J. C. (1964). Water uptake of higher plants as affected by root temperature. *Mededelingen van de Landbouwhogeschool Wageningen*, *64*(4), 1–11.

Kumagai, T. (2011). Transpiration in Forest Ecosystems. *Forest Hydrology and Biogeochemistry* (pp. 389-406). Springer, Dordrecht. https://doi.org/10.1007/978-94-007-1363-5_19

Leuzinger, S., Zotz, G., Asshoff, R., & Körner, C. (2005). Responses of deciduous forest trees to severe drought in Central Europe. *Tree Physiology*, *25*(6), 641–650. https://doi.org/10.1093/treephys/25.6.641

Lévesque, M., Saurer, M., Siegwolf, R., Eilmann, B., Brang, P., Bugmann, H., & Rigling, A. (2013). Drought response of five conifer species under contrasting water availability suggests high vulnerability of Norway spruce and European larch. *Global Change Biology*, *19*(10), 3184–3199. https://doi.org/10.1111/gcb.12268

Lindner, M., Garcia-Gonzalo, J., Kolström, M., Green, T., Reguera, R., Maroschek, M., et al. (2008). Impacts of Climate Change on European Forests and Options for Adaptation. *Report to the European Commission Directorate-General for Agriculture and Rural Development*, *173*.

Lindner, Marcus, Maroschek, M., Netherer, S., Kremer, A., Barbati, A., Garcia-Gonzalo, J., et al. (2010). Climate change impacts, adaptive capacity, and vulnerability of European forest ecosystems. *Forest Ecology and Management*, *259*(4), 698–709. https://doi.org/10.1016/j.foreco.2009.09.023

Lobet, G., Couvreur, V., Meunier, F., Javaux, M., & Draye, X. (2014). Plant Water Uptake in Drying Soils. *PLANT PHYSIOLOGY*, *164*(4), 1619–1627. https://doi.org/10.1104/pp.113.233486

López-Bernal, Á., Alcántara, E., Testi, L., & Villalobos, F. J. (2010). Spatial sap flow and xylem anatomical characteristics in olive trees under different irrigation regimes. *Tree Physiology*, *30*(12), 1536–1544. https://doi.org/10.1093/treephys/tpq095

Lu, J., Sun, G., McNulty, S., & Amatya, D. M. (2005). A Comparison of Six Potential Evapotranspiration Methods for Regional Use in the Southeastern United States. *Journal of the American Water Resources Association*, *41*(3), 621–633.

Luterbacher, J., Dietrich, D., Xoplaki, E., Grosjean, M., & Wanner, H. (2004). European Seasonal and Annual Temperature Variability, Trends, and Extremes since 1500. *Science*, *303*(5663), 1499–1503. https://doi.org/10.1126/science.1093877

Lv, L. (2014). Linking Montane Soil Moisture Measurements to Evapotranspiration Using Inverse Numerical Modeling. Utah State University, Utah, USA.

Maier, M., Schack-Kirchner, H., Hildebrand, E. E., & Schindler, D. (2011). Soil CO2 efflux vs. soil respiration: Implications for flux models. *Agricultural and Forest Meteorology*, *151*(12), 1723–1730. https://doi.org/10.1016/j.agrformet.2011.07.006

Martínez-Vilalta, J., López, B. C., Loepfe, L., & Lloret, F. (2012). Stand- and tree-level determinants of the drought response of Scots pine radial growth. *Oecologia*, *168*(3), 877–888. https://doi.org/10.1007/s00442-011-2132-8

Matías, L., González-Díaz, P., & Jump, A. S. (2014). Larger investment in roots in southern range-edge populations of Scots pine is associated with increased growth and seedling resistance to extreme drought in response to simulated climate change. *Environmental and Experimental Botany*, *105*, 32–38. https://doi.org/10.1016/j.envexpbot.2014.04.003

Mayer, H, Schindler, D., Fernbach, G., & Redepenning, D. (2005). Forstmeteorologische Messstelle Hartheim des Meteorologischen Institutes der Universität Freiburg [Hartheim Forest Research Site of the Meteorological Institute of the University of Freiburg]. *Ber. Meteor. Inst. Univ. Freiburg*.

Mayer, H, Schindler, D., Fernbach, G., & Redepenning, D. (2012). Forstmeteorologische Messstelle Hartheim des Meteorologischen Institutes der Universität Freiburg [Hartheim Forest Research Site of the Meteorological Institute of the University of Freiburg]. *Ber. Meteor. Inst. Univ. Freiburg*.

Mayer, Helmut, Schindler, D., Holst, J., Redepenning, D., & Fernbach, G. (2008). The forest meteorological experimental site Hartheim of the Meteorological Institute, Albert-Ludwigs-University of Freiburg. *Ber. Meteor. Inst. Univ. Freiburg*, *17*, 17-38.

McDowell, N. G. (2011). Mechanisms Linking Drought, Hydraulics, Carbon Metabolism, and Vegetation Mortality. *Plant Physiology*, *155*(3), 1051–1059. https://doi.org/10.1104/pp.110.170704

McElrone, A. J., Choat, B., Gambetta, G. A. & Brodersen, C. R. (2013). Water Uptake and Transport in Vascular Plants. *Nature Education Knowledge*, *4*(5):6

Meinzer, F. C., Goldstein, G., Holbrook, N. M., Jackson, P., & Cavelier, J. (1993). Stomatal and environmental control of transpiration in a lowland tropical forest tree. *Plant, Cell & Environment*, *16*(4), 429–436. https://doi.org/10.1111/j.1365-3040.1993.tb00889.x

Merlin, M., Perot, T., Perret, S., Korboulewsky, N., & Vallet, P. (2015). Effects of stand composition and tree size on resistance and resilience to drought in sessile oak and Scots pine. *Forest Ecology and Management*, *339*, 22–33. https://doi.org/10.1016/j.foreco.2014.11.032

Michelot, A., Bréda, N., Damesin, C., & Dufrêne, E. (2012). Differing growth responses to climatic variations and soil water deficits of Fagus sylvatica, Quercus petraea and Pinus sylvestris in a temperate forest. *Forest Ecology and Management*, *265*, 161–171. https://doi.org/10.1016/j.foreco.2011.10.024

Miyazawa, Y., Tateishi, M., Komatsu, H., Ma, V., Kajisa, T., Sokh, H., et al. (2014). Tropical tree water use under seasonal waterlogging and drought in central Cambodia. *Journal of Hydrology*, *515*, 81–89. https://doi.org/10.1016/j.jhydrol.2014.04.049

Morán-López, T., Poyatos, R., Llorens, P., & Sabaté, S. (2014). Effects of past growth trends and current water use strategies on scots pine and pubescent oak drought sensitivity.

European Journal of Forest Research, *133*(2), 369–382. https://doi.org/10.1007/s10342-013-0768-0

Oren, R., Phillips, N., Ewers, B. E., Pataki, D. E., & Megonigal, J. P. (1999). Sap-flux-scaled transpiration responses to light, vapor pressure deficit, and leaf area reduction in a flooded Taxodium distichum forest. *Tree Physiology*, *19*(6), 337–347. https://doi.org/10.1093/treephys/19.6.337

Poyatos, R., Granda, V., Molowny-Horas, R., Mencuccini, M., Steppe, K., & Martínez-Vilalta, J. (2016). SAPFLUXNET: Towards a global database of sap flow measurements. *Tree Physiology*, *36*(12), 1449–1455. https://doi.org/10.1093/treephys/tpw110

Rabbel, I., Bogena, H., Neuwirth, B., & Diekkrüger, B. (2018). Using sap flow data to parameterize the feddes water stress model for Norway spruce. *Water (Switzerland)*, *10*(3). https://doi.org/10.3390/w10030279

Radcliffe, D. E., Rasmussen, T. C., & Warrick, A. W. (2002). Soil water movement. *Soil Physics Companion* (pp. 85-126).

Rebetez, M., Mayer, H., Dupont, O., Schindler, D., Gartner, K., Kropp, J. P., & Menzel, A. (2006). Heat and drought 2003 in Europe: a climate synthesis. Annals of Forest *Science*, *63*(6), 569–577. https://doi.org/10.1051/forest:2006043

Rind, D., Goldberg, R., Hansen, J., Rosenzweig, C., & Ruedy, R. (1990). Potential evapotranspiration and the likelihood of future drought. *Journal of Geophysical Research: Atmospheres*, *95*(D7), 9983–10004. https://doi.org/10.1029/jd095id07p09983

Rouault, G., Candau, J.-N., Lieutier, F., Nageleisen, L.-M., Martin, J.-C., & Warzée, N. (2006). Effects of drought and heat on forest insect populations in relation to the 2003 drought in Western Europe. *Annals of Forest Science*, *63*(6), 613–624. https://doi.org/10.1051/forest:2006044

Ruiz-Lozano, J. M., Azcon Ruiz-Lozano, R., & Azcon, M. (1995). Hyphal contribution to water uptake in mycorrhizal plants as affected by the fungal species and water status. *Physiologia Plantarum*, *95*(3), 472–478. https://doi.org/10.1034/j.1399-3054.1995.950320.x

Ryel, R. J., Falge, E., Joss, U., Geyer, R., & Tenhunen, J. D. (2001). Penumbral and foliage distribution effects on Pinus sylvestris canopy gas exchange. *Theoretical and Applied Climatology*, *68*(1–2), 109–124. https://doi.org/10.1007/s007040170057

Sabaté, S., Gracia, C. A., & Sánchez, A. (2002). Likely effects of climate change on growth of Quercus ilex, Pinus halepensis, Pinus pinaster, Pinus sylvestris and Fagus sylvatica forests in the Mediterranean region. *Forest Ecology and Management*, *162*(1), 23-37.

Sardans, J, & Peñuelas, J. (2005). Drought decreases soil enzyme activity in a Mediterranean Quercus ilex L. forest. *Soil Biology and Biochemistry*, *37*(3), 455–461. https://doi.org/10.1016/j.soilbio.2004.08.004

Sardans, J, & Peñuelas, J. (2007). Drought changes phosphorus and potassium accumulation patterns in an evergreen Mediterranean forest. *Functional Ecology*, *21*(2), 191–201. https://doi.org/10.1111/j.1365-2435.2007.01247.x

Sardans, Jordi, & Peñuelas, J. (2004). Increasing drought decreases phosphorus availability in an evergreen Mediterranean forest. *Plant and Soil*, *267*(1–2), 367–377. https://doi.org/10.1007/s11104-005-0172-8

Schindler, D., Köstner, B., & Mayer, H. (2004). Drought 2003 at a Scots pine forest. *Impacts of the Drought and Heat in 2003 on Forests* (p. 16).

Schindler, D., Türk, M., & Mayer, H. (2006). CO2 fluxes of a Scots pine forest growing in the warm and dry southern upper Rhine plain, SW Germany. *European Journal of Forest Research*, *125*(3), 201–212. https://doi.org/10.1007/s10342-005-0107-1

Schlyter, P., Stjernquist, I., Bärring, L., Jönsson, A. M., & Nilsson, C. (2006). Assessment of the impacts of climate change and weather extremes on boreal forests in northern Europe, focusing on Norway spruce. *Climate Research*, *31*(1), 75–84. https://doi.org/10.3354/cr031075

Schulze, E. D., Čermák, J., Matyssek, M., Penka, M., Zimmermann, R., Vasícek, F., et al. (1985). Canopy transpiration and water fluxes in the xylem of the trunk of Larix and Picea trees - a comparison of xylem flow, porometer and cuvette measurements. *Oecologia*, *66*(4), 475–483. https://doi.org/10.1007/BF00379337

Silva, B. M., Silva, É. A. da, Oliveira, G. C. de, Ferreira, M. M., & Serafim, M. E. (2014). Plant-available soil water capacity: estimation methods and implications. *Revista Brasileira de Ciência Do Solo*, *38*(2), 464–475. https://doi.org/10.1590/s0100-06832014000200011

Slatyer, R. O. (1937). The significance of the permanent wilting percentage in studies of plant and soil water relations. *The Botanical Review*, *3*(1), 585–636. https://doi.org/10.2307/2420009

Spinoni, J., Naumann, G., Vogt, J., & Barbosa, P. (2015). European drought climatologies and trends based on a multi-indicator approach. *Global and Planetary Change*, *127*, 50–57. https://doi.org/10.1016/j.gloplacha.2015.01.012

Sprenger, M., Volkmann, T. H. M., Blume, T., & Weiler, M. (2015). Estimating flow and transport parameters in the unsaturated zone with pore water stable isotopes. *Hydrology and Earth System Sciences*, *19*(6), 2617–2635. https://doi.org/10.5194/hess-19-2617-2015

Stanke, C., Kerac, M., Prudhomme, C., Medlock, J., & Murray, V. (2013). Health Effects of Drought: A Systematic Review of the Evidence. *PLoS Currents*, *5*. https://doi.org/10.1371/currents.dis.7a2cee9e980f91ad7697b570bcc4b004

Sterck, F. J., Zweifel, R., Sass-Klaassen, U., & Chowdhury, Q. (2008). Persisting soil drought reduces leaf specific conductivity in Scots pine (Pinus sylvestris) and pubescent oak (Quercus pubescens). *Tree Physiology*, *28*, 529–536. https://doi.org/10.1093/treephys/28.4.529

Steudle, E. (2000). Water uptake by plant roots: an integration of views. *Plant and Soil*, *226*(1), 45–56.

Sturm, N., Reber, S., Kessler, A., & Tenhunen, J. D. (1996). Soil moisture variation and plant water stress at the Hartheim Scots pine plantation. *Theoretical and Applied Climatology*, *53*(1–3), 123–133. https://doi.org/10.1007/BF00866417

Teuling, A. J., Van Loon, A. F., Seneviratne, S. I., Lehner, I., Aubinet, M., Heinesch, B., et al. (2013). Evapotranspiration amplifies European summer drought. *Geophysical Research Letters*, *40*(10), 2071–2075. https://doi.org/10.1002/grl.50495

Tilman, D., & Haddi, A. El. (1992). Drought and biodiversity in Grasslands. *Oecologia*, *89*(2), 257-264.

Toll, D., Asquith, J., Fraser, A., Hassan, A., Liu, G., Lourenço, S., et al. (2015). Tensiometer techniques for determining soil water retention curves. In Unsaturated Soil Mechanics

- from Theory to Practice. *Asia-Pacific Conference on Unsaturated Soil* (pp. 15–22). https://doi.org/10.1201/b19248-4

Tyree, M. T. (2007). The Cohesion-Tension theory of sap ascent: current controversies. *Journal of Experimental Botany*, *48*(10), 1753–1765. https://doi.org/10.1093/jxb/48.10.1753

van Genuchten, M. T. (1980). A Closed-form Equation for Predicting the Hydraulic Conductivity of Unsaturated Soils1. *Soil Science Society of America Journal*, *44*(5), 892. https://doi.org/10.2136/sssaj1980.03615995004400050002x

Veihmeyer, F. J., & Hendrickson, A. H. (1949). Methods of measuring field capacity and permanent wilting percentage of soils. *Soil Science*, *68*(1), 75–94. https://doi.org/10.1097/00010694-194907000-00007

Vengadaramana, A., & Jashothan, P. T. (2012). Effect of organic fertilizers on the water holding capacity of soil in different terrains of Jaffna peninsula in Sri Lanka. *Journal of Natural Product Plant Resources*, *2*(4), 500–503.

Vertessy, R. A., Benyon, R. G., O'Sullivan, S. K., & Gribben, P. R. (1995). Relationships between stem diameter, sapwood area, leaf area and transpiration in a young mountain ash forest. *Tree Physiology*, *15*(9), 559–567. https://doi.org/10.1093/treephys/15.9.559

Vicente-Serrano, S. M., Gouveia, C., Camarero, J. J., Begueria, S., Trigo, R., Lopez-Moreno, J. I., et al. (2013). Response of vegetation to drought time-scales across global land biomes. *Proceedings of the National Academy of Sciences*, *110*(1), 52–57. https://doi.org/10.1073/pnas.1207068110

Vogt, R., & Jaeger, L. (1990). Evaporation from a pine forest - using the aerodynamic method and bowen ratio method. *Agricultural and Forest Meteorology*, *50*(1–2), 39–54. https://doi.org/10.1016/0168-1923(90)90137-U

Walter, J. M. N., Fournier, R. A., Soudani, K., & Meyer, E. (2003). Integrating clumping effects in forest canopy structure: An assessment through hemispherical photographs. *Canadian Journal of Remote Sensing*, *29*(3), 388–410. https://doi.org/10.5589/m03-011

Wang, Y. P., & Jarvis, P. G. (1990). Influence of crown structural properties on PAR absorption, photosynthesis, and transpiration in Sitka spruce: application of a model (MAESTRO). *Tree Physiology*, *7*, 297–316. https://doi.org/10.1093/treephys/7.1-2-3-4.297

Watson, D. J. (1947). Comparative Physiological Studies on the Growth of Field Crops: I. Variation in Net Assimilation Rate and Leaf Area between Species and Varieties, and within and between Years. *Annals of Botany*, *11*(1), 41–76. https://doi.org/10.1093/oxfordjournals.aob.a083148

Weber, P., Bugmann, H., & Rigling, A. (2007). Radial growth responses to drought of Pinus sylvestris and Quercus pubescens in an inner-Alpine dry valley. *Journal of Vegetation Science*, *18*(6), 777–792. https://doi.org/10.1111/j.1654-1103.2007.tb02594.x

Wedler, M., Heindl, B., Hahn, S., Köstner, B., Bernhofer, C., & Tenhunen, J. D. (1996). Model-based estimates of water loss from "patches" of the understory mosaic of the Hartheim Scots pine plantation. *Theoretical and Applied Climatology*, *53*(1–3), 135–144. https://doi.org/10.1007/BF00866418

Weiss, M., Baret, F., Smith, G. J., Jonckheere, I., & Coppin, P. (2004). Review of methods for in situ leaf area index (LAI) determination Part II. Estimation of LAI, errors and

sampling. *Agricultural and Forest Meteorology*, *121*(1–2), 37–53. https://doi.org/10.1016/j.agrformet.2003.08.001

Wellpott, A., Imbery, F., Schindler, D., & Mayer, H. (2005). Simulation of drought for a Scots pine forest (Pinus sylvestris L.) in the southern upper Rhine plain. *Meteorologische Zeitschrift*, *14*(2), 143–150. https://doi.org/10.1127/0941-2948/2005/0015

Wösten, J. H. M., & van Genuchten, M. T. (2010). Using Texture and Other Soil Properties to Predict the Unsaturated Soil Hydraulic Functions. *Soil Science Society of America Journal*, *52*(6), 1762. https://doi.org/10.2136/sssaj1988.03615995005200060045x

Yang, X., & You, X. (2013). Estimating Parameters of Van Genuchten Model for Soil Water Retention Curve by Intelligent Algorithms. *Appl. Math. Inf. Sci*, *7*(5), 1977–1983. https://doi.org/10.12785/amis/070537

Zang, C., Pretzsch, H., & Rothe, A. (2012). Size-dependent responses to summer drought in Scots pine, Norway spruce and common oak. *Trees - Structure and Function*, *26*(2), 557–569. https://doi.org/10.1007/s00468-011-0617-z

Zeppel, M. J. B., Wilks, J. V., & Lewis, J. D. (2014). Impacts of extreme precipitation and seasonal changes in precipitation on plants. *Biogeosciences*, *11*(11), 3083–3093. https://doi.org/10.5194/bg-11-3083-2014

Appendices

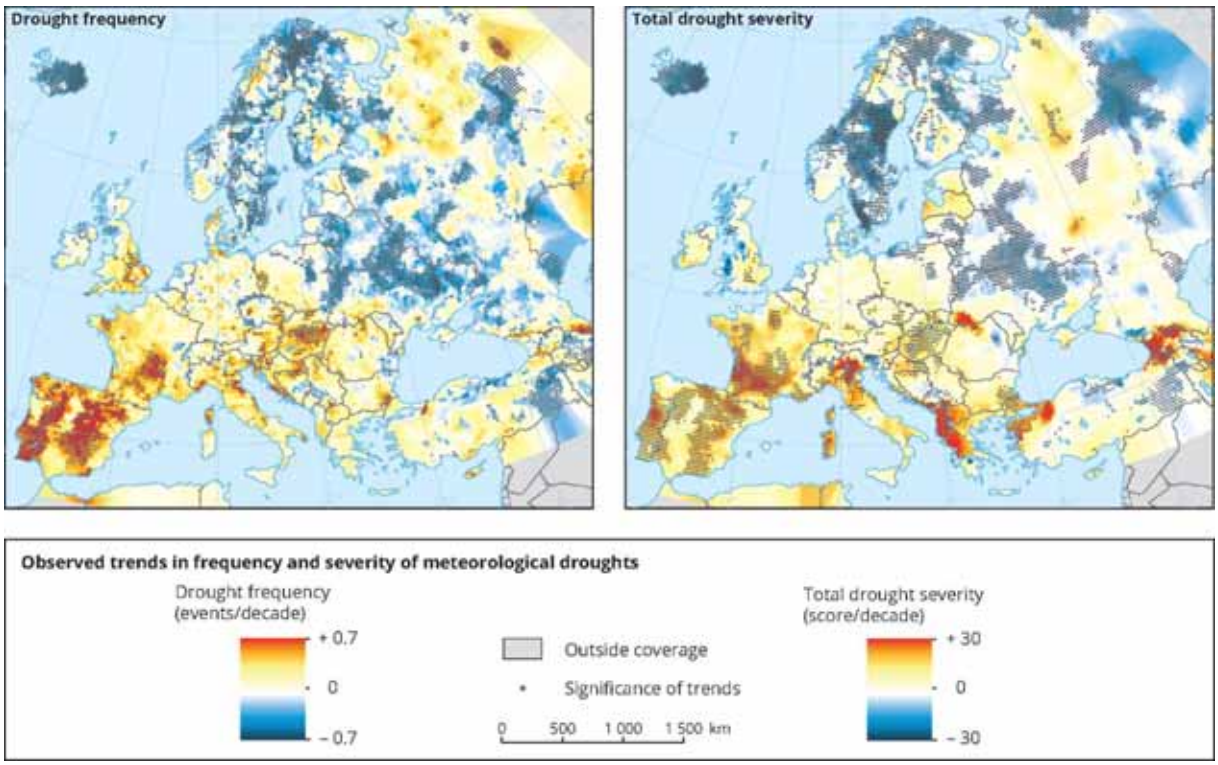

Appendix 1. Trends in frequency (upper) and severity (lower) of meteorological droughts between 1950 and 2012. Trends are based on a combination of three different drought indices - SPI, SPEI and RDI accumulated over 12-month periods. Dots: trends significant at ≥ 95% (https://www.eea.europa.eu/data-and-maps/indicators/river-flow-drought-2/assessment).

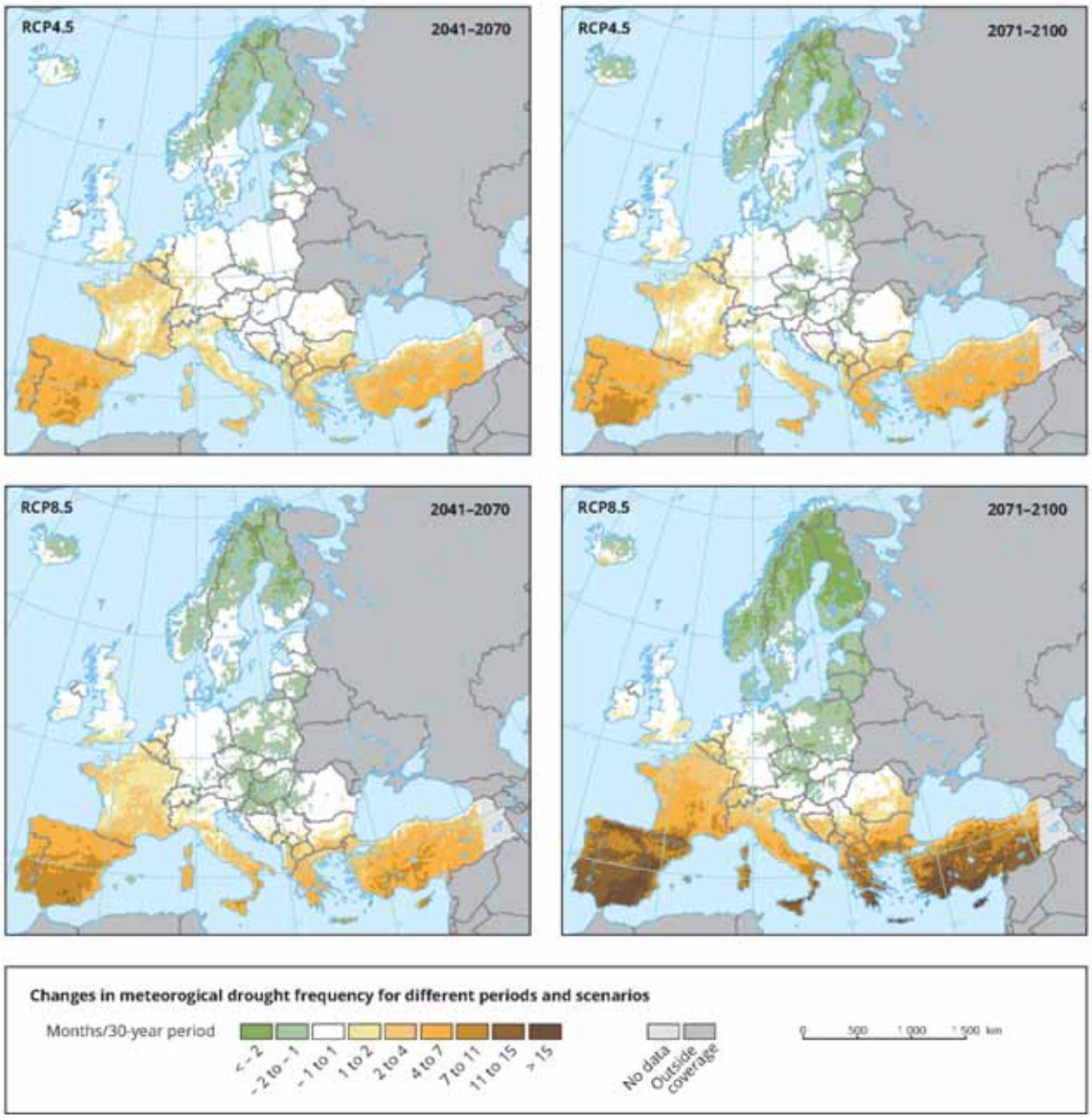

Appendix 2. The maps show changes in the frequency of meteorological droughts for two future periods (2041-2070, left and 2071-2100, right) and for two emissions scenarios (RCP4.5, top and RCP8.5, bottom). Drought frequency is defined as the number of months in a 30 year period with the Standardized Precipitation Index accumulated over a 6 month period (SPI-6) having a value below -2 (https://www.eea.europa.eu/data-and-maps/figures/changes-in-meteorological-drought-frequency)

Appendix 3. Full script of SPWisoM "Simulation.py" file used in this research.

```
from modelCode.Simulation import *

#-----------------------------------
# Step1: load a configuration file
#  the configuration file is loaded and parsed
#  the parsed configuartion will be stored in sim.pre

sim = Simulation("conf.xml", verbosity = 1)

#-----------------------------------
# Step2: modify input data or model parameters
#  water amounts as well as pressure heads in the model are expected in cm
#  since mm is much more usual for prcp and ETpot, the values of the input file
#  are converted from mm to cm
sim.pre.inputData["prcp"]*=0.1 #[mm] to [cm]
sim.pre.inputData["ETp"]*=0.1 #[mm] to [cm]

# overwrite the value for the porespace seperation pressure head [cm] of the
#  model configuration file (just to demonstrate how a model parameter can be
#  overwritten from within a script)
#sim.pre.modelPars["poreSpaceSeperationHead"] = 600
sim.pre.modelPars["doIsotopes"] = False

#-----------------------------------
#Step3: reinitialize the model
# this step is only neccessary, when changes to sim.pre were made after loading the
#  configuration file
sim.reinitialize()

#-----------------------------------
#Step4: run the model
sim.run(verbosity = 1)
#cProfile.run("sim.run(verbosity = 1)")

#-----------------------------------
#Step5: write  results according to the specifications made in the configuration file
sim.write_results()


#optional additional plots...

if 0:

    from modelCode import indices

    import numpy as np
    import matplotlib
    import matplotlib.pyplot as plt
    from mpl_toolkits.axes_grid1 import make_axes_locatable

    cmap_iso = matplotlib.cm.magma
    cmap_theta = matplotlib.cm.Blues
    cmap_temp = matplotlib.cm.coolwarm

    cmaps = {"DExcess": matplotlib.cm.magma,
             "delta18O": matplotlib.cm.magma,
             "delta2H": matplotlib.cm.magma,
             "theta": matplotlib.cm.Blues,
             "head": matplotlib.cm.Blues,
             "temp": matplotlib.cm.coolwarm,
             "uptake": matplotlib.cm.viridis,
```

```
        "evaporation": matplotlib.cm.viridis}

z  = sim.parMat[:,indices.i_z]
dz = sim.parMat[:,indices.i_dz]
n = sim.inputData.shape[0]
extent = (0,n-1,-z[-1],z[0]+dz[0])


f, ((ax1, ax2, ax3, ax4)) = plt.subplots(4, sharex='col', sharey='row', figsize=(10,8))
#plt.tight_layout()

for par, ax in zip(["delta18O", "theta", "evaporation", "uptake"],[ax1, ax2, ax3, ax4]):

    im = ax.imshow(sim.profile[par][:-1,:],
                   vmin=np.min(sim.profile[par][1:,1:]),
                   vmax=np.max(sim.profile[par][1:,1:]),
                   aspect='auto', cmap= cmaps[par],
                   extent = extent)
    ax.plot([0,n-1],[0,0], color='red')
    ax.set_title(par)
    divider = make_axes_locatable(ax)
    cax = divider.append_axes('right', size='5%', pad=0.05)
    f.colorbar(im, cax=cax, orientation='vertical')

plt.show()

```

Appendix 4. Full script of SPWisoM "conf.xml" file used in this research.

```
<?xml version="1.0"?>
<modelConfiguration>
  <time>
    <start>1978-01-01</start>
    <end daysAfterStart = "14974"></end>
    <timeStep>day</timeStep> <!-- choose between day, hour and minute (currently only days are implemented...)-->
  </time>
  <path name = "inputPath" >inputData</path>
  <path name = "outputPath">outputData</path>
  <inputFiles>
    <timeSeries name = "meteo"      delimiter = "\t" path="inputPath" timeStep="D"      >meteo2.csv</timeSeries>
    <timeSeries name = "prcpIsotopes" delimiter = "\t" path="inputPath" gapfill = "backward">prcpIsotopes.csv</timeSeries>
    <timeSeries name = "vegetation"  delimiter = "\t" path="inputPath" gapfill = "linear" >vegetation.csv</timeSeries>
    <table    name = "soils"     delimiter = ";"  path="inputPath"            >soilTypes.csv</table>
    <table    name = "feddes"    delimiter = "\t" path="inputPath"            >feddes.csv</table>
    <table    name = "roots"     delimiter = "\t" path="inputPath"            >roots.csv</table>
    <tableList name = "profiles"  delimiter = "\t" path="inputPath"            >soilProfiles.csv</tableList>
  </inputFiles>
  <vegetation>
    <roots>
      <Feddes>
        <tableRow>feddes.conifer</tableRow>
        <overwrite name = "P4">15000</overwrite>
        <overwrite name = "omega">1</overwrite>
      </Feddes>
      <distribution>
        <!--any valid empiric distribution is the first choice, only if no valid empiric distribution is
          specified, the generic distribution will take effect-->
        <empirical>
          <tableColumn>roots.depth|Pinus</tableColumn>
        </empirical>
        <generic>
          <function>scaledBeta</function>
          <parameter name = "alpha">1</parameter>
          <parameter name = "beta">1.5</parameter>
          <parameter name = "zmax"><tableColumn>vegetation.rootDepth</tableColumn></parameter>

        </generic>
      </distribution>
    </roots>
  </vegetation>

  <soil resolution = "2" depth = "40" bottomTemp = "meteo.temp">
    <initialProfile><tableSection>profiles.initial</tableSection></initialProfile>
    <profileLayers>
      <layer top = "0" bottom = "20">
        <tableRow>soils.Ah1</tableRow>
        <overwrite name = "skeleton">0</overwrite>
      </layer>
      <layer top = "20" bottom = "40">
        <tableRow>soils.Ah2</tableRow>
        <overwrite name = "skeleton">0.5</overwrite>
      </layer>
    </profileLayers>
  </soil>

  <model>
```

```
57      <parameter name = "doIsotopes">0</parameter>
58      <parameter name = "poreSpaceSeperationHead">600</parameter> <!-- values between 0 and 20000
    cm, set it to zero to disable second pore size fraction -->
59      <parameter name = "lowerBoundary">0</parameter> <!-- 0: free drainage, 1: ground water (
    unimplemented), 2: aquiclude (unimplemented) -->
60      <parameter name = "minimumPrcpIntensity">0.05</parameter> <!-- minimum precipitation intensity [cm/
    h] used for daily timesteps with low daily prcp sums  -->
61      <soilEvaporation>
62        <parameter name="depthDecline">1</parameter>  <!-- higher values increase evaporation from the
    top -->
63        <parameter name="maxEvapDepth">20</parameter> <!-- maximum depth of soil evaporation front
    given in cm-->
64      </soilEvaporation>
65
66      <interception>
67        <parameter name = "f_capacity">0.02</parameter> <!-- interception capacity = (LAI + WAI) * f_capacity
    [cm] -->
68        <parameter name = "I_per_PAI">0.33</parameter> <!-- fraction of prcp routed through interception
    storage = min(1, (LAI + WAI) * I_per_PAI) -->
69        <parameter name = "k_ET">0.6</parameter><!-- Tpot = ETpot * (1-exp(-k_ET * (WAI+LAI))); Epot =
    ETpot - Tpot -->
70        <parameter name = "r_ET">0.4</parameter><!-- ratio ov canopy evaporation to transpiration in case of
    wet canopy-->
71      </interception>
72      <gasExchange>
73        <parameter name = "inhomogeneityFactor">100</parameter>
74        <parameter name = "fractionFactor">0.15</parameter> <!-- values between 0.09 and 0.21 -->
75      </gasExchange>
76    </model>
77
78    <!-- change content of this file in order to alter automatic plot labeling-->
79    <parameterDefinitions>modelConfiguration/parDef.xml</parameterDefinitions>
80
81    <outputFiles defaultFormat="%.3f" defaultFigureSize="8x4.5">
82
83      <!-- fileType determines the type of output
84        "" (empty fileType) will not produce any output
85        "csv" will produce a '\t' sepearted text file, where the format property can be used to control precision
86        "pdf" or "png" will produce an image file of the responding file format figureSize (width x height) controls
    figure size
87      -->
88
89      <!-- profileTimeSeries are available by stating "PROFILE_" followed by one of the following parameters:
90        temp                  - soil temperature
91        head                  - soil water pressure head
92        evaporation             - soil evaporation
93        uptake                - plant water uptake
94        theta, f_theta, c_theta       - volumetric water content (all, fine and coarse pores)
95        delta18O, f_delta18O, c_delta18O - soil water delta 18O (all, fine and coarse pores)
96        delta2H,  f_delta2H,  c_delta2H  - soil water delta 2H (all, fine and coarse pores)
97        DExcess,  f_DExcess,  c_DExcess  - soil water Deuterium Excess (all, fine and coarse pores)
98      -->
99      <profileTimeSeries fileType="csv" parameters = "PROFILE_theta"     path="outputPath" format = "%.
    3f">profile_theta</profileTimeSeries>
100     <profileTimeSeries fileType="csv" parameters = "PROFILE_uptake"     path="outputPath" format = "
    %.5f">profile_uptake</profileTimeSeries>
101
102     <profileTimeSeries fileType="pdf" parameters = "PROFILE_theta"     path="outputPath" format = "%.
    3f">profiles</profileTimeSeries>
103     <profileTimeSeries fileType="pdf" parameters = "PROFILE_delta18O"   path="outputPath">profiles</
    profileTimeSeries>
```

```
104     <profileTimeSeries fileType="pdf" parameters = "PROFILE_delta2H"    path="outputPath">profiles</
    profileTimeSeries>
105     <profileTimeSeries fileType="pdf" parameters = "PROFILE_DExcess"    path="outputPath">profiles</
    profileTimeSeries>
106     <profileTimeSeries fileType="pdf" parameters = "PROFILE_evaporation" path="outputPath">profiles</
    profileTimeSeries>
107     <profileTimeSeries fileType="pdf" parameters = "PROFILE_uptake"     path="outputPath">profiles</
    profileTimeSeries>
108     <profileTimeSeries fileType="" parameters = "PROFILE_temp"      path="outputPath">profiles</
    profileTimeSeries>
109
110
111     <!-- timeSeries can be obtained by extracting data from a ceratin depth of a profileTimeSeries (explained
    above)
112          (to do this, give a cm value in square brackets after the specified profile parameter,
113           e.g. PROFILE_theta[10] would yield the value of PROFILE_theta from the position closest to a depth of
    10 cm)
114        additionally available time series are:
115          canopy_storage, canopy_evaporation,  throughfall, runoff, ponding, infiltration, uptake, evaporation,
    percolation, rise, storage
116          throughfall_delta18O, uptake_delta18O, percolation_delta18O, xylem_delta18O (for all in this line 18O
    can also be replaced by 2H)
117          everything that is defined in the input data can also be obtained by using the suffix "INPUT_"
118     -->
119
120     <timeSeries fileType="pdf" parameters = "storage" path="outputPath">storage</timeSeries>
121     <timeSeries fileType="pdf" parameters = "canopy_storage" path="outputPath">storage</timeSeries>
122     <timeSeries fileType="pdf" parameters = "INPUT_ETp; canopy_evaporation; uptake; evaporation"
    path="outputPath" figureSize="20x4.5">waterLoss</timeSeries>
123     <timeSeries fileType="pdf" parameters = "INPUT_delta18O; canopy_delta18O; throughfall_delta18O;
    uptake_delta18O"  path="outputPath" figureSize="8x3">delta18O</timeSeries>
124
125     <timeSeries fileType="" parameters = "PROFILE_theta[10]; PROFILE_theta[50]"  path="outputPath">
    theta_selection</timeSeries>
126
127   </outputFiles>
128
129 </modelConfiguration>
```

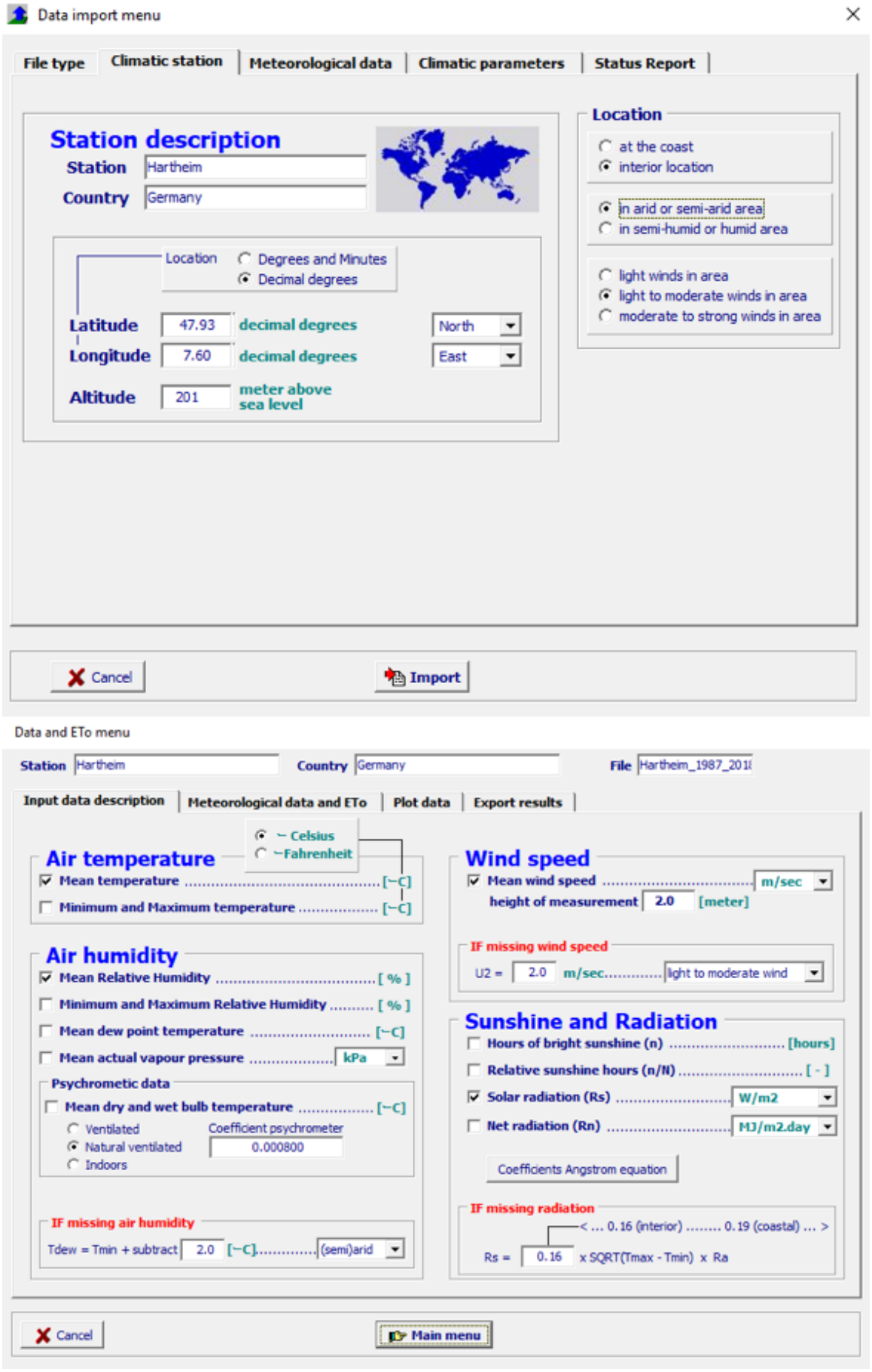

Appendix 5.Screenshots of the FAO ETo Calculator.

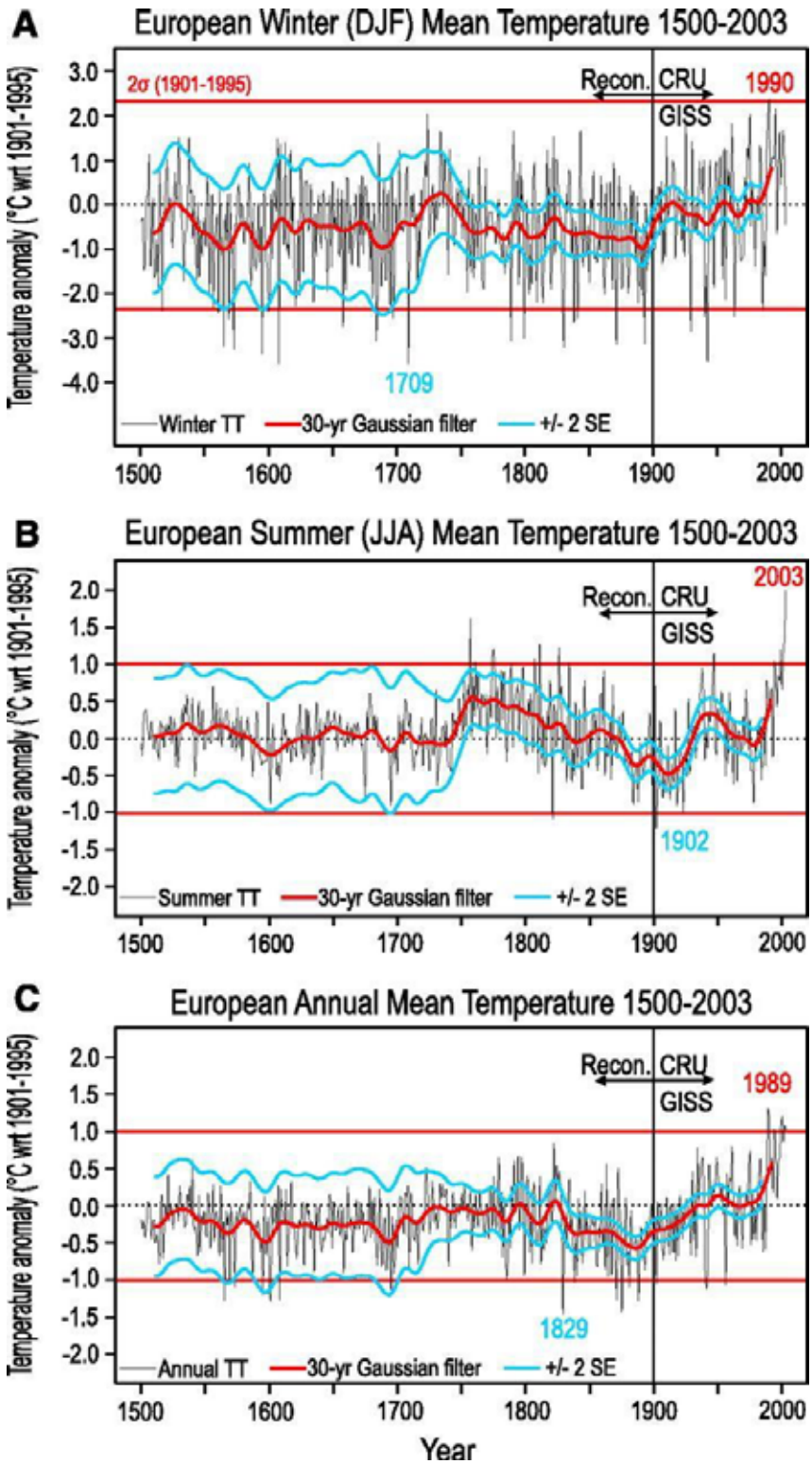

Appendix 6. (A) Winter (DJF), (B) summer (JJA), and (C) annual averaged-mean European temperature anomaly (relative to the 1901 to 1995 calibration average) time series from 1500 to 2003, defined as the average over the land area 25°W to 40°E and 35°N to 70°N (thin black line) from Luterbacher et al. (2004).

Appendix 7. Pan-European distribution of Scots pine (Pinus Sylvestris) (source: https://ec.europa.eu/jrc/en/research-topic/forestry/qr-tree-project/scots-pine).

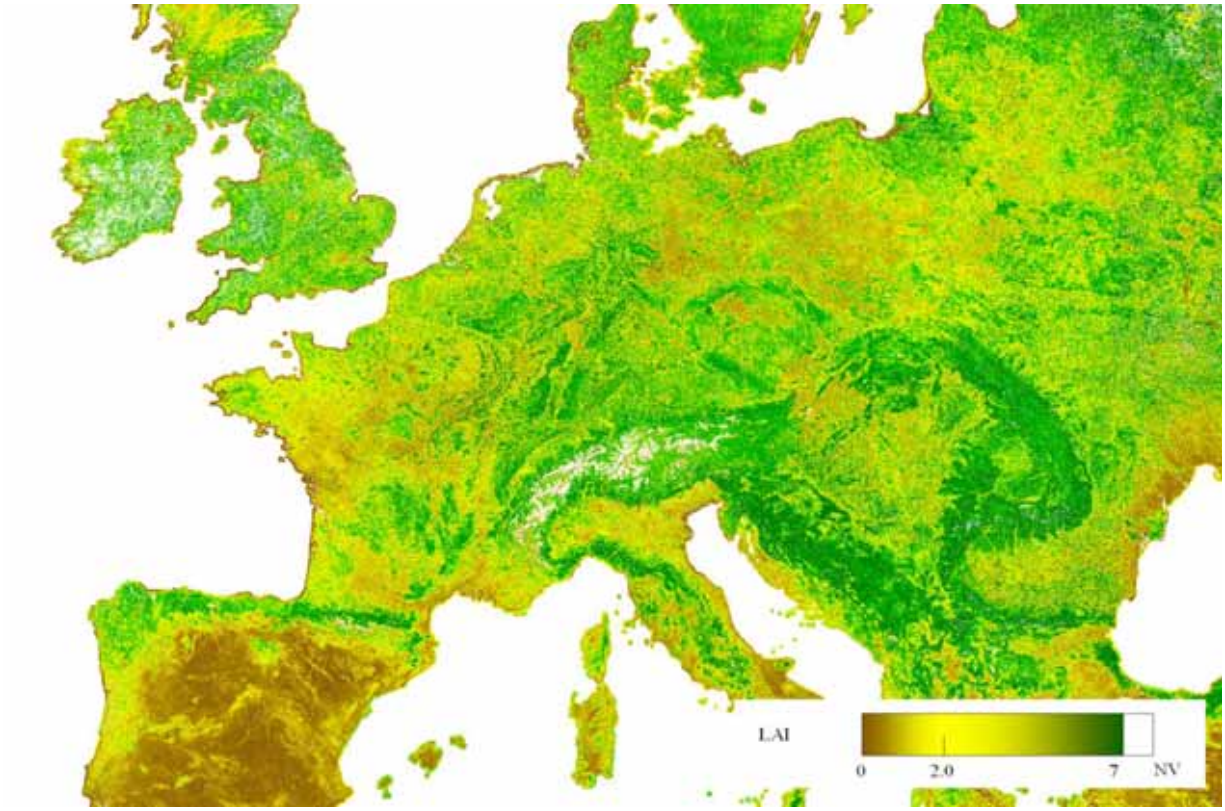

Appendix 8. 300-m resolution leaf area index (LAI) as of 30 June 2019, provided from the Copernicus Global Land Service (CGLS) (source: https://land.copernicus.eu/global/)

Testimony

I herewith declare that I have written this paper on my own and that I have not used any other sources and materials than those indicated. I properly cited the materials I have relied upon. I have not submitted this document as a master thesis elsewhere.

Place and date	Signature